FILTER BANK MULTICARRIER SPREAD SPECTRUM COMMUNICATIONS

by

Daryl Leon Wasden

A dissertation submitted to the faculty of
The University of Utah
in partial fulfillment of the requirements for the degree of

Doctor of Philosophy

Department of Electrical and Computer Engineering

The University of Utah

August 2014

The University of Utah Graduate School

STATEMENT OF DISSERTATION APPROVAL

The dissertation of **Daryl Leon Wasden**

has been approved by the following supervisory committee members:

Behrouz Farhang	, Chair	**03/28/2014** Date Approved
Neal Patwari	, Member	**03/28/2014** Date Approved
Rong Rong Chen	, Member	**03/28/2014** Date Approved
Osama S. Haddadin	, Member	**03/28/2014** Date Approved
Faisal Khan	, Member	**03/28/2014** Date Approved

and by **Gianluca Lazzi** , Chair/Dean of

the Department/College/School of **Electrical and Computer Engineering**

and by David B. Kieda, Dean of The Graduate School.

ABSTRACT

Wireless communications pervade all avenues of modern life. The rapid expansion of wireless services has increased the need for transmission schemes that are more spectrally efficient. Dynamic spectrum access (DSA) systems attempt to address this need by building a network where the spectrum is used opportunistically by all users based on local and regional measurements of its availability. One of the principal requirements in DSA systems is to initialize and maintain a control channel to link the nodes together. This should be done even before a complete spectral usage map is available. Additionally, with more users accessing the spectrum, it is important to maintain a stable link in the presence of significant interference in emergency first-responders, rescue, and defense applications. In this thesis, a new multicarrier spread spectrum (MC-SS) technique based on filter banks is presented. The new technique is called filter bank multicarrier spread spectrum (FB-MC-SS). A detailed theory of the underlying properties of this signal are given, with emphasis on the properties that lend themselves to synchronization at the receiver. Proposed algorithms for synchronization, channel estimation, and detection are implemented on a software-defined radio platform to complete an FB-MC-SS transceiver and to prove the practicality of the technique. FB-MC-SS is shown through physical experimentation to be significantly more robust to partial band interference compared to direct sequence spread spectrum. With a higher power interfering signal occupying 90% of its band, FB-MC-SS maintains a low bit error rate. Under the same interference conditions, DS-SS fails completely. This experimentation leads to a theoretical analysis that shows in a frequency selective channel with additive white noise, the FB-MC-SS system has performance that equals that obtained by a DS-SS system employing an optimal rake receiver. This thesis contains a detailed chapter on implementation and design, including lessons learned while prototyping the system. This is to assist future system designers to quickly gain proficiency in further development of this technology.

CONTENTS

ACKNOWLEDGMENTS

A lot of people have helped me throughout the years to complete the work contained in this dissertation. I almost certainly owe more people than I can list here. With that said, I plan to try to thank some of them.

My brother, Richard Wasden, has stood by me and been there for me since our childhood. His support and friendship over the years have been true and constant. This has been especially true during the intense period of research that I have been pursuing these last five years. I am indebted to him for keeping me working even when things seemed difficult and for helping me focus on the big picture while I am working on the details of a smaller one.

My advisor, Dr. Behrouz Farhang, has been a major source of support, inspiration, guidance, compassion, and encouragement. Without him, this work would not have been possible. I have appreciated his keen mind and solid understanding and knowledge in this area. In addition to aiding me in my professional development, he has provided me with guidance in my personal life that has been a comfort and a value over the years that I have known him.

My parents, Gary and Dawn Wasden, were among the first to encourage me to pursue my passion for technology. These early days of pursuing technological knowledge ultimately led me to the profession of electrical engineering. I will be forever grateful for the early support that led me to further research, and led me to discover one of my greatest passions. Thank you.

Every member of the faculty of the Department of Electrical and Computer Engineering that has come in contact with me has been an inspiration and a guide. I cannot possibly list everyone here. I will never forget the early introductory classes that encouraged me to pursue more knowledge. Every class I have taken has taught me something valuable and contributed to my engineering bag of tricks. The experience and knowledge of the faculty at the University of Utah and their passion and willingness to teach their students has made my time here remarkably productive. I appreciate you all.

I would like to thank Idaho National Laboratory for their continued support of this research. I would especially like to thank David Couch and Jose Loera, whose assistance and support on this project have been helpful. I would like to thank Dr. Hussein Moradi, who—in addition to offering his support for this project—has become a good friend and mentor. I am grateful to him for his support of this project and my professional development.

I would like to thank the National Science Foundation for their financial support during my studies. This Ph.D. dissertation was supported by the National Science Foundation Graduate Research Fellowship under Grant No. 0750758.

CHAPTER 1

INTRODUCTION

Modern wireless communications systems employ a variety of techniques for communicating effectively in many different circumstances [1, 2, 3, 4]. This dissertation provides details for a particularly promising up-and-coming technique based on merging filter bank multicarrier (FB-MC) techniques with spread spectrum techniques. We call the new technique filter bank multicarrier spread spectrum (FB-MC-SS). This chapter provides the motivation for studying FB-MC-SS followed by an outline of the rest of the dissertation. This chapter begins with an overview of single carrier techniques and their short-comings. Next, multicarrier and spread spectrum techniques are examined to overcome the identified weaknesses associated with single carrier systems. Finally, an outline of this dissertation is given which will fully describe the FB-MC-SS technique, its benefits, and its challenges.

1.1 Efficient Single Carrier Communications

Single carrier digital communications systems are among the oldest forms of wireless radio frequency (RF) communications systems. For example, Guglielmo Marconi used wireless telegraphy to communicate digital information early in the history of radio [5]. An efficient single carrier system is characterized by the transmission of a data stream centered at one frequency. This data stream may be transmitted as fast as Nyquist allows for a given bandwidth and a given signal-to-noise ratio (SNR).

A discrete-time implementation of a single carrier transmitter consists of a baseband processor followed by an RF front end. The single carrier receiver consists of a matching RF front end and baseband processor. The baseband processing required at the transmitter is a simple pulse shaping filter, $p_T[n]$. The filter output is passed to a digital-to-analog converter and upconverted to a suitable transmission frequency by the RF front end, as shown in Figure 1.1.

The receiver baseband processing consists of a matched filter, $p_R[n]$, with the correct

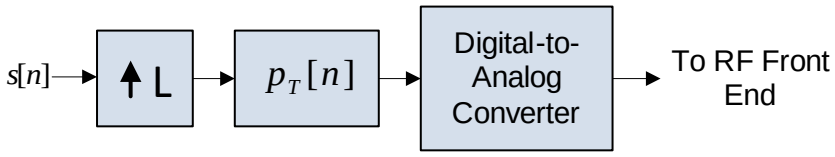

Figure 1.1. The baseband signal processing required for a single carrier transmitter is characterized by passing an impulse sequence $s[n]$ through a pulse shaping filter $p_T[n]$. This is then transformed to an analog signal that is sent to an RF front end for conversion to a suitable frequency for transmission through the wireless medium.

sampling time and carrier frequency. Following the matched filter, an equalizer can be used to correct for any distortion caused by the multipath propagation of the wireless medium. Imperfections or mismatch between high frequency oscillators used in the RF front end, analog-to-digital converters, and digital-to-analog converters can cause the received signal to be distorted. The receiver baseband processing must remove any residual carrier offset as well as lock onto and track the correct symbol timing (which may be drifting). A discrete-time digital implementation for a single carrier receiver is shown in Figure 1.2.

Single carrier systems have been well-studied in the literature; a good reference is [1]. The primary difficulties in engineering a discrete-time digital communication system are a result of the synchronization and distortion compensation requirements at the receiver. Operations required for successful synchronization are timing phase recovery, sampling frequency offset, carrier frequency offset, and channel equalization. These arise from imperfections in the RF front end and from the effects as the signals propagate through the wireless medium.

Despite their usefulness and popularity, single carrier systems have the following three disadvantages:

First, the bandwidth is inversely proportional to the speed of transmission (i.e., doubling the data rate requires doubling the bandwidth). Modern systems that require data rates of tens or hundreds of megabits per second (Mbps) or even gigabits per second (Gbps) require excessively wide bandwidths to be used. The wider bandwidth causes more distortion from the multiple paths (i.e., multipath) of the wireless medium. This requires computationally intensive equalizers to counteract the distortion.

Second, single carrier systems are extremely susceptible to interference. This interference may be caused by natural phenomena (such as lightning or solar flares) or it may be created intentionally as a malicious attack on the system (jamming). In either case, without additional protection, the system will fail.

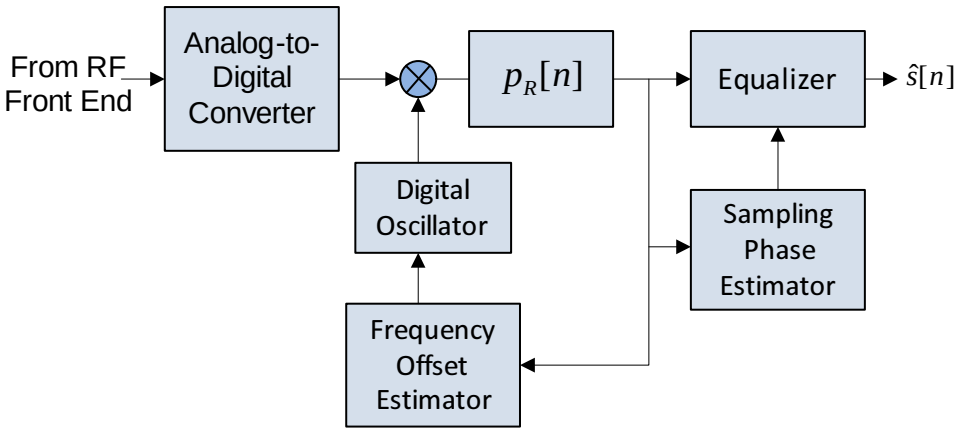

Figure 1.2. The baseband signal processing required for a single carrier receiver is more complex than that for the transmitter. It is characterized by passing the received signal through a matched filter $p_R[n]$. In addition, the carrier offset and signal timing phase must be estimated and tracked due to imperfections in the RF hardware. Likewise, an equalizer is generally needed to undo the effects of the channel.

Third, single carrier systems do not provide efficient multiple user access. These systems require either a time division multiple access (TDMA) or a frequency division multiple access (FDMA) technique in order to share the medium among multiple users. These systems reduce the bandwidth available to all users whether all users are actively using the spectrum or not.

In summary, single carrier systems have the following challenges:

- Higher data rates require unreasonably high complexity equalizers.
- Hostile or unintentional interference leads to a disruption in service.
- Multiuser systems reduce available bandwidth and/or channel access time.

To address these issues, engineers and researchers have developed alternative techniques. In the following sections, we consider two of these alternatives: multicarrier and spread spectrum communication systems.

1.2 Multicarrier Communications

To more effectively combat the effects of the channel in a way that scales to larger bandwidths, multicarrier communications were proposed [6, 7, 8, 9]. A multicarrier system is composed of an aggregated collection of narrow band signals, called the subband signals or subcarriers. Each subcarrier can be viewed as a single carrier system in its own right

operating a slower rate. An efficient implementation of the multicarrier communication concept is the celebrated orthogonal frequency division multiplexing (OFDM) technique [10]. This technique modulates the slower rate data streams onto subcarriers that are orthogonal to each other in the baseband over one symbol period. The need for complex equalization in single carrier systems is eliminated through the use of a cyclic prefix which absorbs the impulse response of the channel. The primary advantages are ISI-free reception and simplicity of implementation. The primary processing requirement consists of an Inverse Fast Fourier Transform (IFFT) at the transmitter and the corresponding forward transform, the Fast Fourier Transform (FFT), at the receiver.

Synchronization algorithms for OFDM have been well-studied in the literature [11, 12, 13, 14]. OFDM is based (not surprisingly) on orthogonal subcarriers. The subcarriers are allowed to overlap in frequency, because the orthogonality allows the different channels to be efficiently extracted at the receiver.

To preserve the orthogonality of the subcarriers, a rectangular or nearly-rectangular filter is used at the OFDM transmitter for pulse shaping. Unfortunately, this type of filter produces relatively large sidelobes on either side of the transmitted bandwidth of each subcarrier. This leads to a signal that is not well-localized in frequency. The fact that OFDM relies on the orthogonality of its subcarriers results in an extreme sensitivity to carrier frequency offset and sampling frequency offset. Both result in significant performance losses due to inter-carrier interference (ICI)—a direct result of the loss of orthogonality between subcarriers. To address these issues, alternatives to OFDM have been considered. Filter bank multicarrier (FB-MC) is one such alternative that has also been studied by various researchers [15, 16, 17, 18].

Two important advantages of FB-MC are:

1. Subcarrier signals are spectrally isolated.

   Each FB-MC subcarrier has good spectral isolation with low out-of-band leakage (resulting in an aggregate signal with low out-of-band leakage). ICI can only exist between adjacent subcarriers due to filtering instead of over multiple subcarriers as in OFDM. External interference only affects the subcarriers occupying the same band instead of leaking to many nearby subcarriers.

2. Signal orthogonality is based on filtering, not subcarrier frequency as in OFDM.

   Sensitivity to carrier frequency offset is greatly reduced due to smaller sidelobes in the pulse shaping filter. Doppler effects have a smaller impact due to filtering.

In addition, spectrum sensing can be easily and accurately performed without much additional processing.

Due to the spectrum sensing ability of the filter bank and the spectral isolation of individual subcarriers, FB-MC is a good candidate for cognitive radio applications [19]. We develop this further after a small digression to explore the benefits of spread spectrum communications.

1.3 Spread Spectrum Communications

A spread spectrum communications system is defined as a communications system that uses much more bandwidth than is strictly necessary to achieve communication [20, 21, 22, 23]. This choice provides the system with an additional gain over narrow band systems at the same data rate. This gain, called the *processing gain*, allows the signal to be detected at particularly low signal-to-noise ratios (SNRs). This is accomplished by providing the intended receiver with additional side information about the way the signal is spread over the additional bandwidth. This allows the intended receiver to despread the signal and acts a type of filter to improve the SNR while rejecting other signals that are either unspread or spread differently. The processing gain therefore provides a reasonable defense against interference (intentional or unintentional). This is one of the primary reasons spread spectrum signals are widely employed in many applications requiring communications in harsh and hostile environments.

Two popular spread spectrum systems in usage today are frequency-hopping spread spectrum (FH-SS) and direct-sequence spread spectrum (DS-SS). More recently, multicarrier spread spectrum techniques have been proposed.

FH-SS relies on the various users in a network using hopping sequences. The same symbol is transmitted over several subcarriers in succession with a differing phase. The sequence and associated phases are known to the intended receivers. The intended receivers may thus collect these signals and coherently combine them to achieve successful communication, with a benefit due to the processing gain.

DS-SS signals are spread across a wide bandwidth by sending a very fast chipping sequence. Each chip may be transmitted at a rate that is an order of magnitude or more greater than the desired symbol rate of the system. Obviously, such high speed transmission results in a much wider bandwidth. The receiver correlates the received signal with the known chipping sequence that was used at the transmitter to spread the signal to the wider bandwidth. A special technique can be used to take advantage of the multipath nature of

the wireless medium. This technique calls for the multiple received paths to be combined coherently to achieve a greater gain—this is the well-studied rake receiver [1].

Another important advantage that spread spectrum communications have over other systems is their ability to allow simultaneous mutltiuser communication in the same bandwidth at the same time. This is achieved through the use of mutually orthogonal (or quasi-orthogonal) spreading sequences that are applied to either DS-SS or FH-SS signals. Each user receives a signal that is distinguishable by correlating with the appropriate spreading sequence intended for that user. This is called code-division multiple access and has been used in cellular networks, personal area networks, and a large number of other multiuser applications.

1.4 Multicarrier Spread Spectrum Communications

More recently, a new spread spectrum technique has emerged: multicarrier spread spectrum (MC-SS) [24, 25, 26, 27, 28]. The basic idea is to transmit redundant information on multiple subcarriers with a slight phase variation on each one. Some researchers combine spreading in frequency and spreading in time to achieve something that is a cross between MC-SS and DS-SS [26]. At the receiver, each subcarrier signal can be passed through a corresponding matched filter. Many options for the combining scheme are available. One important option is to combine the outputs so that the SNR of the combined output is maximized resulting in an optimal system performance. This is referred to as maximum ratio combining (MRC).

MC-SS based on OFDM is given thorough examination in [24] and [28]. These references note that one of the primary advantages of multicarrier spread spectrum is its inherent robustness to narrow band interference. This is due to the ability of an MC-SS receiver to combine disjoint frequency bands such that bands with extremely high interference levels are ignored (or give low weights), effectively reducing their negative impact on the output SNR. Compare this to FH-SS and DS-SS where the strong interference is averaged out by an amount equal to the processing gain of the system. MC-SS is clearly more robust to narrow band and partial band interference compared to FH-SS and DS-SS.

Filter bank-based multicarrier spread spectrum technologies are explored in [26] and [27]. We focus on the technique proposed in [27] with spreading in frequency only. This technique is what we call filter bank-based MC-SS (FB-MC-SS). FB-MC-SS outperforms DS-SS and OFDM-based MC-SS in scenarios with narrow band interference [27, 29]. One key element of the improved performance is that FB-MC-SS can be designed to arbitrarily

lower the effect of out-of-band interference on each subcarrier. This means that narrow band interference stays well isolated and does not affect more than a few subcarriers. Compared with OFDM-based MC-SS where sidelobes of the matched filters receive a significant portion of the spectrum from several neighboring subcarrier bands, the superiority of FB-MC-SS becomes clear.

1.5 Overview of Applications for FB-MC-SS

One interesting application of the techniques developed in this dissertation is for radios which intelligently adapt to other signals and interferences around them (i.e., cognitive radios) [30, 31, 32]. One promise of cognitive radios is to enable a more effective utilization of the limited wireless spectrum through dynamic spectrum access (DSA). A cognitive radio network using DSA, requires a radio to attempt sensing of other users—the primary users (PUs)—of the spectrum. The PUs are usually assumed to operate in a licensed band for which they have full legal rights. The secondary users (SUs)—that is the users of the cognitive radio network—are allowed to opportunistically use the spectrum in the licensed PU band, provided SU activity has no noticeable effect on the performance of the PU network.

Cognitive radio networks require the SUs in a close geographical area to communicate so that spectrum sensing is carried out reliably and nodes may cooperate to maximize the effective usage of the wireless spectrum. One problem this poses is how to establish a control channel with these nodes prior to the spectrum sensing being complete. For this problem, we propose that the filter bank multicarrier spread spectrum technique be used as an underlay control channel (UCC), that is a channel that operates at very low power. Knowledge of the spreading gains allows the SU systems to communicate at low power with other PU signals present in the same bandwidth. In turn, as the spectrum sensing continues, those subcarriers that are identified as occupied by the PU systems can be disabled. Thus, there is a minimal interference during the warm-up of the network, and no interference once the network has converged to a stable configuration. This combination makes the FB-MC-SS modulation format ideal for this type of control channel. More details regarding this application are explored in Chapter 4.

Cognitive radio is not the only interesting application for FB-MC-SS. In fact, FB-MC-SS is useful as a general purpose spread spectrum system as well, finding a variety of applications in the same places as DS-SS and FH-SS. It is useful in any system where low probability of detection, low probability of interception, and low probability of exploitation

are desired. These are common system requirements in military and defense, search and rescue, and many other applications.

1.6 Structure of Dissertation

With this background and these applications in mind, the dissertation proceeds as follows. Chapter 2 introduces the concept of MC-SS mathematically and discusses the benefits, focusing on narrow band suppression. Following this, Chapter 3 gives the mathematical details of an FB-MC-SS system, including details that will be used later to implement synchronization algorithms for a practical receiver. Chapter 4 discusses the usage of FB-MC-SS as a control channel for cognitive radios. Chapter 5 discusses the usage of FB-MC-SS as a general purpose spread spectrum system and compares its performance to DS-SS. Chapter 6 reports on one hardware implementation, including synchronization algorithms of the FB-MC-SS system and empirical evidence of its benefits in the field. Chapter 7 concludes the dissertation and highlights the significant results and contributions made herein.

1.7 Thesis Contributions

This thesis thoroughly explores FB-MC-SS through theoretical studies, computer simulations, and system implementation on a software-defined radio (SDR) platform. While theoretical analysis provides useful insight to the system performance and simulations confirm the accuracy of our theoretical analysis, the system implementation exposes many interesting practical problems. These practical problems are then considered in the development of more theoretical studies. This combination of practical implementation of the system and theoretical analyses with simulations has led to the contributions laid out in the following two paragraphs.

The design and implementation of an FB-MC-SS system on an SDR platform, carrier and timing synchronization algorithms that suit practical implementation, as well as channel estimation and tracking algorithms. To our knowledge, this is the first practical implementation of FB-MC-SS. The results of these studies have been published in *Design and Implementation of a Cognitive Radio Control Channel* [33] and *Design and Implementation of a Multicarrier Spread Spectrum Communication System* [29]. A demonstration of the system was provided at the IEEE International Symposium on Dynamic Spectrum Access Networks (DYSPAN) [34] where it was awarded the *Best Demonstration Award* in 2012.

The implementation of FB-MC-SS and its comparison with DS-SS led us to realize that

even under additive white Gaussian noise, FB-MC-SS outperforms DS-SS. This further led to a comparative study between FB-MC-SS and DS-SS when the latter uses the optimal (and difficult to implement) rake receiver. This study is presented in Chapter 5 and reveals that the simpler FB-MC-SS implementation has a comparable or better performance than the DS-SS system with an ideal rake receiver. The result of this study resulted in the following publications: *Comparison of Direct Sequence Spread Spectrum Rake Receiver with a Maximum Ratio Combining Multicarrier Spread Spectrum Receiver* and a forth-coming journal article.

Throughout this thesis, we use the following notations. Scalars are represented in regular upper and lower case letters. Vectors are represented by boldface lower case letters. Matrices are represented by boldface upper case letters. The notation '$\mathbf{I}$' denotes the identity matrix. The matrix or vector superscripts $(\cdot)^{\mathrm{T}}$ and $(\cdot)^{\mathrm{H}}$ indicate a matrix or vector transpose and conjugate transpose (Hermitian), respectively. The superscript $(\cdot)^*$ indicates element wise complex conjugation. We use $\star$ to denote convolution.

CHAPTER 2

MULTICARRIER SPREAD SPECTRUM

Multicarrier communication systems are among the most popular in modern wireless communication design (e.g., IEEE 802.11ac and 3GPP LTE). The celebrated modulation known as orthogonal frequency division multiplexing (OFDM) is among the most popular multicarrier techniques due to its low-complexity implementation. Other multicarrier techniques exist. One such technique, filter bank multicarrier (FB-MC), has been identified as a candidate for next-generation radios [15]. One advantage of FB-MC systems is the spectral isolation of its subcarriers. In other words, the filtering on each subcarrier effectively rejects interference from nearby subcarriers very efficiently.

This chapter begins by defining traditional MC-SS systems. These systems constitute the largest amount of prior research on MC-SS technology. We summarize the theory for traditional MC-SS in Section 2.1. Then, we present the results of past researchers and identify advantages and disadvantages from their work. We address the primary advantages defined in the literature. We then discuss some of the known disadvantages. This prepares us for an exploration of an alternative MC-SS system that strengthens the known advantages of MC-SS while removing many of the disadvantages.

2.1 Traditional MC-SS Systems

As described in [15], an OFDM system may be viewed as a special case of an FB-MC-SS system with a special pulse shaping filter. We present the details of FB-MC-SS systems in Chapter 3 and draw the parallel interpretation of OFDM. In this section, we examine traditional MC-SS systems based on the OFDM-style modulation.

For a traditional MC-SS system, the transmit waveform, $x_{mc}(t)$, may be expressed as

$$x_{mc}(t) = \sum_{n=-\infty}^{\infty} s[n] \sum_{k=0}^{N-1} \gamma_k \Pi(t - nT_{FFT} - nT_{CP}) e^{j2\pi f_k (t - T_{CP} - nT_{FFT} - nT_{CP})}, \qquad (2.1)$$

where $s[n]$ is the transmit symbol, γ_k is the unit amplitude complex spreading gain for the kth subcarrier, $\Pi(t)$ is a rectangular pulse shape with the duration $T_{FFT} + T_{CP}$, and f_ks are chosen on a regular grid in frequency with spacing $1/T_{FFT}$. Each symbol can be thought of as a Discrete-Time Fourier Transform (DTFT) of window duration T_{FFT} periodically extended with a duration T_{CP} at the beginning (the cyclic prefix). This is efficiently computed in the digital domain by using the Fast Fourier Transform, copying the cyclic prefix, and passing the output through a digital-to-analog converter.

We consider a channel with a fixed impulse response. The complex baseband equivalent impulse response of the channel is given as $c_{BB}(t)$. We lump together an additive white Gaussian noise process and an interference term into $\nu(t)$—this is the noise-plus-interference process. The received signal at baseband may be expressed as

$$y_{mc}(t) = x_{mc}(t) \star c_{BB}(t) + \nu(t), \tag{2.2}$$

where $\star$ denotes linear convolution. For clarity of presentation, we ignore the noise-plus-interference term. Due to the cyclic prefix, the transient period that occurs during symbol transitions can be ignored at the receiver. The remaining portion of the received symbol appears to be the transmitted signal circularly convolved with the complex baseband impulse response of the channel. The well-known property of the DFT that circular convolution in time is equal to multiplication in frequency implies that the distortion of the channel is perfectly canceled out by applying a DFT. Each subcarrier passes through an orthogonal channel. These subcarrier channels are sufficiently narrow band so that a flat-fading approximation holds. The receive symbol on each subcarrier is distorted by the channel frequency response, denoted $C_{BB}(e^{j2\pi f})$.

The received signal can be equalized by a single tap weight per subcarrier, w_k. Then the subcarrier outputs can be combined to form an estimate of the symbol transmitted at time n, $\hat{s}[n]$. This is expressed as

$$\hat{s}[n] = \sum_{k=0}^{N-1} w_k \int_{T_{CP}+n(T_{FFT}+T_{CP})}^{(n+1)(T_{FFT}+T_{CP})} y_{mc}(t) e^{-j2\pi f_k t} dt. \tag{2.3}$$

The tap weight selection has a high degree of influence on the system performance. This is described with more detail in Section 2.3.

2.2 Other MC-SS Techniques

There are SS techniques other than MC-SS. The two most prominent techniques are direct sequence spread spectrum (DS-SS) where the spreading code is a sequence of short

duration pulses modulated by the transmit symbols and frequency hopping spread spectrum (FH-SS) where the spreading code consists of a known random hopping sequence on several subcarrier bands. This chapter is primarily concerned with what we call traditional MC-SS.

In addition to traditional MC-SS, there are other multicarrier spreading schemes than the one discussed in this thesis. These combine spreading in time and spreading in frequency. A good introduction to these is presented in [24] in the context of multicarrier code division multiple access (MC-CDMA) schemes. They are given the names MC-CDMA, multitone CDMA (MT-CDMA), and multicarrier direct sequence CDMA (MC-DS-CDMA). We present these distinct multicarrier spread spectrum techniques under the names MC-SS, MT-SS, and MC-DS-SS, respectively.

The MC-SS waveforms considered are the same as traditional MC-SS. These systems are characterized by spreading in the frequency domain only. While most systems have used the OFDM-style modulation for spreading in frequency, a notable exception is [27] which suggests using FB-MC modulation instead. We refer to this as FB-MC-SS and discuss its advantages in Section 2.4.

MT-SS waveforms use multiple subcarriers; each one applies a spreading sequence in time. The subcarriers are wideband such that the subcarrier spectra overlap significantly. According to [24], the primary advantage of these systems is to increase the length of the spreading code to accomodate a larger number of multiuser codes. In light of the subcarrier overlap, the outputs are correlated and result in lower gains in the presence of strong narrow band interference. These systems are less useful as general spread spectrum systems. For these reasons, we explore them no further.

MC-DS-SS waveforms use spreading in time and in frequency as discussed in [26, 25]. The subcarrier spectra are not allowed to overlap. Spreading in time and frequency both have benefits. Similarities are explored further in Chapter 5 of this thesis where it is shown analytically that spreading in time and frequency both provide the same performance under white noise. MC-DS-SS requires a high complexity rake receiver structure on each subcarrier to achieve optimal performance. We choose MC-SS in lieu of MC-DS-SS, because the implementation is simpler, more practical, and there is no performance degradation. For more information on the trade-offs of spreading in time and frequency, refer to Chapter 5.

2.3 Advantages of Traditional MC-SS Systems

The primary advantage of SS systems in general (e.g., DS-SS, FH-SS, and MC-SS) is the processing gain. The processing gain of any SS system is defined as the signal-to-

interference-plus-noise ratio (SINR) at the combined detector output compared to the SINR at the input to the receiver. An SS system uses side information about the spreading to achieve these gains. In MC-SS, the side information is the distinct phase rotation sequence applied to different subcarriers.

In [24], various weighting schemes are analyzed. These correspond to choosing the weights, w_k, in our system. One consideration is orthogonality restoring combining (ORC) also known as zero-forcing (ZF). It is noted that ZF combining leads to noise amplification on low-power subcarriers. This leads to a suboptimal bit error rate (BER) performance. Equal gain combining (EGC) weights all subcarrier outputs equally. This simple scheme does not amplify the noise very much, but it is shown to be suboptimal, too. A scheme denoted maximum ratio combining (MRC) can be used to obtain an optimal estimate. The MRC weights the subcarrier outputs in a way that after combining, the SINR is maximized. For more details. It is shown that this scheme is optimal in the case of a single user.

The MRC weights are chosen to be proportional to the measured SINR on each subcarrier output with the constraint that the output is an unbiased estimate of the symbol. This maximizes the SINR at the output of the combiner from (2.3). It is intuitive that weighting the outputs in this manner, any signal that is narrow band in nature will only affect a small number of subcarrier outputs. These weights will be lowered, while the higher SINR outputs will be given higher weights. This results in a system that adapts to suppress narrow band interference.

2.4 Improving Traditional MC-SS Systems

OFDM waveforms are more susceptible to carrier frequency offsets (CFOs) and Doppler shifts [35, 11, 36, 37]. A CFO causes an equal phase rotation on each subcarrier. A Doppler shift results in a different phase rotation on each subcarrier. Both result in a loss of orthogonality of all subcarriers. Compared to an equivalent single carrier system, the CFO results in a lower BER performance. Traditional MC-SS is based on OFDM waveforms. Therefore, it suffers from the same problems. In [35], it is shown that FB-MC-SS waveforms are more robust to CFO and Doppler.

OFDM waveforms use a rectangular pulse shape. This pulse shape has a frequency response equal to a sinc function. This function has high side lobes adjacent to the main lobe, and these decrease slowly across frequency. This results in spectral leakage. In other words, the narrow band suppression that is usually touted as one of the primary advantages of MC-SS waveforms is lower than it otherwise could be if nonoverlapping subcarriers were

used instead.

This is one of the primiary advantages of FB-MC-SS. It was suggested as a candidate for MC-SS waveforms in [27] with nonoverlapping filters used for each subcarrier signal where it was shown that such a waveform has a robust performance in the presence of partial and narrow band interference. It is shown in [27] that FB-MC-SS waveforms outperform DS-SS and other MC-SS waveforms in terms of bit error rate (BER) due to the locality of their interference. We derive analytical expressions for the SINR performance of DS-SS and the proposed FB-MC-SS system in Chapter 5 of this thesis. In FB-MC-SS systems, the partial or narrow band interference is limited to only those subcarriers that coincide in frequency with the interfering signal with very low leakage interfering with the adjacent subcarriers. Thus, these adjacent subcarriers maintain a high SINR that contributes a higher quality signal for the detector. We confirmed the results of [27] empirically in [29] by measuring the BER of a practical system.

2.5 Evidence of FB-MC-SS Performance

Before diving into the details of FB-MC-SS in the subsequent chapters, we motivate the work presented in this thesis by presenting experimental evidence of the performance benefits of MC-SS (and FB-MC-SS in particular) compared with a DS-SS system. The two spread spectrum communication systems were implemented: one for DS-SS and one for FB-MC-SS. Both systems were implemented on the same software-defined radio (SDR) platform. This means that they used the same RF front end and analog/digital circuitry with the same strengths, weaknesses, and defects. A controlled level of interference was introduced in an RF isolation chamber, and the bit error rate (BER) was measured.

A description of the experimental setup follows. The RF front end was configured to operate at a center frequency of 2.48 GHz. The experiment occurred in an RF isolation chamber retrofitted with RF and office equipment, chairs, computers, etc. The RF isolation chamber isolates the system from other RF signals to maintain the same interference conditions for both systems. The receive antenna was connected to a power splitter with half the power going to the system and the other half going to a spectrum analyzer; see Figure 2.1 and Figure 2.2 for the spectrum measurements. The antenna locations were adjusted until they were reasonably far apart and a frequency selective (multipath) channel was observed on the spectrum analyzer. Then, the antennas remained motionless while the experiments were executed. All experiments were executed under identical layout.

This interference was kept at a constant power spectral density (PSD) for both systems.

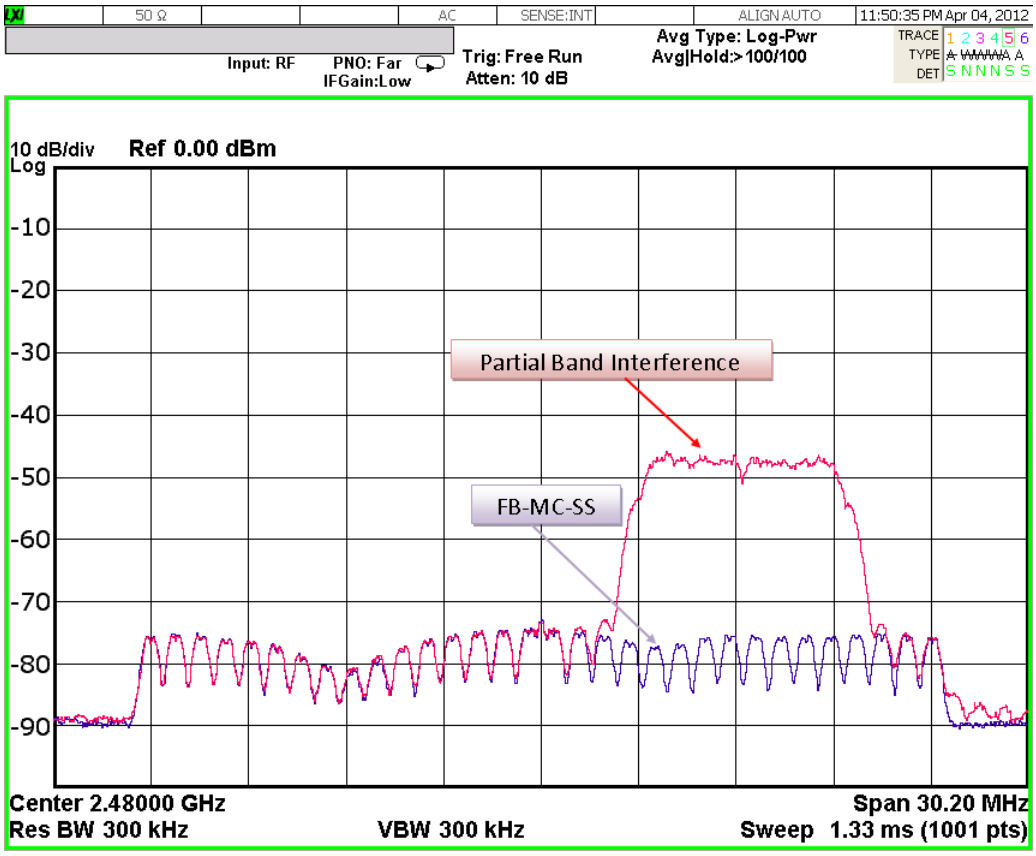

Figure 2.1. FB-MC-SS received signal spectrum with partial band interference present.

The systems were operating in an RF isolation chamber to remove uncertainty caused by the time variation of the wireless channel. The precisely controlled interference signal was received with a PSD 30 dB higher than the received PSD for the DS-SS and FB-MC-SS systems. Figures 2.1 and 2.2 show the received signal and received interference spectrum for two different experiments. These were measured for the FB-MC-SS system in the presence of the high power interference signal generated by an Agilent RF signal generator, E4438C. Figure 2.1 shows the signal with a partial band interference, and Figure 2.2 shows the sliding wideband interference covering half of the FB-MC-SS bandwidth. The interference waveform shown in Figure 2.2 was slid through the SS signals to obtain the BER measurements in Figure 2.3. Both the DS-SS and FB-MC-SS systems were adjusted so that the received PSD was the same. Under these similar conditions—equal received signal PSD and interference PSD—the FB-MC-SS system significantly outperforms the DS-SS system.

Two experiments were executed to verify the benefits of the FB-MC-SS system. First, a partial-band jammer was introduced while the system was operating. The power spectrum

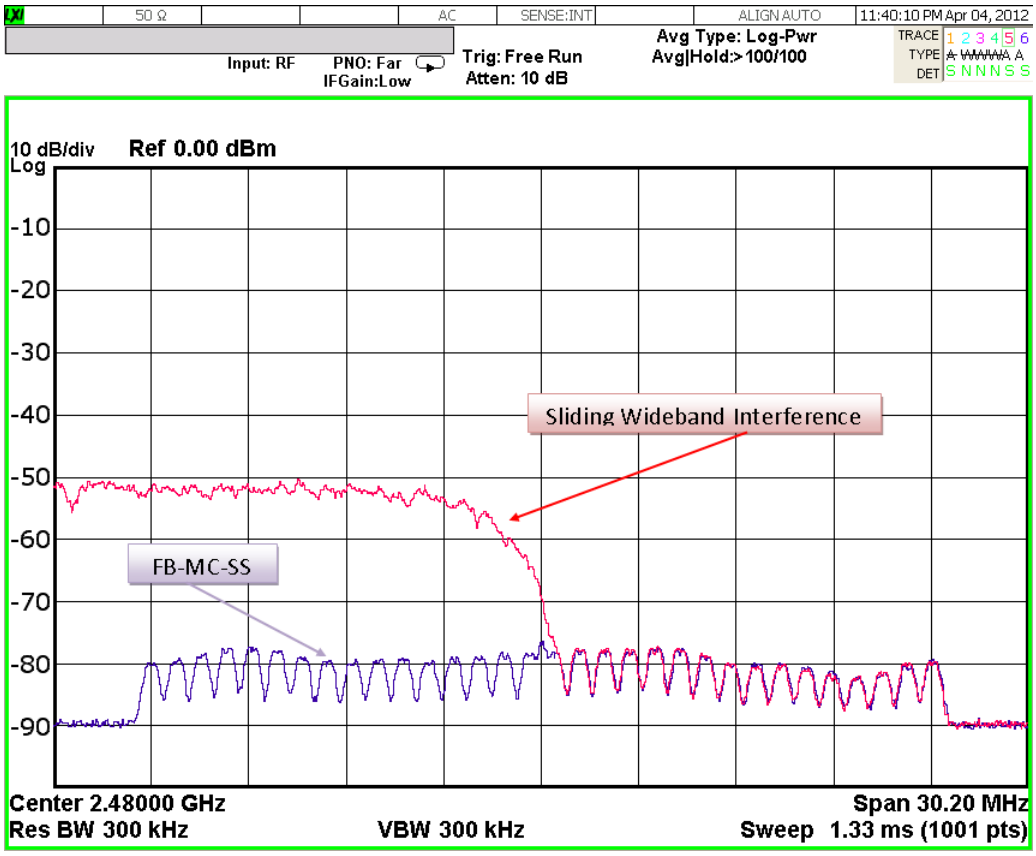

Figure 2.2. FB-MC-SS received signal spectrum with sliding wide band interference present and covering half of the available spectrum.

of the signal and the interference can be seen in Figure 2.1. Two traces are visible. One is the system operating without interference. This trace was held, and then the interference was introduced before taking this screen shot. The constellation diagrams of both the FB-MC-SS and DS-SS systems are plotted in Figure 2.4. Increasing the power of this partial band interference has a negligible effect on the constellation of the FB-MC-SS system, while increasing it to a point that is higher than the processing gain of the DS-SS system results in such a noisy constellation that reliable communication is impossible. The bit error rate (BER) observed by the DS-SS receiver at the time of the screen shot was 0.480 averaged over 1000 frames, each one containing 940 bytes of data. At the same time, the FB-MC-SS system using MRC maintained a reliable communication link with no bit errors. No coding was applied to either system.

For the second experiment, an interfering signal was generated with wider bandwidth than the system. The signal was then swept through the operating band. Figure 2.2 shows

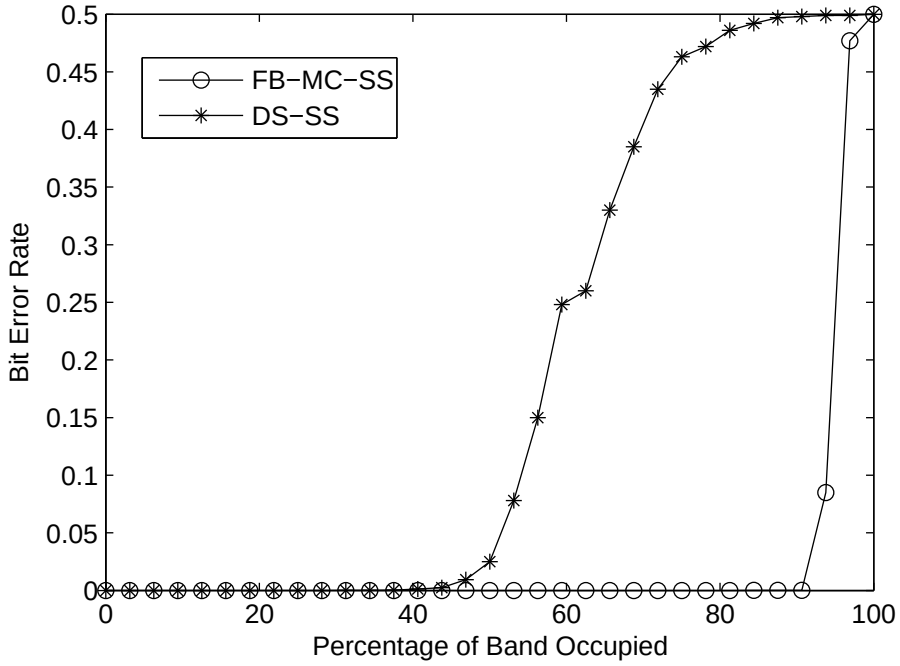

Figure 2.3. Measured BER vs. percentage of band occupied (DS-SS and FB-MC-SS)

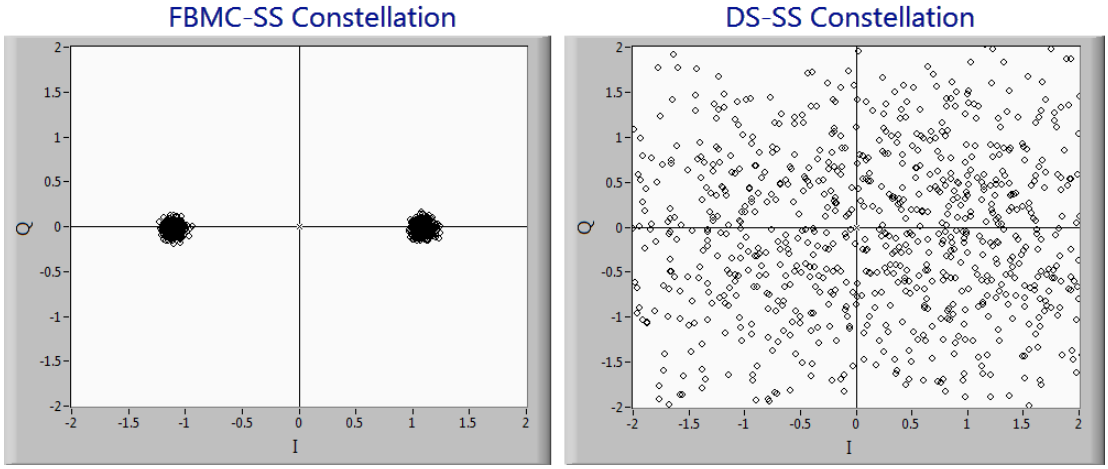

Figure 2.4. Measured constellation diagram with partial-band interference present.

the spectrum when the interference covered half of the band. At this point, the DS-SS system observed a BER of 0.035 while the FB-MC-SS system was error free. The measured constellation diagrams of both systems are shown in Figure 2.5.

Figure 2.3 plots the BER as a function of the percentage of the band occupied by the interfering signal for the FB-MC-SS and the DS-SS system. Under these conditions, we can

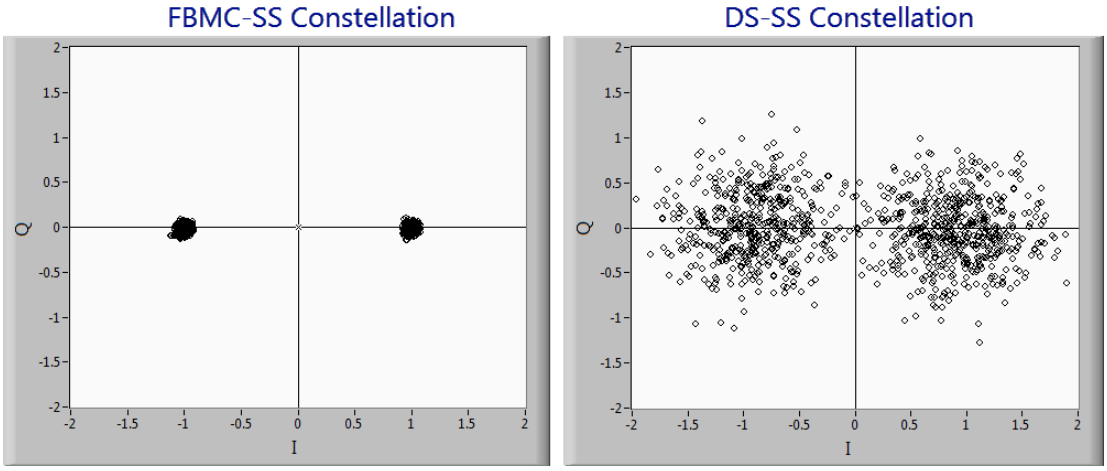

Figure 2.5. Measured constellation diagram with sliding wide-band interference covering half of the available bandwidth.

see that the DS-SS system starts to fail when about half of the band is occupied, while the FB-MC-SS system maintains a robust communication link until all but a few subcarriers are left unoccupied.

A key observation is that the DS-SS system averages out the interfering signals. Therefore, high powered interference (greater than the processing gain) anywhere in the bandwidth can reduce the system effectiveness, whereas the FB-MC-SS system can ignore selective portions of the bandwidth that are identified as interfering. This is accomplished automatically through the MRC mechanism.

Figure 2.3 plots the time averaged BER of a DS-SS transceiver and an FB-MC-SS transceiver as a function of the percentage of the band occupied by the interfering signal. These results indicate the robust performance of the FB-MC-SS system in terms of partial-band interference. When a sufficiently high number of subcarriers are not experiencing a strong interference, the BER remains low—yielding a high quality of service. The system only fails as the interference bandwidth approaches the entire band. On the other hand, the DS-SS system experiences a high degree of failure when approximately half of the band is shared between the interference and the signal. Constellation diagrams of the received signals are presented in Figures 2.4 and 2.5. These reveal the SNR performance for DS-SS and FB-MC-SS in the presence of the interference signals shown in Figures 2.1 and 2.2, respectively. Clearly, FB-MC-SS outperforms DS-SS in terms of partial band interference. For DS-SS to obtain better performance, the receiver complexity increases significantly [23].

More details about the theory of FB-MC-SS with nonoverlapping subcarriers are ex-

plained in Chapter 3. A practical implementation based on this theory is presented in Chapter 6.

2.6 Summary

In summary, the performance of spread spectrum waveforms is characterized by their processing gains. Higher processing gains lead to more robust performance in the presence of other (interfering) signals. Thus, DS-SS and MC-SS both exhibit a partial band interference suppression effect. MC-SS suppresses the narrow band interference to a greater degree because the partial band interference only interferes with some of the signal chips. This is possible because each chip in MC-SS is spread to a distinct frequency, whereas for DS-SS, each chip is spread across the entire band, suffering a similar amount of interfference. In MC-SS, the portions suffering from a high degree of interference can be selectively removed (or given weights that are extremely small). Among multicarrier waveforms that might be employed for MC-SS, the FB-MC-SS waveform based on filtered multitone (FMT) has nonoverlapping subcarriers with very good spectral isolation. This means that the interference affects a minimal number of subcarriers and the others achieve their full potential in terms of SINR performance. This leads to higher quality of service for FB-MC-SS systems. Contrast this with the popular OFDM-style modulation where adjacent subcarriers overlap completely, and the spectral isolation of each is very poor. While MC-SS of any form proves to be better than simple DS-SS systems at partial band suppression, FB-MC-SS significantly outperforms DS-SS in practical scenarios. This was illustrated by the experimental evidence provided in Section 2.5. With this motivation, Chapter 3 discusses the details and theory of operation for the FB-MC-SS system proposed and implemented as part of this thesis. Chapter 5 extends this study and compares FB-MC-SS with DS-SS analytically when noise PSD is uniform over the band of transmission. This study shows that FB-MC-SS has a comparable or better performance than DS-SS when the latter uses the optimal rake receiver.

CHAPTER 3

FILTER BANK MULTICARRIER SPREAD SPECTRUM

Before proceeding into the details of the proposed FB-MC-SS system, we present block diagrams of the proposed transceiver. The role and significance of various sub-blocks in the system are discussed without getting ourselves involved with the mathematical details. In doing this, we will be able to justify our choice of FMT for spreading our FB-MC-SS signal in frequency as opposed to other multicarrier modulation formats. We then proceed with the full mathematical details of the system.

In the proposed system, the transmitter is effectively a synthesis filter bank. We call this the transmitter filter bank (TxFB). The input to the TxFB is the sequence of information bits that we wish to transmit. The TxFB output is upconverted to an RF carrier frequency for transmission. As shown in the next section, the TxFB is characterized by an impulse response that we represent by $g(t)$ followed by an RF modulator. This simplistic model of the transmitter is presented in Figure 3.1. These are the same signal processing blocks required for an equivalent single carrier system.

Figure 3.2 presents a block diagram of the receiver of the FMT-based spread spectrum system. After demodulating the received RF signal, the baseband processor at the receiver performs one matched filter for each subcarrier frequency occupied by the transmitter pulse shaping filter $g(t)$. These symbol streams each carry redundant information. The streams are combined in an optimal way that maximizes the SNR of the combined output. This results in a special kind of matched filter for the overall system—one that adapts itself to

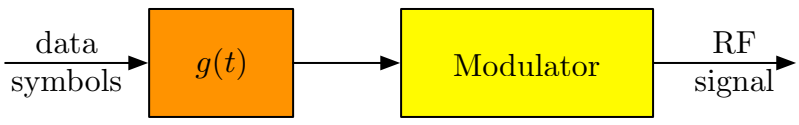

Figure 3.1. Block diagram of transmitter in an FB-MC-SS system.

fit the channel conditions. We call this the *adaptive matched filter*.

It is also possible to use a single-carrier technique with a filter matched to $g(t)$. We call this the *simple matched filter*. In the absence of channel distortion and the presence of white noise, these two matched filters are equivalent. In this case, they lead to the system output shown in Section 3.2.1. The simple matched filter output is a sequence of high amplitude pulses that can be clearly identified even when the FB-MC-SS signal is at or below some noise level. These pulses remain in the presence of channel distortion. They carry sufficient information for timing and carrier acquisition and tracking. Implementation algorithms that make use of these FB-MC-SS signal properties for timing recovery, carrier recovery, and tracking algorithms are introduced in this chapter. More implementation details of these algorithms and other alternatives are provided in Chapter 6.

The output of the simple matched filter (represented by the box labeled "matched filter" in the figure) is used for synchronization, and the adaptive matched filter is used for data detection. To implement the adaptive matched filter, the output signal from the demodulator block is passed to an analysis polyphase filter bank (APFB) along with the recovered timing information from the simple matched filter. The APFB extracts the received signal of each subcarrier and samples them at the optimal timing phase. The usage of an APFB is what makes the adaptive filter practical and allows us to obtain the robust performance that makes FB-MC-SS desirable.

The output samples from the APFB are passed to a channel estimator. The channel estimator provides information about the complex channel gain and the power of noise plus interference at each subcarrier frequency. The last block of the receiver uses this information to perform maximum ratio combining (MRC) prior to detection of the data symbol. The MRC maximizes the SNR by calculating a coherent weighted average of the detected data symbols from each subcarrier with weights proportional to the subcarrier SNR. Intuitively, the higher power, less noisy outputs are given higher weights and the lower power, more noisy outputs are given lower weights under the constraint that the weights should sum to one.

At this point, we wish to make a few comments with regard to the choice of FMT in our design. We note that in the context of bandwidth efficient FB-MC data transmission, FMT is the least efficient method. FB-MC systems that are based on cosine modulated filter banks (CMFB) and offset-QAM (OQAM) modulation allow more subcarriers per unit of bandwidth. This concept is depicted in Figure 3.3.

Clearly, if independent symbols are to be transmitted over different subcarriers, CMFB

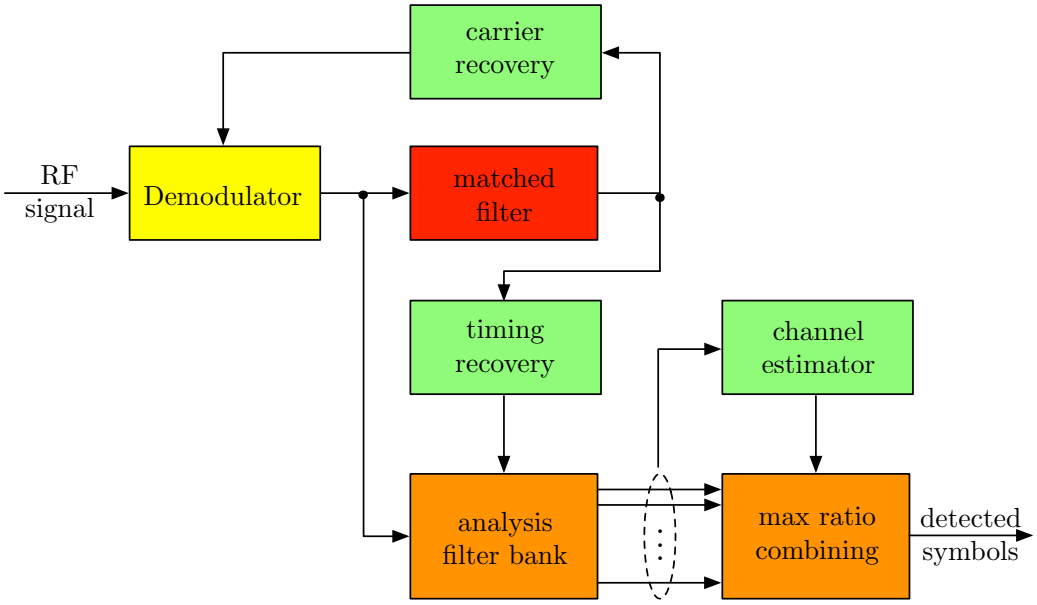

Figure 3.2. Block diagram of the receiver for the proposed filter bank MC-SS system.

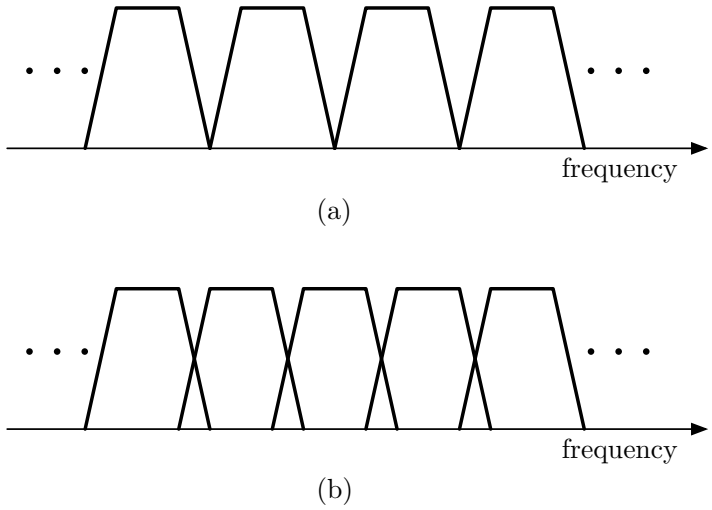

Figure 3.3. Bandwidth efficiency comparison of FMT against more bandwidth efficient multicarrier schemes. (a) FMT; (b) CMFB/OQAM.

or OQAM-based FBMC will result in higher bit rates, [15]. However, one should note that the goal here is not to increase the number of transmitted bits per unit of bandwidth. The goal of a spread spectrum system in general, and the proposed FMT-based system in particular, is to spread each information symbol over a bandwidth that is much wider than required by the data rate. This allows the transmit power to be comparable to or lower

than the noise level and still achieve robust communication.

The parameter that characterizes the level of robustness achieved by a particular form of spreading is the *processing gain*, defined as the ratio of the SNR after processing to the SNR prior to processing by the receiver. Hence, as long as the same processing gain is established through different FB-MC-SS systems, it becomes immaterial to say which system is better for spreading purposes. In Appendix A, we have evaluated the processing gain of the FMT-based spread spectrum system. The processing gain is found to be identical with other MC-SS systems that use the more closely packed subcarrier transmission schemes. In light of this fact, we have chosen FMT. As shown throughout this thesis, this particular choice offers simplicity in various aspects of the system implementation.

3.1 Transmitter Design

Figure 3.4 presents a block diagram of the transmitter in an FB-MC-SS system. In such a system, the concept of spreading a signal to a wider bandwidth may be accomplished in a number of ways. From a signal processing perspective, the spreading may either be accomplished in time (by transmitting some chipping sequence or spreading code modulated by each symbol) or in frequency (by transmitting the same symbol on different subcarriers with a spreading code). In addition, we may employ any combination of these two techniques.

In this thesis, we limit our design to the case where spreading is only across frequency and each data symbol is spread over all active subcarriers. The input signal in Figure 3.4 is an impulse train of data symbols $s[n]$ at the spacing of T seconds. Mathematically, this is expressed as

$$s(t) = \sum_{n} s[n]\delta(t - nT). \tag{3.1}$$

In this chapter, we refer to $h(t)$ as the *prototype filter*, following the filter bank literature [38]. The prototype filter, $h(t)$, is a common pulse shaping filter, identical for all subcarriers. Ideally, $h(t)$ should be chosen to be a well-designed lowpass filter. Accordingly, one may note that the set of filters $\gamma_0 h(t)$ through $\gamma_{N-1} h(t)$ are to band-limit the stream of data symbols and apply the spreading gain factors γ_0 through γ_{N-1}. These filters are followed by a set of modulators that shift the spectra of these band-limited signals to the set of subcarrier frequencies f_0 through f_{N-1}. This modulation results in redundant data being spread across a broad band. We also note that Figure 3.4 is an expanded version of the first block in Figure 3.1, and as demonstrated in Figure 3.1, the output $x(t)$ has to be

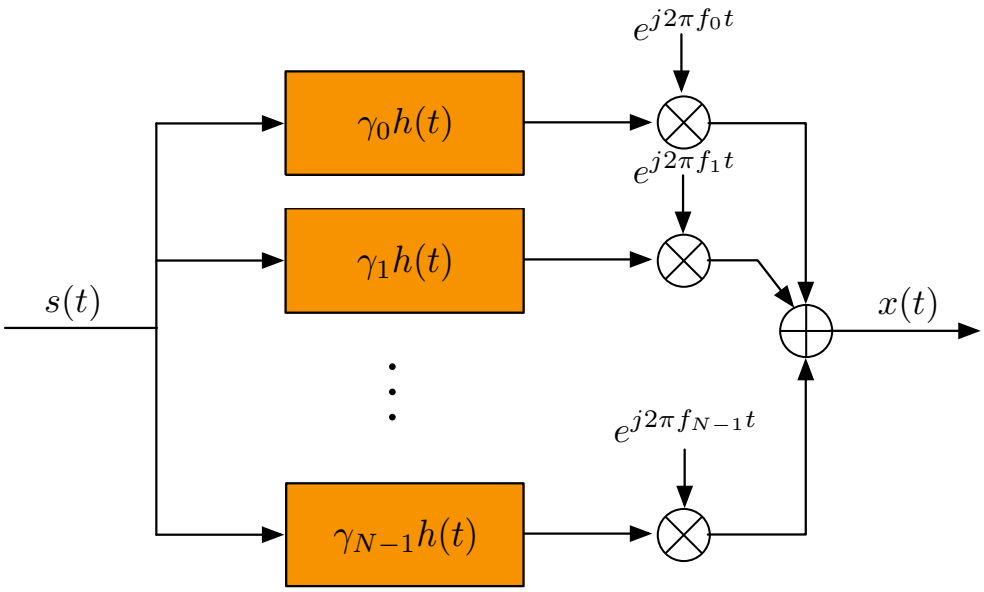

Figure 3.4. Block diagram of a transmitter for MC-SS system.

up-converted to an RF band before transmission. Here, we have ignored the modulator block for brevity.

A few comments on the choice of $h(t)$ are in order. As it will become clear later, $h(t)$ should be a square-root Nyquist filter, meaning that $h(t) \star h^*(-t)$ should be a Nyquist filter with regular zero-crossings at integer multiples of T. The notation $\star$ denotes convolution and the superscript $*$ means conjugation. It is common for $h(t)$ to be designed as a real-valued even function of time so that $h^*(t) = h(t) = h(-t)$. We assume this to be the case in the design adopted in this thesis.

Using (3.1), the output of the transmitter is obtained as

$$x(t) = \sum_{n} \sum_{k=0}^{N-1} \gamma_k s[n] h(t - nT) e^{j2\pi f_k t} \tag{3.2}$$

with the subcarrier frequencies f_k selected such that $f_k T$ is an integer for $k = 0, 1, \cdots, N-1$. As a result of this choice, $e^{j2\pi f_k t} = e^{j2\pi f_k (t-nT)}$ for integer choices of n. This property allows us to rearrange (3.2) as follows,

$$x(t) = \sum_{n} s[n] g(t - nT) \tag{3.3}$$

where

$$g(t) = h(t) p(t) \tag{3.4}$$

and

$$p(t) = \sum_{k=0}^{N-1} \gamma_k e^{j2\pi f_k t}. \tag{3.5}$$

Note that $g(t)$ is factored as a multiplication of the prototype filter $h(t)$ and another function of time, $p(t)$, that is determined by the spreading gains γ_k and the subcarrier frequencies f_k.

Equation (3.3) has the following interpretation. The MC-SS signal $x(t)$ is obtained by passing the data stream, $s[n]$, through the pulse shaping filter $g(t)$. Varying the choice of $g(t)$—determined by the prototype filter $h(t)$, the spreading sequence γ_k, and the subcarrier frequencies f_k—result in various forms of MC-SS systems with different properties. When $h(t)$ is a rectangular pulse with a width of $T = T_{\text{FFT}} + T_{\text{CP}}$, that is equal to the length of the FFT window T_{FFT} plus the length of a cyclic prefix T_{CP} (as in an OFDM system) and the subcarrier frequencies f_k are at the regular interval $1/T_{\text{FFT}}$, then $x(t)$ will be an OFDM-based MC-SS signal. On the other hand, if $h(t)$ is the impulse response of a square-root raised-cosine filter with a roll-off factor α and a symbol rate $1/T$, and the frequencies f_k are chose on a regular interval $(1+\alpha)/T$, then $x(t)$ will be an FMT-based spread spectrum signal, i.e., the FB-MC-SS design that we develop in this chapter. Other choices of $h(t)$ and f_k that lead to other types of FB-MC-SS are also possible (e.g., CMFB and OQAM-based systems); see [39] for a review of various forms of FB-MC systems.

As noted earlier, the choice of FMT for multicarrier modulation is to take advantage of its simplicity. This, in turn, results in a simple and robust FB-MC-SS system. In our design, we choose N to be an even integer, set the roll-off factor $\alpha = 1$, and choose the subcarrier frequencies f_k at the positions $\pm\frac{1}{T}$, $\pm\frac{3}{T}$, $\cdots$, $\pm\frac{N-1}{T}$. More specifically, we let $f_0 = -\frac{N-1}{T}$, $f_1 = -\frac{N-3}{T}$, $\cdots$, $f_{N-1} = \frac{N-1}{T}$. The spreading gain factors γ_k are chosen as

$$\gamma_k = e^{j\theta_k}, \quad \text{for } k = 0, 1, \cdots, N-1. \tag{3.6}$$

where the angles θ_k are a set of phase angles that may be chosen to improve on the properties of the FB-MC-SS waveform. Among various choices, $\theta_k = \pi k^2/N$ is an interesting one. It belongs to the class of polyphase codes [40]. It leads to a transmit signal $x(t)$ with a moderately low peak-to-average-power ratio (PAPR)—a consideration that one may wish to take note of in designing the pulse shape $g(t)$. For later reference, we note that, in accordance with (3.6), the following identities hold for all choices of θ_k:

$$|\gamma_k|^2 = 1, \quad \text{for } k = 0, 1, \cdots, N-1. \tag{3.7}$$

Although the formulations given above are in terms of continuous-time signals and filters, practical generation of the transmit waveform is conveniently performed in discrete-time using efficient signal processing blocks. More specifically, the transmit waveform may be generated using the structure presented in Figure 3.5 where $\uparrow L$ denotes an L-fold expander and $g[n]$ is the corresponding discrete-time version of $g(t)$.

In some applications, on-demand activation and deactivation of subcarriers at the transmitter is desired (e.g., dynamic spectrum access). In this case, the system is efficiently implemented according to a polyphase synthesis filter bank structure. Otherwise, a single polyphase filter suffices. See [4, 38] for details.

3.2 Receiver Design

In this section, we discuss the mathematical basis for the implementation of the various blocks in the receiver structure that was introduced earlier in Figure 3.2. This provides a solid foundation for synchronization algorithms and circuits to be proposed later. Converting these proposed mathematical formulations into an efficient FPGA hardware implementation is discussed in Chapter 6.

3.2.1 Preliminaries

Clearly, any carrier and timing recovery method should take advantage of the properties of the modulation method that has been used to construct the transmitted signal. We thus begin our discussion here by exploring some of the properties of the pulse shape $g(t)$.

Consider the case where the channel is ideal and demodulation is performed perfectly, hence the demodulator output is the transmit baseband signal $x(t)$ given by (3.3). After passing $x(t)$ through a filter matched to the transmit pulse shape $g(t)$—that is, the simple matched filter—the overall impulse response of the system is obtained as

$$\eta(t) = g(t) \star g^*(-t). \tag{3.8}$$

Using (3.4) and (3.5) in (3.8) and noting that by design $h(-t) = h(t)$, we obtain

$$\eta(t) = \left(\sum_{k=0}^{N-1} \gamma_k h(t) e^{j2\pi f_k t} \right) \star \left(\sum_{l=0}^{N-1} \gamma_l^* h(t) e^{j2\pi f_l t} \right). \tag{3.9}$$

Next, we note that $h(t)e^{j2\pi f_k t}$ and $h(t)e^{j2\pi f_l t}$ may be thought of as a pair of modulated filters. By design, such a pair of filters either has a common band (when $f_k = f_l$) or

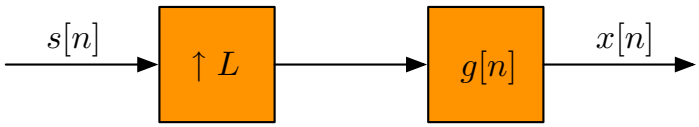

Figure 3.5. Digital implementation of transmitter in a filter bank MC-SS system.

covers nonoverlapping bands. In the latter case, $h(t)e^{j2\pi f_k t} \star h(t)e^{j2\pi f_l t} = 0$, and this term contributes nothing to the sum. Hence, (3.9) reduces to

$$\eta(t) = \sum_{k=0}^{N-1} |\gamma_k|^2 \left(h(t)e^{j2\pi f_k t} \star h(t)e^{j2\pi f_k t} \right). \tag{3.10}$$

Straightforward manipulations of (3.10) and recalling that $|\gamma_k| = 1$ from (3.7) lead to

$$\eta(t) = \beta(t)\rho(t) \tag{3.11}$$

where $\rho(t) = h(t) \star h(t)$, by design, is a Nyquist pulse whose peak appears at $t = 0$, and

$$\beta(t) = \sum_{k=0}^{N-1} e^{j2\pi f_k t}. \tag{3.12}$$

One may notice that $\beta(t)$ is the summation of N complex sine-waves all of the amplitude unity. Hence, the Fourier transform of $\beta(t)$ is effectively a sampled version of a rectangular pulse, as demonstrated in Figure 3.6. Note that the samples in the frequency domain are spaced by $2/T$. This implies that $\beta(t)$ is a train of sinc pulses spaced in time at the interval $T/2$. At $t = 0$ and non-integer multiples of T, all the components of $\beta(t)$ have zero phase. Therefore, they add up to the value N. At the points where t is an odd multiple of $T/2$, all the components of $\beta(t)$ have phase of π. Therefore, they add up to the value of $-N$. An example of $\beta(t)$ for the case where $N = 16$ is presented in Figure 3.7. As N increases and approaches infinity, the train of sinc pulses approaches an impulse train, and thus $\eta(t)$ will approach a waveform consisting of a number of impulses (narrow and tall pulses, when N is finite but large) whose magnitudes are the samples (or the negated samples) of the Nyquist pulse $\rho(t)$. Interestingly, when the roll-off factor $\alpha = 1$, one finds that there are only three non-zero samples of $\rho(t)$, with values of -0.5, 1, and -0.5 at the positions $t = -T/2$, 0, and $T/2$, respectively. From this, we see that when $\alpha = 1$ and $N \to \infty$,

$$\eta(t) = -0.5\delta(t + T/2) + \delta(t) - 0.5\delta(t - T/2). \tag{3.13}$$

This result becomes a reasonable approximation when N is finite but sufficiently large. Now, we define a more precise expression,

$$\beta_0(t) = \beta(t)\Pi\left(\frac{t}{T_0}\right) \tag{3.14}$$

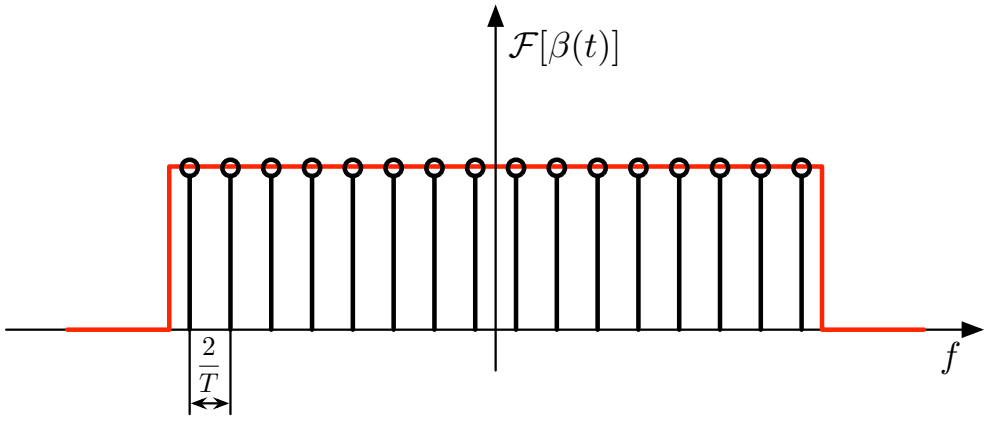

Figure 3.6. Demonstration of the Fourier transform of $\beta(t)$.

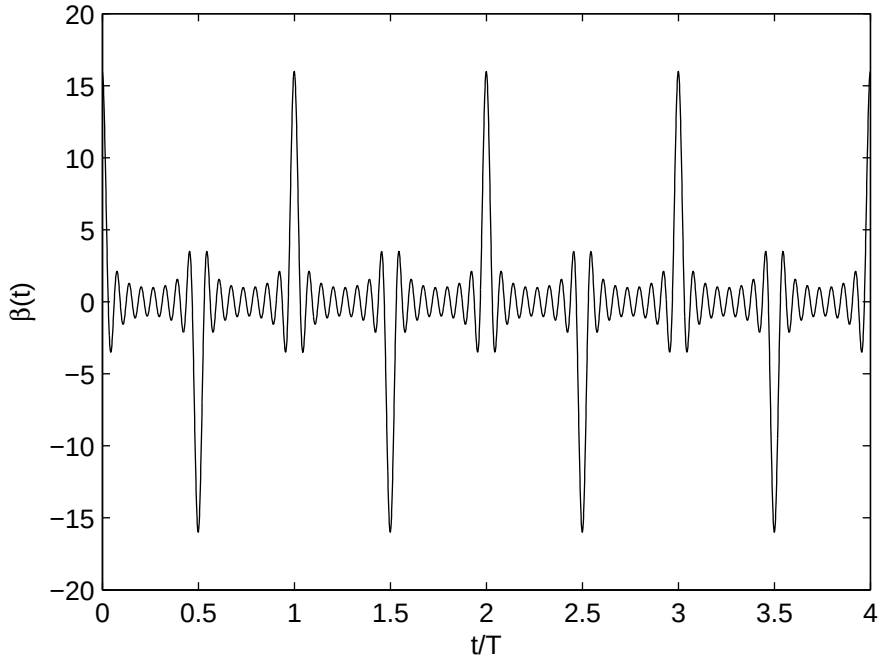

Figure 3.7. An example of $\beta(t)$.

where $\Pi(\frac{t}{T_0})$ denotes a rectangular pulse with a properly chosen width of T_0 and, accordingly, we write (3.13) as

$$\eta(t) = -0.5\beta_0(t + T/2) + \beta_0(t) - 0.5\beta_0(t - T/2). \tag{3.15}$$

Equation (3.15) is the system response between the input $s(t)$ and the output of the matched filter $g^*(-t)$. Hence, using (3.1), one finds that the output of the matched filter is given by

$$z(t) = \sum_n s[n] \left(-0.5\beta_0 \left(t + \frac{T}{2} - nT \right) + \beta_0(t - nT) - 0.5\beta_0 \left(t - \frac{T}{2} - nT \right) \right) + \nu_0(t). \tag{3.16}$$

Figure 3.8 presents a typical signal at the matched filter output where, for clarity of presentation, $\beta_0(t)$ is replaced by a unit impulse. Note that at the position nT, an impulse with amplitude $s[n]$ appears. At mid-point $(n + 0.5)T$, $z(t)$ is zero, if $s[n] \neq s[n + 1]$, or is an impulse with amplitude $-s[n]$, if $s[n] = s[n + 1]$. This interesting property has many practical uses that will be discussed later.

Next, we discuss the effects of nonidealities in the channel.

3.2.1.1 Impact of Carrier Frequency Offset

Assume that the channel is ideal, but there exists a carrier frequency offset Δf_c between the transmitter and receiver. Then, (3.9) will become

$$\eta(t) = \left(\sum_{k=0}^{N-1} \gamma_k h(t) e^{j2\pi(f_k + \Delta f_c)t} \right) \star \left(\sum_{l=0}^{N-1} \gamma_l^* h(t) e^{j2\pi f_l t} \right). \tag{3.17}$$

For the case where $0 < \Delta f_c < 2/T$, subcarrier filters at bands k and $k + 1$ will overlap with the transmitted signal from the kth band. Noting this, from (3.17), we obtain

$$\eta(t) = \sum_{k=0}^{N-1} \left(h(t) e^{j2\pi(f_k + \Delta f_c)t} \star h(t) e^{j2\pi f_k t} \right) + \sum_{k=0}^{N-2} \gamma_k \gamma_{k+1}^* \left(h(t) e^{j2\pi(f_k + \Delta f_c)t} \star h(t) e^{j2\pi(f_k + \frac{2}{T})t} \right). \tag{3.18}$$

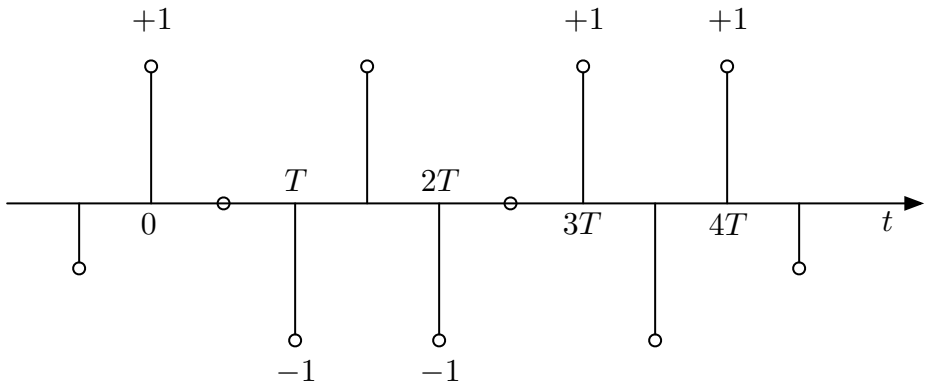

Figure 3.8. A typical signal exemplifying $z(t)$. In this example, the transmitted symbol sequence is $s[n] = \{+1, -1, -1, +1, +1\}$.

Straightforward manipulation of the terms in (3.18) leads to

$$\eta(t) = \beta(t)\left(h(t)e^{j2\pi\Delta f_c t} \star h(t)\right) + \kappa(t)\left(h(t)e^{j2\pi(\Delta f_c - \frac{2}{T})t} \star h(t)\right) \tag{3.19}$$

where $\beta(t)$ is given by (3.12) and

$$\kappa(t) = e^{j(4\pi/T)t}(\beta(t) - e^{j2\pi f_0 t}). \tag{3.20}$$

To simplify (3.19), we note that for typical values of N, the term $e^{j2\pi f_0 t}$ in (3.20) compared to $\beta(t)$ is negligible, and thus may be ignored. In addition, $\beta(t)$ is significant for values of t in the vicinity near integer multiples of $T/2$. For these choices of t, $e^{j(4\pi/T)t} \approx 1$. Considering these approximations for sufficiently large N, (3.19) may be replaced by

$$\eta(t) = \beta(t)\varrho(t) \tag{3.21}$$

where

$$\varrho(t) = h(t)e^{j2\pi\Delta f_c t} \star h(t) + h(t)e^{j2\pi(\Delta f_c - \frac{2}{T})t} \star h(t). \tag{3.22}$$

Clearly, for $\Delta f_c = 0$, $\varrho(t)$ reduces to $\rho(t)$. As Δf_c deviates from zero, $\varrho(t)$ deviates from $\rho(t)$. However, some special features of it that can be used for synchronization purposes still remain nearly the same. In particular, $|\varrho(t)|$ preserves the shape of $|\rho(t)|$ to a great extent and its amplitude reduces only slightly over a relatively wide range of Δf_c. To demonstrate this, a set of plots of $|\varrho(t)|$ for different choices of Δf_c is presented in Figure 3.9.

3.2.1.2 Impact of Channel Impulse Response

When the channel is nonideal, i.e., $c(t) \neq \delta(t)$, $\eta(t)$ of (3.13) becomes

$$\eta(t) = -0.5c'(t + T/2) + c'(t) - 0.5c'(t - T/2) \tag{3.23}$$

where

$$c'(t) = c(t) \star \beta_0(t). \tag{3.24}$$

For sufficiently large values of T, the three terms on the right-hand side of (3.23) remain nonoverlapping. In fact, for typical values of T and the spread of channel impulse response, $c'(t)$ always remain a relatively narrow and tall pulse, or a cluster of narrow and tall pulses. In Chapter 6, we use the above results to suggest methods for timing recovery and carrier synchronization. These methods have been implemented on a software-defined radio platform to prove the practicality of their possible deployment in practice.

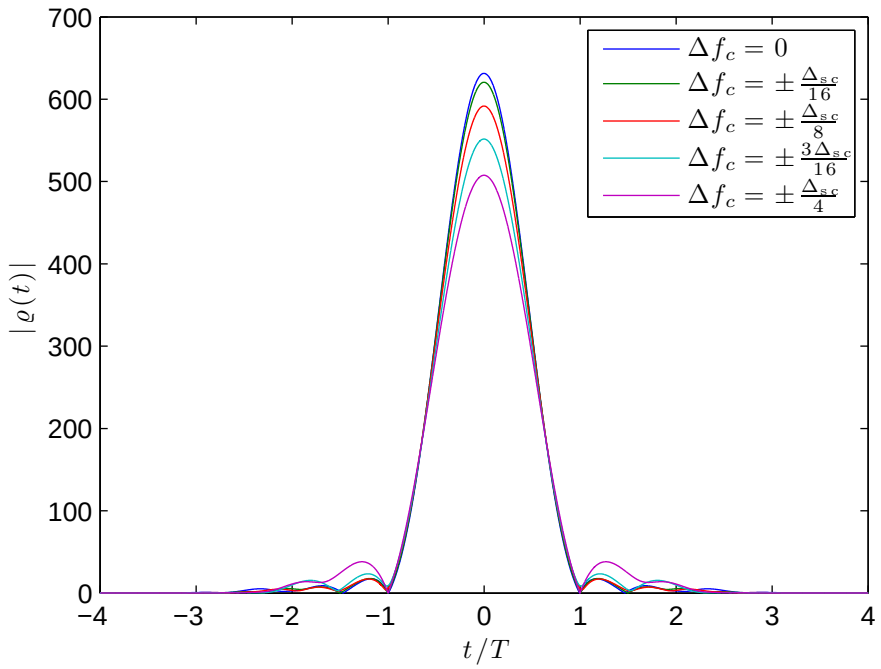

Figure 3.9. Plots of $|\varrho(t)|$ for different choices of Δf_c. $\Delta_{\text{sc}} = 2/T$ denotes the spacing between subcarriers.

3.2.2 Timing Recovery

As discussed above, the matched filter output $z(t)$ consists of a sequence of narrow pulses at the spacing of $T/2$. These pulses are always present at the time instants that are even multiples of $T/2$ and these correspond to the center of the data symbols. On the other hand, at the time instants that are odd multiples of $T/2$, the presence of such pulses depends on the information symbols transmitted before and after the time instant. As demonstrated in Figure 3.8, a pulse will appear only when the two symbols are the same.

Obviously, many methods exist for using the properties of these pulses to find the time instants associated with the even factors of $T/2$—the desired timing phase for sampling the symbols. One particular choice of these methods that provides a good match to one hardware setup is presented in Chapter 6.

3.2.3 Carrier Recovery

Algorithms for carrier acquisition and tracking can also be devised by taking advantages of the pulses generated at the output of the matched filter. Algorithms can also be devised based on the effect of a carrier frequency offset and how much the signal deviates from an ideal response. This is given by (3.21). Either this or another frequency estimator can be

used as the error signal in a phase-locked loop (PLL). Obviously, a variety of choices from the literature on PLLs can be used for both carrier acquisition and tracking [4, 41]. One computationally simple algorithm is developed in Chapter 6.

3.2.4 Channel Estimation

Once the received signal is carrier compensated and the timing information is obtained, the sampled signal at the outputs of the receiver analysis filter bank satisfies the following set of equations:

$$z_k(nT) = \gamma_k C_{\mathrm{BB}}(e^{j2\pi f_k}) s[n] + \vartheta_k(nT) \text{ for } k = 0, 1, \cdots, N-1 \tag{3.25}$$

where $C_{\mathrm{BB}}(e^{j2\pi f_k})$ is the equivalent baseband channel frequency response at the frequency f_k and $\vartheta_k(nT)$ arises from the contributions from noise and interfering signals that may exist in the band of transmission. We assume the channel impulse response contains M samples, and using this a priori information, we perform a standard least squares estimator to obtain the frequency response of the channel $\hat{C}_{\mathrm{BB}}(e^{j2\pi f_k})$. When $s[n]$ is known, this technique provides a unique estimate. When $s[n]$ is unknown, it provides an estimate with a sign ambiguity or, equivalently, a phase ambiguity of $\pm\pi$.

As discussed in the next section, the implementation of an optimum receiver, through maximum ratio combining, requires the estimates of the variance of each element of the interference vector $\boldsymbol{\vartheta}(nT) = [\vartheta_0(nT)\ \vartheta_1\ \cdots\ \vartheta_{N-1}]^T$. Once the channel estimate is obtained, these interference/noise estimates can be calculated as

$$\vartheta_k(nT) = z_k(nT) - \hat{s}[n]\gamma_k \hat{C}_{\mathrm{BB}}(f_k) \tag{3.26}$$

and averaging the magnitude squared over a few choices of n. This technique requires the estimated channel gain and the estimated symbol $\hat{s}[n]$. Other techniques are possible that do not require this knowledge. One such technique will be explained in Chapter 6.

3.2.5 Maximum Ratio Combining

Following the principle of maximum ratio combining, [1], an unbiased minimum variance estimate of $s[n]$ is obtained as

$$\hat{s}[n] = \mathbf{w}_o^{\mathrm{H}} \mathbf{z}(nT), \tag{3.27}$$

where $\mathbf{z}(nT) = \left[\ z_0(nT) z_1(nT) \cdots z_{N-1}(nT)\ \right]^{\mathrm{T}}$ and the tap-weight vector $\mathbf{w}_o$ is given by

$$\mathbf{w}_o = \frac{1}{\sum_{k=0}^{N-1} \frac{|\hat{C}_{\mathrm{BB}}(e^{j2\pi f_k})|^2}{\sigma_k^2}} \begin{bmatrix} \frac{\gamma_0 \hat{C}_{\mathrm{BB}}(e^{j2\pi f_0})}{\sigma_0^2} \\ \frac{\gamma_1 \hat{C}_{\mathrm{BB}}(e^{j2\pi f_1})}{\sigma_1^2} \\ \vdots \\ \frac{\gamma_{N-1} \hat{C}_{\mathrm{BB}}(e^{j2\pi f_{N-1}})}{\sigma_{N-1}^2} \end{bmatrix}. \tag{3.28}$$

Here, σ_k^2 is the variance of $\vartheta_k(nT)$ which was obtained by averaging the magnitude squared output of (3.26). This result is derived in Appendix B.

CHAPTER 4

APPLICATION 1: COGNITIVE RADIO CONTROL CHANNEL

There has been considerable interest in a more efficient utilization of the spectrum in academia, government, and industry [43, 44]. A *cognitive radio* is a radio that is intelligent—in the sense that it is aware of its environment and able to adapt to environmental conditions. One application of cognitive radios is to improve the efficiency of spectrum utilization. This is accomplished by having the radio sense the spectrum to search for holes in usage. These holes occur whenever a primary user (PU), a licensed user of the spectrum, is not operating in a particular band at a particular time and in a particular location. The secondary users (SUs) may then opportunistically exploit these holes without interfering with PU systems. These holes occur over blocks of frequency, time, and space [45].

A *cognitive radio network* (CRN) is a network consisting of many cognitive radio nodes. These nodes engage in joint sensing of the spectrum to reduce the probability of an SU interfering with a PU. This allows them to fulfill the awareness requirement—the ability to sense PUs and distinguish between PU activity and PU inactivity.

CRNs hold promise as a forward-looking technology to achieve better spectrum management. As wireless activity has become a ubiquitous part of modern life, the demand for services continues to grow. In addition to more services, faster service is also required to maximize network efficiency. This idea has led to a considerable amount of work going into developing cognitive radio networks [46]. Of particular note is the IEEE 802.22 standard [47, 48] that was recently ratified. IEEE 802.22 is a standard for deploying wireless regional area networks (WRANs) in TV whitespaces from 54–862 MHz. Its purpose is primarily to bring broadband internet access to hard-to-reach, lowly populated areas (typically, in rural areas). With this in mind, the standard describes a base station with multiple users (termed customer-premises equipment or CPEs). The base station is assumed to have cabled access to the internet in order to access and provide updates to a national spectrum

sensing database.

The primary mechanism for dynamically allocating the spectrum for various users is the central database. However, SUs (or CPEs) do engage in sensing and share that information with the base station. This allows the base station to make decisions regarding the network topology and to send periodic updates to the central database which is supposed to contain up-to-date information about which frequency bands are available in various geographical regions. The SUs (or CPEs) are equipped with a global positioning system (GPS) to determine their approximate location. This is then used by the base station to look up which channels assignments are valid. This, in turn, determines the creation/destruction of links from CPEs to the base station.

The method of a control channel used in IEEE 802.22 is based on the rendezvous technique. The base station is assumed to have prior knowledge of frequency availability from the database. So, it periodically broadcasts data on unreserved channels. The CPEs hop from channel to channel, trying to listen for one of these broadcasts. Once the CPE and base station have made a connection, authentication and connection registration may proceed gradually. This is a relatively long process, and avoiding it is one of the motivations for developing an "always available" control channel such as the one that would be offered by FB-MC-SS. We provide more details in the next section.

4.1 Challenges in Cognitive Radio Network Design

Construction of a CRN presents a number of challenges, the most obvious of which is how to fulfill the "awareness" requirement. Each node must be able to sense the channel to identify the unused portions of the spectrum, and share this information with the other nodes to allow the cognitive nodes to communicate reliably while avoiding the portions of the frequency band used by legacy devices.

Various methods for channel/spectrum sensing have been explored in the literature, e.g., see [49, 50, 51]. However, the more challenging task is to find an effective method for exchanging the sensed information among the nodes within the cognitive network. Such an exchange of information clearly requires a communication channel called a control channel. This shared information may be pooled together at some central location or through some ad hoc algorithm.

The emphasis of this chapter is on the design and development of a control channel that lends itself to (i) ease of implementation, (ii) minimum interference to the primary users, and (iii) robust performance under various channel conditions. Following some logical reasoning

from the present literature (see Section 4.2), we identify spread spectrum techniques that lay a communication channel below the primary users (PUs) noise temperature, [30], as the most reasonable and reliable candidate for the control channel in cognitive radios. This is called an *underlay control channel* (UCC) for obvious reasons. We note that although direct sequence spread spectrum (DS-SS) and frequency hopping spread spectrum (FH-SS) techniques are the most widely established spread spectrum techniques, multicarrier spread spectrum (MC-SS) is a better fit for the application of interest to this chapter. This follows from the fact that, compared to DS-SS and FH-SS, MC-SS is significantly more robust against narrow band and partial band interference, [24, 26, 27, 28, 52], and the presence of PU signals may be viewed as partial band interference to the UCC. Moreover, as will be shown, MC-SS can be straightforwardly adapted to avoid transmission over the active PU bands similar to an overlay approach, [53]. Hence, MC-SS imposes a minimum taxation to the PUs, a very desirable property.

To implement MC-SS systems, two approaches are proposed in the literature. The first approach constructs an MC-SS waveform following the celebrated method of orthogonal frequency division multiplexing (OFDM), [24]. The second approach uses a filter bank multicarrier (FB-MC) technique, [26, 27]. Since in the latter approach the spectrum of each subcarrier is more localized than its counterpart in the former, FB-MC-based SS (namely, FB-MC-SS) systems are more robust to partial-band interferences than OFDM-SS systems.

Among different choices of FB-MC waveforms, we have identified filtered multitone (FMT) as the most appropriate choice for the application of interest to this chapter. As demonstrated throughout this thesis, FMT-SS has a number of appealing properties that lend themselves to a robust implementation. The often difficult tasks of timing and carrier synchronization can be implemented trivially, thanks to the particular properties of FMT-SS that were developed in Chapter 3. Furthermore, in Chapter 6, we report the design, implementation, and evaluation of the proposed FMT-SS scheme on a software-defined radio platform.

In the next section, we present motivations for applying FB-MC-SS as a control channel in cognitive radio networks. We provide a taxonomy of control channels and present more details about various control channels that have been proposed in the cognitive radio literature. We show how our radio fits into this taxonomy in order to provide more clarity for its purpose in CRNs.

4.2 Control Channels: A Taxonomy

Cognitive radios provide a promise of more efficient spectrum utilization [30], [54]. Cognitive radio networks must perform several tasks to utilize the available spectrum. To avoid interfering with PUs, the nodes must perform spectrum sensing. To avoid the so-called hidden terminal problem, the spectrum usage information must be shared between nodes [55], [56], [57]. This information can either be shared locally in clustered groups [32], [58] or globally by the whole network [59], [60]. In either case, sharing spectral information requires internode communication or, in other words, a shared control channel is needed [54], [61].

In addition, many researchers focusing on medium access control (MAC) strategies for cognitive radio networks assume that a control channel is available for sharing spectral information and/or scheduling resources [62], [63], [64]. However, this is by no means a trivial task [65], and hence, a variety of methods have been proposed in the literature to establish control channels for cognitive radios.

The control channels have been classified by different authors under different taxonomies [65]. In this paper, we categorize the available control channel methods as follows:

1. Dedicated Control Channel (DCC): A dedicated narrow band licensed channel is used to transmit control signals, e.g., see [66] and [67]. This method is also referred to as an out-of-band control channel, [65], because the control channel operates in a frequency band that does not overlap with any of the PU bands.

2. Common Control Channel (CCC): The nodes in a cognitive radio network may dynamically establish a CCC in some ad hoc manner, within the PU bands, e.g., see [32, 68, 53]. The terminology *rendezvous* is often used to refer to this type of control channel [69], [70].

3. Underlay Control Channel (UCC): A spread spectrum technique is adopted to establish a common control channel, e.g., see [71] and [72]. In this case, the control channel uses the entire frequency band, including portions with PU activities. However, to remain invisible to the PUs, the transmit power should be at a level comparable to the noise temperature [30].

When there is a dedicated band available for use as a DCC, then the control channel is guaranteed. This method is the simplest and, when it is feasible, it is likely to be applied. However, such a dedicated channel may not always be available. For this reason, many

researchers have proposed techniques of establishing a control channel either in some ad hoc manner (through rendezvous or what we call CCC) or else using a spread spectrum technique (i.e., through a UCC) to mitigate the effective interference seen by PUs.

The CCC (or rendezvous) technique has been found very useful and has been well-studied [69, 70, 73, 74]. The basic idea is to send out test messages searching for the other users by hopping from one band to another until a common band is found and control messages can be sent. While this technique is very popular, there are two weaknesses. The first problem is linked to the hidden terminal problem when an SU radio cannot sense a PU transmitter, but a PU receiver is nearby (and can sense the PU transmitter), thus any transmission by the SU radio will result in significant PU interference. The second problem is associated with time to rendezvous. There is always some time associated with the search for a common channel. This search must occur every time a new network is established, and it must occur every time a PU collision causes interference with an already established control channel. This problem has been addressed previously. For example, in [70], a spread spectrum technique (adaptive frequency hopping) was used to avoid the need to rendezvous again in the event of a PU transmission. The use of ultra-wideband (UWB) technology to establish a control channel has also been suggested [61], [71], [75]. The interested readers may refer to [65] for a broader discussion on control channels, including various classifications.

To overcome these weaknesses, several researchers have suggested the use of spread spectrum techniques as a UCC [71], [72], [66]. This channel occupies the entire band with a low transmit power such that the PUs who are nearby will see the transmission as comparable to the noise temperature [30]. In this way, the entire band is used, but there is only a minimal impact on the PUs. The FMT-SS UCC proposed in this document further reduces the impact of the control channel to the PUs by masking out subcarrier transmission for frequency bands that coincide with PU activities once such PU activities are recognized. This ability to dynamically select the bands of transmission may be seen as an additional bonus not offered by competing technologies, such as UWB and the traditional DS-SS and FH-SS, making the FMT-SS UCC an ideal choice for cognitive radio networks.

4.3 FB-MC-SS as a Control Channel

Multicarrier communications have been proposed for control channels due to the flexibility of their spectral presence [59]. The possibility of using noncontiguous bands is noted as being particularly useful in [31]. That is, there may be several narrow band PUs occupying a relatively small portion of the overall spectrum. The SUs may wish to harvest other

portions of this spectrum for their own benefit while avoiding the disjoint sections being used by active PUs. The most prominent multicarrier technique in usage today is OFDM. In this scenario, however, FB-MC-SS stands out as a strong contender for the next generation of dynamic spectrum access systems. Filter bank techniques allow the system designer to reduce the out-of-band leakage by increasing the order of the underlying prototype filter. For FB-MC-SS, disabling subcarriers results in a minimal loss provided a sufficiently fine-grained subcarrier spacing is used. FB-MC-SS leads to a technique that avoids much interference with PUs through a low transmit power before PU location (in space, time, and frequency) are completely known. Once the network PU usage map is complete (through collaborative spectrum sensing), the FB-MC-SS system can avoid interfering completely by disabling subcarriers in and near active PU bands. This is similar in spirit to suggested overlay techniques, e.g. [76], while at the same time retaining the advantages of underlay techniques (i.e., large processing gain, low transmit power, and robustness to interference).

In addition, filter banks can be used as both a communication method and a spectrum sensing mechanism for cognitive radios [19]. One very obvious requirement for SU receivers is to accurately and efficiently sense the spectrum. One popular way to measure power spectral density (PSD) is by using Welch's method which is based on averaging many windowed FFT outputs together to form an estimate [77]. Another technique with higher accuracy is the multitaper technique pioneered by Thomson [78]. In [79], the close relationship of the multitaper technique with the filter bank approach to PSD estimation was shown. This close relationship leads to a very accurate approach to spectrum sensing. This is a benefit that our system receives almost for free. By averaging the filter bank outputs, we arrive at a very accurate estimation of the PSD in the vicinity of our radio. By combining these estimates from all radios in an area, we lower the probability of having hidden terminal situations—situations where SUs would interfere with undetected PUs without knowing.

As mentioned, this spectrum sensing ability of the SU radios is obtained almost for free since it is part of the modulation scheme being used. In systems employing OFDM-style modulation, they obtain the popular (but less accurate) Welch's method for about the same additional cost. Compare this with systems employing DS-SS or FH-SS as a UCC. Such systems would have to employ an additional technique (e.g., filter banks or periodograms) in order to achieve spectrum sensing. Thus, again we find FB-MC-SS to be an efficient design for CRN applications.

Another requirement for SU receivers is that they should be robust to incumbent PU transmission. If a PU starts to transmit in the middle of a packet, then we would like to

still be able to receive that packet, even if the transmitter has to back off of those bands now occupied by the PU. In the case that the PU does not occupy the entire bandwidth, the SU receivers will automatically adapt their maximum ratio combining weights to adjust for the incumbent PU, and the packet will not be lost. This is a direct result of the robustness of FB-MC-SS to narrow band interference (called narrow band interference suppression by some authors).

In addition to these benefits at a cognitive radio receiver, the transmitter also benefits. The SU is required to avoid interference with all nearby PUs. This hard requirement must be met—any interference from the SUs to the PUs should be at a level comparable to the case if no SUs were operating. Otherwise, the licensed PUs would not have access to the spectrum for which they have already paid.

As noted previously, this is achieved through spectrum sensing. When PU activity is sensed, the SU should immediately vacate that channel to avoid interfering. FB-MC-SS allows interruption of several subcarriers to occur even in the middle of a packet transmission without appreciably affecting the quality of the transmission. As noted in Chapter 3, FB-MC-SS sends redundant information on multiple subcarriers. It can drop several subcarriers at frequencies when a PU transmission has been detected. Unless almost all of the spectrum is occupied by the PUs, this will not lead to significant packet loss.

Spectrum sensing always takes some amount of time. It is impossible for an SU to respond to PU activity before it is aware of the presence of a PU. Therefore, the transmit power should be kept as low as possible in case an incumbent PU is not detected immediately. Again, we see that FB-MC-SS with its high processing gain is a perfect fit for this requirement. With power control feedback, the SUs can communicate with relatively low transmit power levels to avoid much interference with PUs. This is especially important in the case that a PU detection must propagate through to the central base station and then back to the SU (perhaps on a separate band of frequencies). This allows the SUs to have only a minor impact (low level of interference) to a PU before the PU presence is known. Also, as noted above, the SU can eliminate its impact completely once the PU presence is discovered.

4.4 Summary

The advantages discussed in this chapter show that FB-MC-SS is ideal for usage as an underlay control channel in cognitive radio networks. Specifically, these advantages are the following.

- A dedicated band is not required.
- There is no latency in setting up the control channel (as opposed to CCC).
- It is possible to adapt quickly to incumbent PU transmissions.
- Transmission is robust to variations in resource availability over time.
- The control channel is "always available" as long as there is available bandwidth.
- FB-MC-SS comes with a built-in, highly accurate spectrum sensing mechanism
- It has the ability to use noncontiguous bandwidths with ease (unlike DS-SS and FH-SS) [69, 70], and UWB [75, 71].

Along with these advantages, a system implementation and design should be practical. Such a practical design is explored with attention to the full details of implementation in Chapter 6. These advantages along with a practical and implementable design make FB-MC-SS an attractive option for transmission/reception of control signaling in the next generation of cognitive radio networks for dynamic spectrum access applications.

CHAPTER 5

APPLICATION 2: SPREAD SPECTRUM COMMUNICATIONS

Spread spectrum systems are commonly used in harsh and hostile environments due to their resistance to jamming, interference, and noise. Traditional spread spectrum techniques include direct sequence spread spectrum (DS-SS), frequency hopping spread spectrum (FH-SS), and more recently, multicarrier spread spectrum (MC-SS) [1, 20, 80, 22, 25, 24]. FH-SS techniques tend to require a relatively long time for code synchronization based on scanning techniques [21, 81]. DS-SS techniques are often used to mitigate interference (e.g., in multiple access scenarios) [20, 80]. MC-SS techniques have been noted to have a stronger resistance to narrow and partial band interference compared to DS-SS and FH-SS [27, 28, 24, 52].

Traditional MC-SS techniques use a multicarrier modulation format similar to orthogonal frequency division multiplexing (OFDM). In the literature, these techniques are typically called MC-SS techniques. Alternatives to these techniques are hybrid techniques combining the spreading mechanisms of DS-SS and MC-SS. These have been studied by several researchers [82, 83, 84, 85, 86]. These techniques have typically been called direct sequence MC-CDMA (DS-MC-CDMA) and multitone CDMA (MT-CDMA) (highlighting their usage for multiple access scenarios). MT-CDMA has the distinguishing characteristic that subcarrier bands are allowed to overlap significantly. This is done in an attempt to accommodate longer spreading codes and a higher number of users [87, 24]. References [25] and [24] provide an excellent overview of these works, highlighting their advantages and disadvantages, with special focus on the multiuser case.

Although most works assume the celebrated OFDM signaling for various MC-SS waveforms, a few works have noted the possibility of using filter banks to implement systems that behave more robustly in the presence of narrow/partial band interference; e.g., [27, 52, 33, 29, 26, 88]. While most of these works consider the case of spreading each

data symbol across frequency only, the works in [26] and [88] emphasize that the spreading should be performed in both time and frequency. The subcarrier bandwidths should be selected so that their frequency responses can be considered independent of one another. In [26], it was also assumed that each subcarrier band can be approximated by a flat gain. Clearly, under the condition that the subcarrier bands are contiguous, these two conditions cannot be true simultaneously. In [88], thus, the second condition was relaxed, i.e., some variation in the subcarrier bands was allowed in the model. Accordingly, it was argued in [88] that the optimal detector for each subcarrier component is still a rake receiver. The outputs from these rake receivers are then combined, using a maximum ratio combining mechanism. The numerical results presented in [88] show that an FB-MC-SS with a small number of subcarriers, a rake receiver per subcarrier, and a maximum ratio combiner at its output, performs similar to or better than its single carrier counterpart.

The MC-SS systems of [26] and [88], while interesting, are significantly different from the filter bank-based multicarrier spread spectrum (FB-MC-SS) technique that has been considered in [27, 52, 33, 29] and we follow up in this chapter. As opposed to the systems in [26] and [88], we consider spreading in frequency only. Each subcarrier band is designed so that the channel may be approximated by a flat gain, thus allowing equalization using a single-tap per subcarrier. Furthermore, as noted above, [26] and [88] use a relatively small number of subcarriers, comparable to the number of multipaths in the channel. We consider a much larger number of subcarriers. For the purpose of analysis, we let this number tend to infinity. For this limiting case, we find that the optimum implementations of the studied FB-MC-SS and DS-SS approach the same performance. This implies that the FB-MC-SS waveform may be used in similar applications where DS-SS is already employed (e.g., applications that require low probability of detection, low probability of interception, and low probability of exploitation).

The analysis presented in this chapter is inclined in favor of the DS-SS system, as we make the idealistic assumption that multipath components are resolvable. Also, we ignore intersymbol interference (ISI) effects in DS-SS. However, as it is well-understood in the literature [89, 90, 91], DS-SS rake receivers are always subject to some performance loss due to unresolved paths and ISI effects. The analysis results show that in the limiting case, spreading in time and in frequency both exhibit a similar performance. The simulations confirm this finding for realistic scenarios where noise and interference are the dominant source of system error. One strong advantage of the FB-MC-SS system that is studied in this chapter compared to that of [88] (an improved version of [26]) is a far simpler

implementation. This stems from the fact that each subcarrier does not require a rake receiver to achieve the full benefits of spreading.

This chapter is organized as follows. Section 5.1 presents the structure of the DS-SS model along with a derivation of its signal-to-noise ratio. Section 5.2 similarly presents the structure of the FB-MC-SS model and its derived signal-to-noise ratio. Section 5.3 provides a comparison between the two derivations and shows that, in the ideal case, the two will offer the same signal-to-noise ratio performance. Section 5.4 backs up the derivation with evidence from numerical simulations of the two systems.

5.1 Direct Sequence Spread Spectrum Model

The DS-SS system considered in this chapter is shown in Figure 5.1. In this section, we explain the details of the individual blocks in this figure and present equations that quantify its performance under ideal conditions.

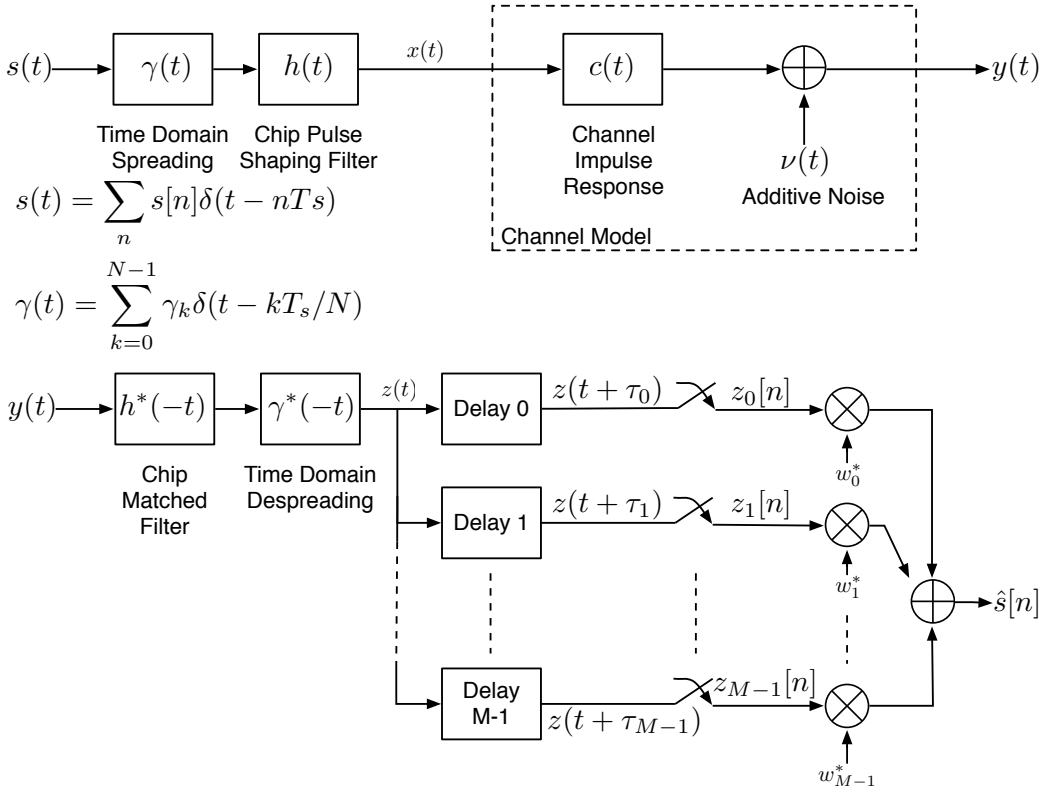

Figure 5.1. Block diagram of the DS-SS system under consideration. The top diagram represents the transmitter and channel model. The lower diagram represents the rake receiver structure.

5.1.1 Transmitter and Channel Model

The DS-SS transmitter converts a sequence of data symbols $s[n]$ to a continuous-valued transmit signal $x(t)$. We assume that the data symbols $s[n]$ are from a quadrature amplitude modulated (QAM) constellation. The continuous-time signal $s(t)$ of data symbols $s[n]$ is formed as shown in Figure 5.1 where T_s denotes the symbol interval and N is the processing gain. This is spread in time by passing $s(t)$ through the spreading block $\gamma(t)$ whose functionality is also indicated in Figure 5.1. The result is then band limited through the pulse shaping filter $h(t)$ to form the transmit signal

$$x(t) = \left[\sum_n s[n]\delta(t - nT_s)\right] \star \gamma(t) \star h(t). \tag{5.1}$$

The baseband equivalent channel is modeled as a multipath channel with L resolvable paths characterized by the impulse response

$$c(t) = \sum_{l=0}^{L-1} c_l \delta(t - \tau_l) \tag{5.2}$$

where τ_l is the lth multipath component delay and c_l is the lth path gain. The received signal, at the channel output, is thus obtained as

$$y(t) = \sum_{l=0}^{L-1} c_l x(t - \tau_l) + \nu(t) \tag{5.3}$$

where $\nu(t)$ the additive noise at the channel output. We assume that $\nu(t)$ is white within the band of interest and has a two-sided power spectral density $N_0/2$.

5.1.2 Rake Receiver

At the receiver, the received signal is passed through the matched filter $h^*(-t)$ and the despreading matched filter $\frac{1}{N}\gamma^*(-t)$. Assuming that $|\gamma_k|^2 = 1$, for $k = 0, 1, \cdots, N-1$, this leads to the L rake finger outputs[1] for $l = 0, 1, \cdots, L-1$, we have

$$z(t + \tau_l) = \sum_{n=-\infty}^{\infty} s[n] c_l g(t - nT_s) + \eta(t + \tau_l) \tag{5.4}$$

where $g(t) = h(t) \star h^*(-t)$ and $\eta(t)$ is signal component arising from channel noise and intersymbol interference (ISI) due to channel dispersion. Note that the additional factor $\frac{1}{N}$ is added to the despreading matched filter to account for averaging over the N chips

[1] In writing (5.4), we have assumed that N is sufficiently large so that ISI among adjacent symbols is negligible and thus can be ignored.

of each data symbol. Assuming that $h(t)$ is a Nyquist pulse, we define the signal samples $z_l[n] = z(nT_s + \tau_l)$ and $\eta_l[n] = \eta(nT_s + \tau_l)$, we obtain

$$z_l[n] = s[n]c_l + \eta_l[n], \quad \text{for } l = 0, 1, \cdots, L-1. \tag{5.5}$$

This can be written in vector form as

$$\mathbf{z}[n] = s[n]\mathbf{c} + \boldsymbol{\eta}[n], \tag{5.6}$$

where $\mathbf{z}[n] = [z_0[n]\ z_1[n]\ \cdots\ z_{L-1}[n]]^{\mathrm{T}}$, $\mathbf{c} = [c_0\ c_1\ \cdots\ c_{L-1}]^{\mathrm{T}}$, and $\boldsymbol{\eta}[n] = [\eta_0[n]\ \eta_1[n]\ \cdots\ \eta_{L-1}[n]]^{\mathrm{T}}$.

A linear optimal detector may compute an unbiased estimate of $s[n]$ as

$$\hat{s}[n] = \mathbf{w}^{\mathrm{H}}\mathbf{z}[n]. \tag{5.7}$$

where $\mathbf{w}$ is a tap-weight vector whose optimum value is found by minimizing $E[|s[n] - \hat{s}[n]|^2]$ subject to the constraint $\mathbf{w}^{\mathrm{H}}\mathbf{c} = 1$. This problem has the solution

$$\mathbf{w}_{\mathrm{o}} = \frac{1}{\mathbf{c}^H\mathbf{R}^{-1}\mathbf{c}}\mathbf{R}^{-1}\mathbf{c} \tag{5.8}$$

where $\mathbf{R} = \mathrm{E}[\boldsymbol{\eta}[n]\boldsymbol{\eta}^{\mathrm{H}}[n]]$.

Substituting (5.8) in (5.7) and evaluating the signal-to-interference-plus-noise ratio (SINR) at the output of the linear optimal detector, we obtain

$$\mathrm{SINR}_{\mathrm{ds}} = \sigma_s^2\mathbf{c}^{\mathrm{H}}\mathbf{R}^{-1}\mathbf{c} \tag{5.9}$$

where σ_s^2 is the variance of the sequence $s[n]$. For a large processing gain, N, which is our assumption here, one may assume that the ISI in the system is negligible and thus can be ignored. Moreover, if the multipath components in the channel are sufficiently spaced, one will find that the elements of the vector $\boldsymbol{\eta}[n]$ are uncorrelated with one another, hence, $\mathbf{R} = \frac{N_0}{N}\mathbf{I}$. Note that N_0 is the variance of the elements of $\boldsymbol{\eta}[n]$ and this follows since we have assumed $g(t)$ is a Nyquist filter (equivalently, $h(t)$ is a square-root Nyquist filter). Under these conditions, (5.9) may be simplified as

$$\mathrm{SNR}_{\mathrm{ds}} = N\frac{\sigma_s^2}{N_0}\mathbf{c}^{\mathrm{H}}\mathbf{c}. \tag{5.10}$$

For this result, we have replaced SINR with SNR on the left-hand side, as the ISI has been assumed to be absent.

5.2 FB-MC-SS Model

The FB-MC-SS system considered in this chapter is shown in Figure 5.2. In this section, we explain the details of the individual blocks in this figure and present equations that quantify its SNR performance.

We reuse similar notations from Section 5.1 for operations and elements that may be thought of as the frequency-domain duals of those expressed in the time-domain for DS-SS. For example, the spreading sequence in the DS-SS system was expressed by the continuous time impulse sequence $\gamma(t)$ which consisted of a series of N impulses whose amplitudes are the spreading gains $\gamma_0, \gamma_1, ..., \gamma_{N-1}$. Moreover, in the case of DS-SS, $h(t)$ was used to denote the transmitter pulse shaping filter. It was a square-root Nyquist filter designed for chip spacing of $T_c = T_s/N$. Here, $h(t)$ is also a square-root Nyquist filter, but designed for symbol spacing of T_s.

5.2.1 Transmitter and Channel Model

As with the DS-SS system, we begin with a discrete time sequence of symbols $s[n]$ taken from a QAM constellation. Each symbol is spread across frequency through the spreading gains $\gamma_0, \gamma_1, ..., \gamma_{N-1}$. The result is passed through a synthesis filter bank whose subband filters are obtained from $h(t)$ as the prototype filter, hence,

$$h_k(t) = h(t)e^{j2\pi f_k t} \tag{5.11}$$

where f_k is the center frequency of the kth subband. Hence, the transmit signal, $x(t)$, is obtained as

$$x(t) = \sum_n s[n] \sum_{k=0}^{N-1} \gamma_k h_k(t - nT_s). \tag{5.12}$$

Also, it follows that the received signal is given by

$$y(t) = \sum_{n=-\infty}^{\infty} s[n] \sum_{k=0}^{N-1} \gamma_k h_k(t - nT_s) \star c(t) + \nu(t). \tag{5.13}$$

To proceed, we write

$$h_k(t - nT_s) \star c(t) = c_k^{\mathrm{f}} h_k(t - nT_s) + \epsilon_k(t) \tag{5.14}$$

where c_k^{f} is the channel gain at the center of the pass band of $h_k(t)$, and $\epsilon_k(t)$ is a residual ISI term arising from a small variation of the channel gain around the center gain c_k^{f}.

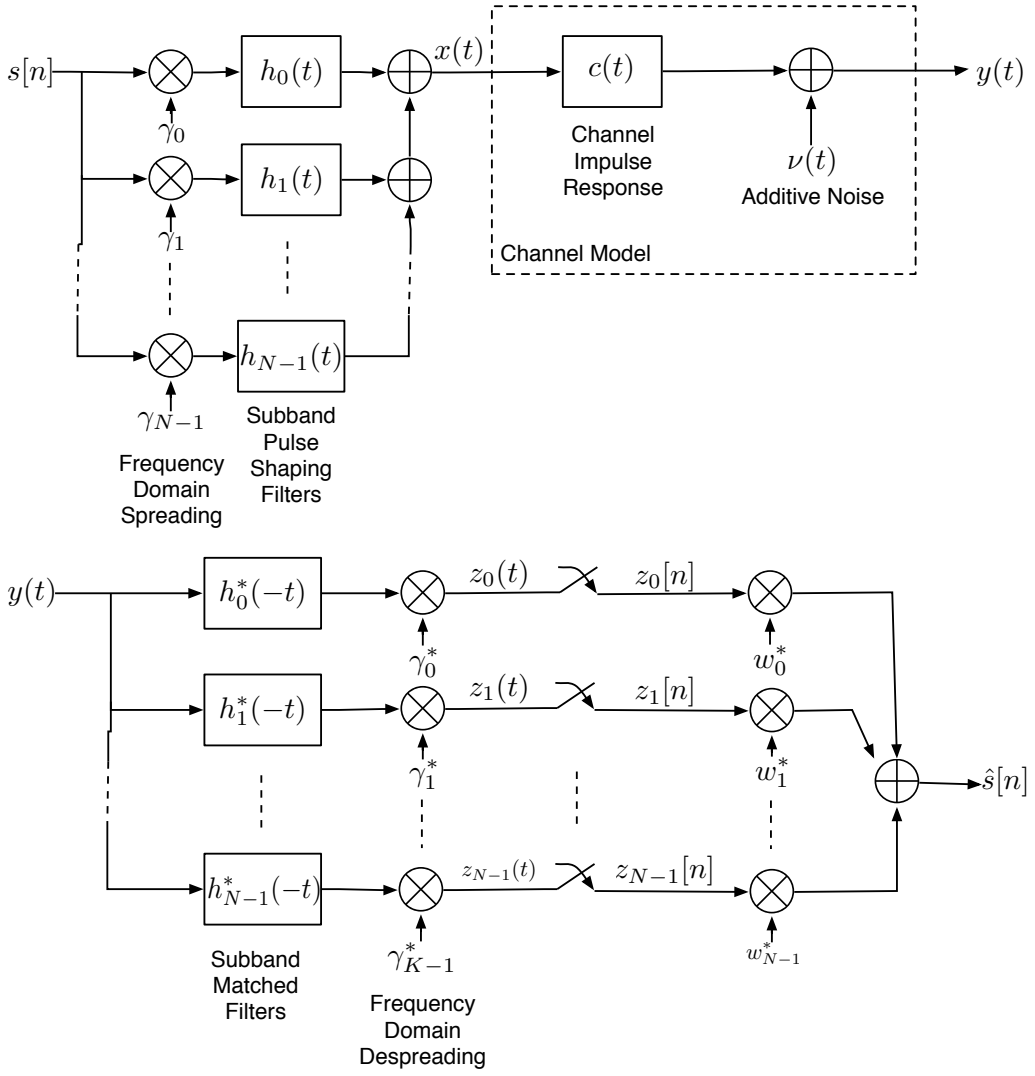

Figure 5.2. Block diagram of FB-MC-SS model under consideration. The top diagram represents the transmitter and the channel model. The lower diagram represents the maximal ratio combining receiver structure.

The superscript 'f' signifies the fact that reference is made to the channel response in the frequency-domain. Next, substituting (5.14) in (5.13), we obtain the received signal

$$y(t) = \sum_{n=-\infty}^{\infty} s[n] \sum_{k=0}^{N-1} \gamma_k c_k^{\mathrm{f}} h_k(t - nT_s) + \epsilon(t) + \nu(t) \tag{5.15}$$

where $\epsilon(t) = \sum_n s[n] \sum_{k=0}^{N-1} \gamma_k \epsilon_k(t)$.

5.2.2 Maximal Ratio Combining Receiver

Following the receiver block diagram in Figure 5.2 and assuming that the spreading gains satisfy the identity $|\gamma_k|^2 = 1$, one will find that the analyzed subband signals can be written as

$$z_k(t) = \sum_n s[n] c_k^{\mathrm{f}} g(t - nT_s) e^{j2\pi f_k t} + \eta_k(t), \tag{5.16}$$

for $k = 0, 1, \cdots, K-1$, where we have noted that $h_k(t) \star h_k^*(-t) = h(t) \star h^*(-t) e^{j2\pi f_k t}$ and have defined $g(t) = h(t) \star h^*(-t)$. Also, $\eta_k(t) = \gamma_k^* h_k^*(-t) \star (\epsilon(t) + \nu(t))$.

Next, taking the samples $z_k(t)$, for $k = 0, 1, \cdots, N-1$, at $t = nT_s$ and collecting the result in a vector equation, we obtain

$$\mathbf{z}[n] = s[n]\mathbf{c}^{\mathrm{f}} + \boldsymbol{\eta}[n] \tag{5.17}$$

where the vectors $\mathbf{z}[n]$, $\mathbf{c}^{\mathrm{f}}$ and $\boldsymbol{\eta}[n]$ are defined in the same way as their counterparts in Section 5.1. The term $e^{j2\pi f_k n T_s}$ disappears from the left-hand side, because it is guaranteed to be equal to one based on the chosen frequencies. Also, following the same line of derivations as in Section 5.1, here, the linear optimal detector (5.7) has the tap-weight vector

$$\mathbf{w}_{\mathrm{o}} = \frac{1}{(\mathbf{c}^{\mathrm{f}})^{\mathrm{H}} \mathbf{R}^{-1} \mathbf{c}^{\mathrm{f}}} \mathbf{R}^{-1} \mathbf{c}^{\mathrm{f}} \tag{5.18}$$

and the output signal-to-interference-plus-noise ratio

$$\mathrm{SINR}_{\mathrm{fb}} = \sigma_s^2 (\mathbf{c}^{\mathrm{f}})^{\mathrm{H}} \mathbf{R}^{-1} \mathbf{c}^{\mathrm{f}}. \tag{5.19}$$

Moreover, for a large processing gain, N, one may assume that the channel has a flat gain over each subcarrier band, hence, ISI in the system is negligible and thus can be ignored. This, in turn, is equivalent of saying one can remove $\epsilon(t)$ from the right-hand side of (5.15). Under this condition, here, $\mathbf{R} = N_0 \mathbf{I}$ and, hence, (5.19) simplifies to

$$\mathrm{SNR}_{\mathrm{fb}} = \frac{\sigma_s^2}{N_0} (\mathbf{c}^{\mathrm{f}})^{\mathrm{H}} \mathbf{c}^{\mathrm{f}}. \tag{5.20}$$

5.3 Comparison

In this section, we compare the SNR results that were derived in Sections 5.1 and 5.2. To this end, we note that for the channel model (5.2),

$$c_k^{\mathrm{f}} = \sum_{l=0}^{L-1} c_l e^{-j2\pi f_k \tau_l}, \quad \text{for } k = 0, 1, \cdots, N-1. \tag{5.21}$$

Next, if we form the matrix

$$\mathbf{A} = \begin{bmatrix} e^{j2\pi f_0 \tau_0} & e^{j2\pi f_0 \tau_1} & \dots & e^{j2\pi f_0 \tau_{L-1}} \\ e^{j2\pi f_1 \tau_0} & e^{j2\pi f_1 \tau_1} & \dots & e^{j2\pi f_1 \tau_{L-1}} \\ \vdots & \vdots & \ddots & \vdots \\ e^{j2\pi f_{N-1} \tau_0} & e^{j2\pi f_{N-1} \tau_1} & \dots & e^{j2\pi f_{N-1} \tau_{L-1}} \end{bmatrix} \tag{5.22}$$

the two channel vectors $\mathbf{c}$ and $\mathbf{c}^{\mathrm{f}}$ are related as

$$\mathbf{c}^{\mathrm{f}} = \mathbf{A}\mathbf{c}. \tag{5.23}$$

Substituting (5.23) into (5.20), we obtain

$$\mathrm{SNR}_{\mathrm{fb}} = \frac{\sigma_s^2}{N_0} \mathbf{c}^{\mathrm{H}} \mathbf{A}^{\mathrm{H}} \mathbf{A} \mathbf{c}. \tag{5.24}$$

Next, we note that for large values of N, $\mathbf{A}^{\mathrm{H}}\mathbf{A} \approx N\mathbf{I}$. As N increases, this approximation becomes more precise. Accordingly, we argue that for typical cases, using practical choices of N in the order of 100 or greater,

$$\mathrm{SNR}_{\mathrm{fb}} = N \frac{\sigma_s^2}{N_0} \mathbf{c}^{\mathrm{H}} \mathbf{c} \tag{5.25}$$

which is the same result as (5.10). This shows the limiting behavior of both systems. As the processing gain N increases, both DS-SS (with an ideal rake receiver) and FB-MC-SS (with an ideal maximum ratio combiner) approach the same performance. However, differences exist in more realistic systems. This is demonstrated next through computer simulations.

5.4 Simulations

In this section, we present a number of simulation results to compare the performance of DS-SS and FB-MC-SS over a wireless channel in an urban area setting. We examine and compare the SINR values at the output of both systems.

5.4.1 Channel Parameters

We consider a channel with the total bandwidth 50 MHz. For the DS-SS system, we allow the total bandwidth of the chip pulse shaping filter to be $(1.0 + \alpha) \times 50$ MHz and we use a roll-off $\alpha = 0.1$, while for the FB-MC-SS system, the total bandwidth allowed is 50 MHz with a prototype filter $\alpha = 1.0$ and only every other subcarriers are active. This implies, to achieve the same data rate, the FB-MC-SS system has a lower number of (frequency-domain) chips per symbol compared to the (time-domain) chips per symbol of the DS-SS signal. The processing gain of FB-MC-SS is derived in [33] and for our setup

here is shown to be twice the number of its chips. Hence, for the results presented here, FB-MC-SS and DS-SS have the same processing gain. Furthermore, one may note that here a slight advantage to DS-SS is granted, by allowing a slightly wider bandwidth, in order to highlight the strong advantages of FB-MC-SS over DS-SS in terms of SINR.

For our study, the channel model parameters c_i and τ_i, introduced in (5.2), are chosen according to the COST 207 models listed in Table 7.3 of [92]. The relevant parameters from this table are taken and listed here in Table 5.1. There are four different channel models: (a) Rural Area (RA); (b) Typical Urban (TU); (c) Bad Urban (BU); and (d) Hilly Terrain (HT). Here, we do not consider variation/fading of the channel, and simply generate random channels with the specified delays (that are fixed for each model), and each respective gain, c_i, is treated as a zero-mean complex Gaussian random variable with the specified power/variance. We note that this choice of path gains does not follow the models of COST 207 exactly, but we believe it is acceptable for the sake of comparison.

Our simulator for the DS-SS system follows the block diagram of Figure 5.1. The combination of the modulator, the channel impulse response (5.2), and the demodulator are lumped together by the equivalent baseband response

$$c_{\mathrm{BB}}(t) = \sum_{l=0}^{L-1} c_l e^{-j2\pi\tau_l f_c} \delta(t - \tau_l). \tag{5.26}$$

We also note the terms $e^{-j2\pi\tau_l f_c}$ have the impact of adding an additional phase to the

Table 5.1. The relevant parameters of the Cost 207 model used for the simulations.

Rural Area		Typical Urban	
Tap Delay	Ave. Power	Tap Delay	Ave. Power
0.0 μs	1.00	0.0 μs	0.50
0.2 μs	0.63	0.2 μs	1.00
0.4 μs	0.10	0.6 μs	0.63
0.6 μs	0.01	1.6 μs	0.25
		2.4 μs	0.16
		5.0 μs	0.10
Bad Urban		Hilly Terrain	
Tap Delay	Ave. Power	Tap Delay	Ave. Power
0.0 μs	0.50	0.0 μs	1.00
0.4 μs	1.00	0.2 μs	0.63
1.0 μs	0.50	0.4 μs	0.40
1.6 μs	0.32	0.6 μs	0.20
2.4 μs	0.63	15.0 μs	0.25
6.6 μs	0.40	17.2 μs	0.06

combined coefficients $c_l e^{-j2\pi\tau_l f_c}$. However, since c_l has an arbitrary phase, the equivalent baseband channel model (5.26) can be simplified as

$$c_{\mathrm{BB}}(t) = \sum_{l=0}^{L-1} c_l \delta(t - \tau_l) \tag{5.27}$$

where the coefficients c_l, as in (5.2), for each realization of the channel, are a set of complex Gaussian random variables. Accordingly, the system model of Figure 5.1 is simplified as in Figure 5.3.

In the case of the FB-MC-SS system, there are N parallel subcarrier channels whose center frequencies are spaced apart by Δf. Hence, following the same line of derivations to those that lead to the simplified system model of Figure 5.3, here, we obtain Figure 5.4. In this diagram, the equivalent baseband channels for subcarriers are modeled as

$$c_{\mathrm{BB},k}(t) = \sum_{l=0}^{L-1} c_l e^{-j2\pi\tau_l k\Delta f} \delta(t - \tau_l), \tag{5.28}$$

for $k = 0, 1, \cdots, N-1$. The noise components $\nu_k(t)$ are a set of identically independent white Gaussian noise processes with the two-sided power spectral density $N_0/2$.

In our simulation, we set $\Delta f = \frac{50}{N}$ MHz with $N = 256$. The sampling rate was set to 100 MS/s. The FB-MC-SS system was implemented with $N = 256$ active subcarriers spanning 50 MHz resulting in a subcarrier spacing of approximately $\Delta f = 97.7$ kHz. This implies a baud interval of 10.24 μs. The DS-SS system was implemented with $N = 512$ chips per symbol and a chip period of 0.02 μs resulting in a baud interval of 10.24 μs as well. As noted previously, the DS-SS system has twice as many chips per symbol to match the same processing gain as FB-MC-SS [33].

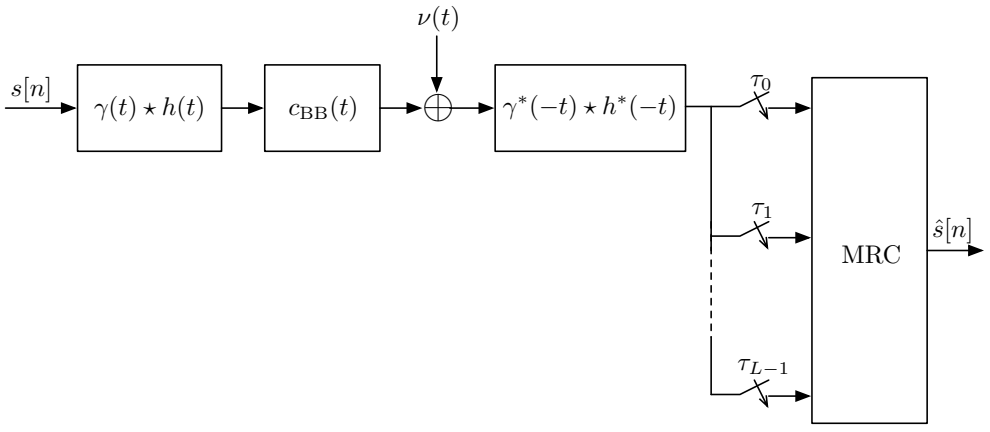

Figure 5.3. The simplified block diagram of DS-SS that is used for simulations.

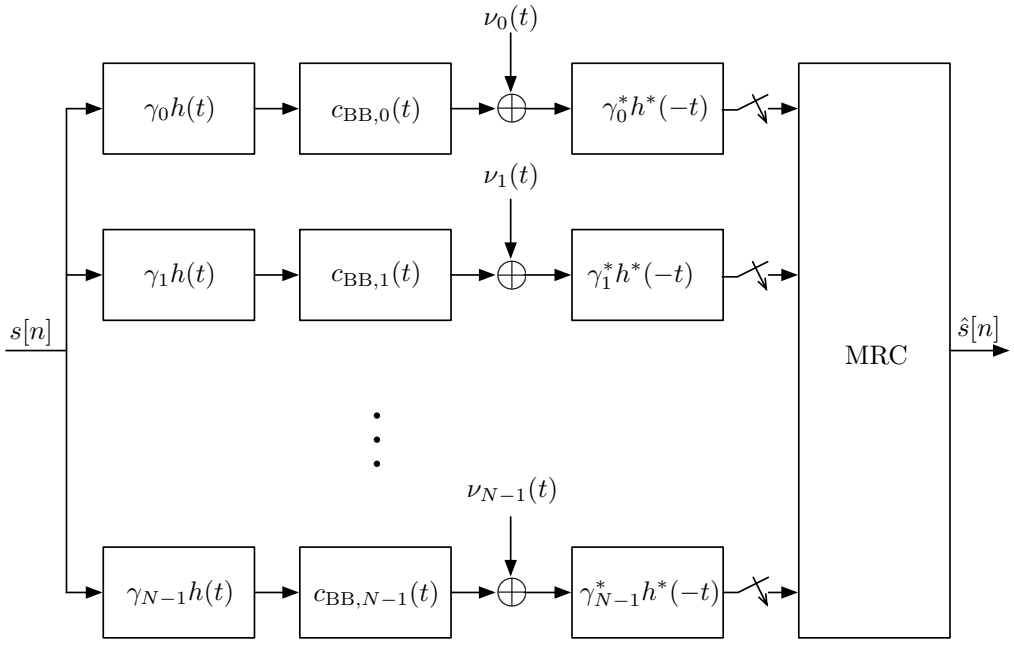

Figure 5.4. The simplified block diagram of FB-MC-SS that is used for simulations.

Given this setup, Monte Carlo simulations were processed according to the following procedure.

1. A new channel was generated according to the parameters in Table 5.1.
2. A packet of 1000 BPSK symbols was generated for DS-SS and FB-MC-SS.
3. The symbols were convolved with the channel.
4. Complex white Gaussian noise samples were added to the data with variance σ^2.
5. The DS-SS signal was matched filtered; the various delays were maximal ratio recombined (i.e., rake receiver).
6. Each subcarrier of the FB-MC-SS signal was matched filtered and the outputs were maximal ratio combined.
7. The SINR for the detection sequences are measured and stored in a file.
8. A new packet was generated until 100 packets had been generated (going back to step 2).

9. A new channel was generated until 1000 channels had been generated (going back to step 1).

The simulation parameter, σ^2, was varied to observe the effects of noise on the system. After running these simulations, the average SINR of both systems was computed from the samples. Note that we used the same source of randomness (channel generation and noise samples) to evalulate both systems' performances. The results are summarized in Table 5.2.

5.4.2 Discussion of Results

First, consider the noiseless case. In this case, the DS-SS system self-interference is pronouncedly higher than that of the FB-MC-SS system. This is because the randomly generated spreading code is not self-orthogonal when shifted by one or more chip intervals. In addition, there is a fractional intersymbol interference, as the duration of channel impulse response extends over multiple chips.

Table 5.2. Simulation Results

Rural Area		
Received SNR	DS-SS SINR	FB-MC-SS SINR
∞ dB	43.4 dB	54.9 dB
10 dB	38.3 dB	46. dB
0 dB	26.0 dB	27.1 dB
-10 dB	17.0 dB	17.1 dB
Typical Urban		
Received SNR	DS-SS SINR	FB-MC-SS SINR
∞ dB	36.0 dB	54.5 dB
10 dB	32.6 dB	37.1 dB
0 dB	25.4 dB	27.2 dB
-10 dB	17.0 dB	17.2 dB
Bad Urban		
Received SNR	DS-SS SINR	FB-MC-SS SINR
∞ dB	36.2 dB	54.7 dB
10 dB	31.7 dB	37.0 dB
0 dB	25.6 dB	27.0 dB
-10 dB	16.9 dB	17.0 dB
Hilly Terrain		
Received SNR	DS-SS SINR	FB-MC-SS SINR
∞ dB	33.8 dB	54.9 dB
10 dB	30.8 dB	37.1 dB
0 dB	25.1 dB	27.2 dB
-10 dB	16.8 dB	17.2 dB

The channel spreading in time on FB-MC-SS, on the other hand, has a somewhat different impact. This can be best-explained by considering a two tap channel and the equivalent baseband response across subcarriers. The interference from these subcarriers is correlated according to a linear phase. Another contributing factor is a *self-equalization* property that comes about by combining subcarrier signals on different subcarriers. As highlighted in (5.14), the channel effect on each subcarrier channel may be quantified by a flat gain c_k^{f} and a disturbed response characterized by $\epsilon_k(t)$. The MRC aligns the flat gains and constructively adds them together. This process, at the same time, averages the disturbed responses, and hence, nullifies the impact of the channel response to a level very close to zero. These two properties explain the almost interference free performance of FB-MC-SS. When channel noise is absent (received SNR is infinity), FB-MC-SS SINR (SIR, to be more exact) is a large value (55 dB), irrespective of the type of the channel. This is not the case for DS-SS.

At lower values of received SNR, as one would expect, SINR is dominated by channel noise, and the results are predictably obtained by adding the processing gain to the received SNR. For the experiments here, the processing gain is 512 ($\equiv$ 27 dB).

We presented theoretical derivations that show that when the channel noise is white, in the limit, as the number of subcarriers increases, a maximal ratio combining (MRC) detector for the filter bank multicarrier spread spectrum (FB-MC-SS) system offers the same performance as an ideal rake receiver using an MRC detector for an equivalent direct sequence spread spectrum (DS-SS) system. We provided simulation results to confirm these findings. The Monte Carlo simulations showed that the two systems have a similar performance in the case of low SNR. At the same time, we found that the performance of FB-MC-SS is substantially greater in the high SNR regimes.

Spread spectrum systems are usually employed at low SNR. Thus, the important fact that in these low SNR regimes, the FB-MC-SS system with MRC and the DS-SS system with an ideal rake receiver perform equally may lead one to prefer FB-MC-SS since it has a simpler implementation and does not require long search times to find all significant channel impulse response taps. Thus, FB-MC-SS is an attractive alternative system with similar performance to DS-SS for any applications in which DS-SS has historically been used.

CHAPTER 6

SYSTEM IMPLEMENTATION

This chapter discusses various options that may be used to implement the transmitter and receiver systems required to modulate and demodulate the data symbols in FB-MC-SS. We present multiple possibilities for implementing the transmitter and receiver. These options have all been implemented in a software-defined radio (SDR) platform. From theoretical analysis and through physical experimentation, we have identified many of the advantages and disadvantages of the various approaches presented here. Anywhere alternative implementation options are present, a discussion of the advantages and disadvantages of alternative subsystems is presented.

The SDR platform utilized is based on the National Instruments FlexRIO architecture. A block diagram of this architecture is provided in Figure 6.1. The FlexRIO FPGA module is an NI PXIe-7965R equipped with a Xilinx Virtex-5 FPGA and 512 MB of onboard memory (DRAM). The NI FlexRIO adapter module is an NI 5781, and more recently replaced by the NI 5791. The NI 5781 module is equipped with dual 100 MS/s 14-bit analog-to-digital converters (ADC) and dual 100 MS/s 16-bit digital-to-analog converters (DAC). These ADC and DAC modules are connected to the Ettus daughterboard to sample the baseband signal. The Ettus RF front-end is an XCVR2450 operating in the 2.4 to 2.5 GHz band. The NI 5791 has similar ADC and DAC capabilities, but includes an RF front-end so that the Ettus board is no longer required—making the system more compact. The NI Real-Time Controller is an NI PXIe-8133. This controller is basically a host PC equipped with an Intel Core i7-820 processor (1.73 GHz quad-core) and 4 GB of RAM. The controller is running a real-time operating system which is programmable using NI LabVIEW Real-Time. Communication between the controller and the FPGA module is facilitated by a high speed Direct Memory Access (DMA) interface.

The NI SDR system was chosen for its flexibility and programmability. While most of the signal processing is implemented on the FPGA module, the more structurally com-

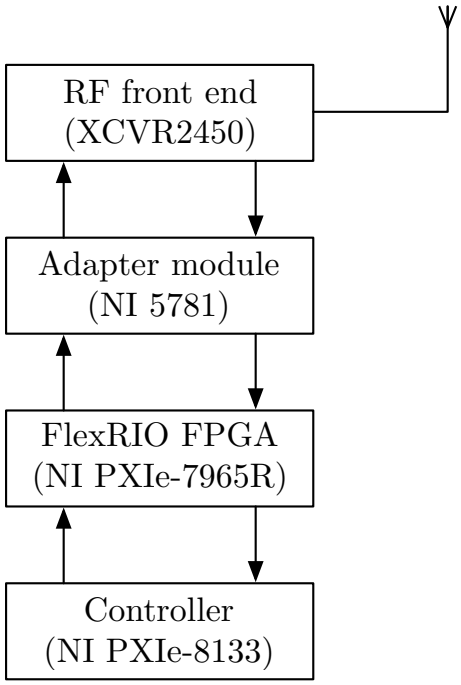

Figure 6.1. A block diagram of the National Instruments SDR platform used for testing the system implementation.

plicated but less time-critical components of the system (namely, channel estimation and computation of the MRC coefficients) are delegated to the controller. These tasks operate in real-time but require far less frequent updates compared to the timing and carrier recovery portions of the system.

In Section 6.1, we discuss the implementation of the core signal processing required by the transmitter. Two alternative (but equivalent) implementations are explored. The rigid pulse shaping filter implementation is preferred in situations where transmitter complexity is a major concern. However, it is found to be somewhat inflexible for certain applications. In particular, it is unable to activate/deactivate subcarriers in order to sculpt itself to the channel conditions (e.g., for dynamic spectrum access applications). It is found that an alternative, slightly higher complexity implementation based on a synthesis filter bank is preferred in order to maintain the degree of flexibility that these applications demand.

In Section 6.2, we discuss the implementation of the core signal processing required by the receiver. This consists of matching the filters of the subcarriers and combining them. Two options that are analogous to those presented for the transmitter are discussed. The two options have trade-offs in terms of computational complexity, performance, and the

ability to sense the spectrum. These are discussed and design recommendations are made in Subsection 6.2.3.

In Sections 6.4–6.6, the problems associated with equalization in a multipath channel, carrier recovery and tracking, symbol timing recovery and tracking, and MRC weight estimation are explored. Section 6.7 explains the benefits and drawbacks associated with adding differential encoding and decoding to the system. Section 6.8 provides a discussion of these techniques and explores the trade-offs. It includes recommendations for system designers regarding the choice and ordering of the algorithms.

Several appendices are included at the end of this thesis that may be useful to system designers. Appendix C contains the details for implementing a variable delay in the analysis polyphase filter bank. Most descriptions of polyphase filter banks assume that the system delay is constant. The variable delay mechanism allows one to compute the outputs at an arbitrary delay within a single baud interval. It is possible to apply this update once every baud interval without observing a transient in the output. Appendix C also contains helpful hints for dealing with delays that fall outside of one baud interval. This is especially important in situations where the sampling clock at the transmitter and receiver are mismatched. After a sufficient amount of time passes, one is likely to need to advance or delay by a full baud interval to avoid dropping data. Appendix D contains a description about the effects of finite word lengths on signal processing. Recommendations are given about choosing the word lengths for various subsystems in the FB-MC-SS architecture.

6.1 Transmitter Core Signal Processing

As discussed in Chapter 3, the transmitter consists of generating a number of narrow band signals. These narrow band signals are each multiplied by a different complex spreading gain γ_k and modulated to nonoverlapping subcarriers. Then, the narrow band signals are summed to obtain the transmit signal. The process can be divided into a symbol sequence that is convolved with a simple pulse shaping filter. Mathematically, this pulse shaping filter can be written as

$$g(t) = h(t) \sum_{k=0}^{L-1} \gamma_k e^{j2\pi f_k t}, \tag{6.1}$$

where $h(t)$ is a square root raised cosine filter, the γ_ks represent the spreading code used, and the f_ks are chosen as in Chapter 3.

The core signal processing requirement at the transmitter is to compute the convolution of this pulse shaping filter with the symbol sequence, $s[n]$, that we desire to transmit. As described in Chapter 3, this operation may be written as

$$x(t) = \sum_{n=-\infty}^{\infty} s[n]\delta(t - nT_b) \star g(t), \tag{6.2}$$

where $x(t)$ is the transmit signal, $s[n]$ is the symbol sequence, $\delta(t)$ is the Dirac delta function, T_b represents the baud interval, $\star$ denotes convolution, and $g(t)$ is as defined in (6.1).

Many options exist for implementing this signal processing structure. Each option results in varying degrees of computational complexity and system flexibility. While we have presented continuous-time equations to describe the system operation, discrete-time signal processing operations may be used to conveniently implement equivalent system blocks. We discuss two implementation options in the subsections that follow, and then present suggestions on their usage to system designers in Subsection 6.1.3.

6.1.1 Rigid Pulse Shaping Filter

The simplest structure for implementing the transmitter is known as the *rigid pulse shaping filter*. The structure is rigid in the sense that its spreading gains are fixed and cannot be changed on-the-fly. This assumption results in a time-invariant closed-form solution for $g(t)$. Thus, the sampled version $g[n] = g(nT_s)$ may be precomputed and stored in a memory for later processing. From here, an efficient implementation of the filter, $g[n]$, is possible.

Consider the fact that $L - 1$ out of every L input samples to the filter are zero (where $T_b = LT_s$ is the baud or symbol interval of our system). We should be able to exploit this fact to achieve an efficient digital implementation. The theory of multirate signal processing was built around this idea, among others [4, 38]. The well-known multirate filtering technique (known as an interpolation filter) reduces the complexity of the pulse shaping filter significantly. A block diagram depicting the structure is shown in Figure 6.2. $R_0(z)$ through $R_{L-1}(z)$ are the Type 2 polyphase components of $G(z)$, where $G(z)$ is the z-transform of $g[n]$. Note that the same symbol is passed through L polyphase filters. Then the polyphase filter outputs are read out in a specific sequence to obtain the output signal. If we use a filter with an impulse response duration equal to K times the baud interval T_b, then each polyphase filter has K discrete-time coefficients. Thus, we require K multiplications and $K - 1$ additions for every output sample.

Furthermore, we recognize the special nature of our input in the case of binary phase-shift keying (BPSK). BPSK provides maximum robustness which is one of the primary goals of

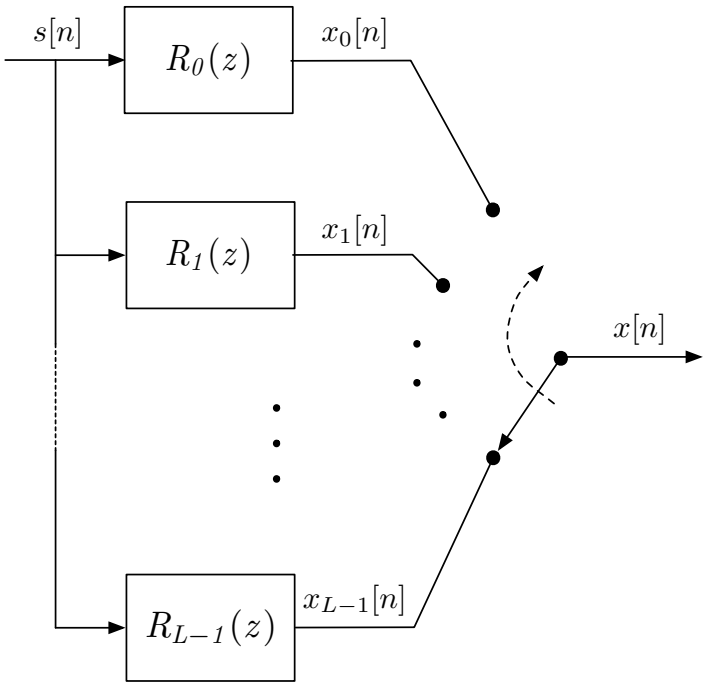

Figure 6.2. A block diagram depicting a polyphase interpolation filter used for implementing the rigid pulse shaping filter.

spread spectrum communications systems. In this case, the input sequence is either $+1$ or -1. But, multiplication by $+1$ or -1 is trivial and only requires an adder/subtractor module. This means that we may implement our filter without any explicit multiplications and only a small number of addition/subtraction operations. If we use a filter with a duration K times longer than the baud interval, then we require $K-1$ addition/subtraction operations per output sample and a memory of size LK.

To reduce the complexity even further, we can choose our spreading gains to have a special structure such that the output is real-valued. Specifically, if we choose gains with conjugate symmetry, specifically if $\gamma_k = \gamma_{L-k}^*$, then $g(t)$ will be real-valued to reduce the computational complexity by a factor of two since every complex-valued adder/subtractor can be replaced by a real-valued adder/subtractor (a real-valued adder/subtractor only requires one half the resources of a complex adder/subtractor).

There is one important drawback to this structure. To change a single γ_k using this structure—or to activate/deactivate a single subcarrier—requires all LK coefficients to be recomputed and reloaded. This process may require a significant number of clock cycles in an FPGA implementation. To make matters worse, the signal should not be transmitted

during this update time to prevent unexpected transients from occurring. These transients would be the result of a pulse shape where half the filter coefficients being updated and the other half not being updated.

6.1.2 Flexible Synthesis Filter Bank

An alternative to the rigid pulse shaping filter is the *flexible synthesis filter bank* or just *synthesis filter bank* structure. This structure requires a block that multiplies the incoming symbols by the desired spreading sequence, then the IFFT of this sequence is computed, followed by a bank of polyphase filters. The IFFT plus polyphase filters follow the classical synthesis polyphase filter bank structure [4, 38]. The only difference is the presence of the common input with the spreader feeding the IFFT.

Implementation of the spreader requires additional memory for retaining the spreading code. Large spreading codes for larger processing gains may be stored in a block RAM on the FPGA. For smaller processing gains, it may be stored in distributed memories. Either way, this significantly increases the footprint of the design compared to the case of the rigid pulse shaping filter.

To reduce the computational complexity, it is possible to cache the IFFT of the spreading sequence and modulate this by the transmit symbol sequence, $s[n]$. Again, in the important case of BPSK symbols, this implies that no multiplication is required, just a sign change on the cached IFFT outputs. If the spreading code changes infrequently, then the cost of computing the IFFT cache is small. As in the case of the rigid pulse shaping filter, we assume the use of a filter with a duration K times longer than the baud interval. In this case, the complexity of the spreading and IFFT operations are amortized over many symbol periods so that they contribute almost nothing to the overall cost. As such, the number of multiplications per output symbol approaches K and the number of additions per output symbol approaches $K - 1$. This is similar to the unoptimized design of the rigid pulse shaping filter from Subsection 6.1.1.

In the case that updates to the spreading coefficients must occur frequently (i.e., when subcarriers are turned on and off regularly), the cost of the IFFT and spreader do not become amortized over many symbol periods. Therefore, the additional computations cannot be neglected. This results in L additional multiplications for the spreading sequence and roughly $L/2 \log_2(L)$ additional multiplications for the IFFT operation. The L multiplications from spreading can easily be replaced with a simple negation (sign inversion) circuit in the important case of BPSK symbol sequences. Thus, the additional cost stems mainly

from the IFFT. The signal processing required to implement the flexible synthesis filter bank is shown in Figure 6.3. The zero inputs at the top and bottom of the IFFT produce a guard band on either side of the baseband signal. This guardband reduces the filtering requirement after the DAC. Additional zeros are inserted between each active subcarrier as per discussion in Section 3.1.

Unlike the rigid pulse shaping filter, the flexible synthesis filter bank design allows the spreading code to be updated from symbol to symbol without worrying about a transient. A single subcarrier may be activated/deactivated in one clock cycle. When adjusting the spreading code, a hybrid combination of the new and old spreading sequence present in the system will not result in a transient discontinuity. Thus, the system need not be disabled during updates to the spreading code as was the case for the rigid pulse shaping filter. Despite its additional complexity, this property makes the synthesis filter bank attractive in situations that require substantial flexibility over the subcarrier activity and/or spreading code.

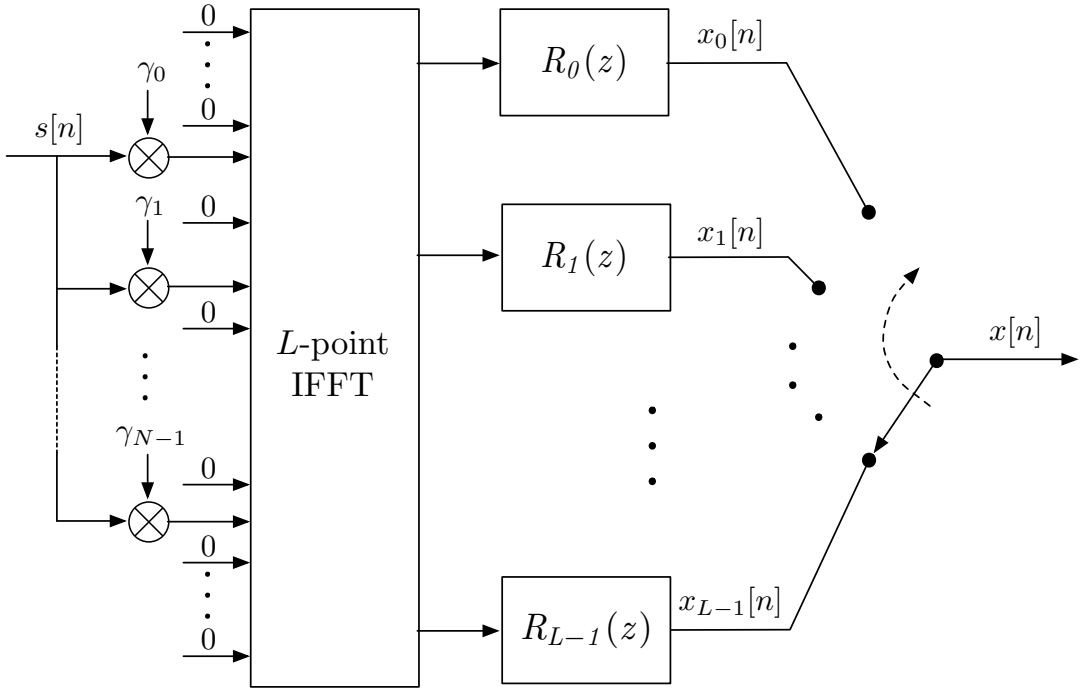

Figure 6.3. Block diagram of a synthesis filter bank implementation at the transmitter, according to the method presented in Subsection 6.1.2.

6.1.3 Discussion: Transmitter Core Signal Processing

Clearly, the rigid pulse shaping filter results in a far smaller resource requirement on the FPGA. It is recommended to use this design in situations where the spreading coefficients do not need to be updated quickly and subcarriers do not need to be activated or deactivated quickly. These restrictions mean that it is not a good fit for cognitive radio and dynamic spectrum access applications where the activation and deactivation of subcarriers is based on availability and must be updated in real-time.

The flexible synthesis filter bank results in the option to update the spreading coefficients on a symbol by symbol basis. The spreading coefficients can be updated by writing to the coefficient memory directly. This very important advantage allows the system to use disjoint bands whenever they are available and evacuate them quickly when the primary users return. For this reason, the flexibility offered by the synthesis filter bank approach is important for cognitive radio and dynamic spectrum access systems. In systems that require these benefits, it is recommended to use the synthesis filter bank even though the computational complexity is greater than the rigid pulse shaping filter.

6.2 Receiver Core Signal Processing

Again, referring to the derivations in Chapter 3, the signal seen at the receiver input may be expressed as

$$y(t) = x(t) \star c_{BB}(t) + \nu(t), \tag{6.3}$$

where $c_{BB}(t)$ is the complex baseband equivalent of the channel impulse response (a series of delta functions with complex-valued gains) and $\nu(t)$ represents the additional noise and interference from the channel. The core signal processing requirement is to consider each of the subcarrier signals and combine them together into a single number that can be used as a sufficient statistic for symbol detection. The method used to achieve this goal may vary depending on the type of performance and complexity that we desire. It may also depend on the type of system. For example, are we trying to prevent interference in a multiuser scenario or are we more concerned with obtaining optimal performance in the presence of malicious jamming attacks?

We present two possibilities for system implementation in the next two subsections. These are both based on filtering operations. The first possibility is analogous to the rigid pulse shaping filter at the transmitter. It requires that a fixed spreading code be known in advance, and it offers a low complexity implementation. Then, we consider a more flexible (and slightly higher computational) alternative, and show the advantages we obtain from

using it. We discuss the advantages and disadvantages of both system implementations and make recommendations for system designers in Subsection 6.2.3.

6.2.1 Rigid Matched Filter

The receiver implementation analogous to the rigid pulse shaping filter is the *rigid matched filter*. We also refer to the outputs of the rigid matched filter as the *simple matched filter* outputs. This terminology is useful in later sections of this chapter. The simple matched filter outputs are useful in synchronization and may be computed using either the rigid matched filter structure or the more flexible filter bank structure with an accumulator at its output.

The rigid matched filter is a finite-impulse response (FIR) filter that is matched to the transmit pulse shaping filter, $g(t)$. Mathematically, this simple matched filter may be expressed as

$$g^*(-t) = h(t) \sum_{k=0}^{L-1} \gamma_k^* e^{j2\pi f_k t}, \tag{6.4}$$

where all quantities are the same as defined for (6.1), and we have used the fact that $h(t)$ is a real-valued even function of time (see Chapter 3). Again, for implementation, it is possible to sample this signal to obtain $g_M[n] = g^*(-nT_s)$. The subscript M in $g_M[n]$ is to clearly identify it as the filter matched to $g[n]$. From here, a polyphase decimation filter may be used to compute only those outputs needed for synchronization and detection [4, 38].

The overall structure is a discrete-time implementation of the following equivalent operation expressed in continuous-time,

$$z(t) = y(t) \star g^*(-t), \tag{6.5}$$

where $z(t)$ represents the simple matched filter output signal. As shown in Chapter 3, when $c_{BB}(t) = \delta(t)$ and $\nu(t) = 0$, the output may be expressed as the product of a Nyquist pulse and a special quantity, $z(t) = p(t)\beta(t)$. In Chapter 3, the special quantity $\beta(t)$ is defined as the sum of L sinusoids, each at one of the active subcarrier frequencies. We repeat the definition here for clarity,

$$\beta(t) = \sum_{k=0}^{L-1} e^{j2\pi f_k t}, \tag{6.6}$$

where all quantities are as defined previously. When the output of (6.5) is sampled at the correct timing phase, $z[nL] = z(nLT_s)$, the output will be a good estimate of the transmitted symbol. For the case of the rigid matched filter, this is the decision statistic

used for symbol detection. One may note that it is essentially the same output that would be achieved by giving equal weight to each subcarrier filter and combining them. Thus, it is equivalent to the equal gain combining (EGC) method discussed in Chapter 3 with its associated strengths and weaknesses. While EGC may have acceptable performance in some applications, it has no optimality properties. To achieve an optimal performance, one requires the flexibility offered by an analysis filter bank.

6.2.2 Flexible Analysis Filter Bank

This section describes an alternative signal processing structure for the receiver. This structure is analogous to the flexible synthesis filter bank used by the transmitter that was outlined in Subsection 6.1.1. We call it the *flexible analysis filter bank* or simply the *analysis filter bank* structure. This structure passes the input signal through a set of polyphase filters feeding an IFFT. Following the IFFT, the subcarrier signals are despread and equalized separately prior to the computation of a weighted average. The weight of each subcarrier signal is made proportional to its SNR. The output is the decision statistic used for symbol detection. This is the MRC block, and it results in a very robust, highly flexible structure.

The polyphase filters plus IFFT are part of the classical analysis polyphase filter bank structure [4, 38]. We assume that the outputs are oversampled by some small integer for synchronization purposes. This integer is typically 1, 2, or 4 for the designs that we consider. For an example with an oversampling factor of 2, see Figure 6.4.

To save space, the despreading operation is not depicted. It may be absorbed into the channel estimator, maximum ratio combiner, and simple matched filter output calculator separately. In implementing the system, it can be convenient for all three systems to share a single despreader block placed at the filter bank output.

The simple matched filter outputs are required for some synchronization algorithms. Other algorithms operate directly on the subcarrier outputs. If algorithms are chosen that do not require the simple matched filter outputs, then it is unnecessary to include the matched filter output calculator.

One obvious advantage of this system is the performance gain obtained through use of the MRC. This gain increase is the result of two different components. First, there is an increased robustness to narrow and partial band interference. Second, the system has an ability to adapt reception according to the signal strengths. This exploits the frequency selectivity of the channel and provides a certain amount of self equalization. For the frequency selectivity gain, the baud interval must be chosen to be much larger than the

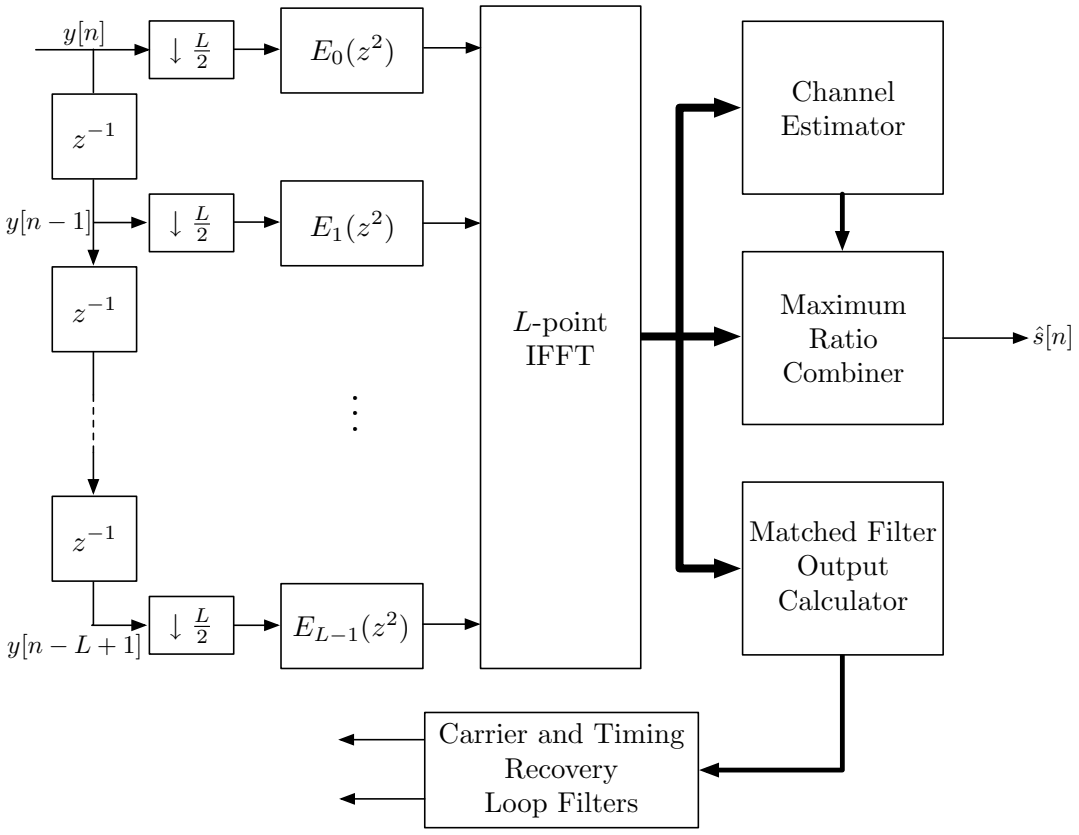

Figure 6.4. Block diagram of the polyphase analysis filter bank used in the receiver design.

delay spread of the wireless channel.

A second important advantage of the filter bank structure is its ability to alter its spreading sequence in mid-operation (i.e., from baud interval to baud interval). This advantage allows codes to change over time, allowing systems to add even more security by altering their spreading sequence in a time-varying manner. This should make such systems even more difficult to detect by unintended receivers. This area will be explored in future research.

A third advantage of the filter bank structure is its ability to compute different timing phase outputs without a transient response. This benefit requires only a modest increase in memory and a few additional multiplexors in the design. This is explored in more details in Appendix C at the end of this chapter. The results are used in Section 6.3 in conjunction with the timing phase recovery and tracking.

A fourth advantage is additional timing and carrier recovery methods that are available based on the filter bank outputs. These methods are based on the wider pulses (in the time

domain) of the subcarrier output signals. Thus, the utility function for timing recovery derived from these outputs is also a wider, more gradually changing function as shown in Section 6.3. Consider what happens if a timing lock is lost due to noise or interference or for some other reason. The simple matched filter output (shown in Chapter 3) has a nice sharp peak at its main pulse; the energy, however, falls off 1–2 samples away from the main pulse. At these locations, the system has very little information about which direction to go. This is not the case for algorithms based on combining the individual utility function of each subcarrier output. More detailed comparisons are provided in Section 6.3. Comparisons of the advantages and disadvantages of carrier recovery methods based on the simple matched filter outputs and the filter bank outputs are available in Section 6.4.

As noted before, if the simple matched filter outputs are desired (e.g., for synchronization), it is possible to compute them from the filter bank outputs. The sum of the filter bank outputs at one time instant is equal to the simple matched filter output at the same instant. Thus, the simple matched filter outputs may be computed by simply running a complex-valued accumulator at the output of the despreader. This is shown as the *matched filter output calculator* in Figure 6.4.

In dynamic spectrum access applications that use cognitive radios, this method of reception results in the ability to sense the spectrum using the filter bank outputs. See Chapter 4 for more details.

6.2.3 Discussion: Receiver Core Signal Processing

The rigid matched filter can be implemented easily but it is unable to adapt its performance to the observed channel. This results in a system that experiences a performance loss similar to DS-SS. To see this, consider that one way of looking at the simple matched filter output is as the output of a match filtered DS-SS signal with a multilevel chipping sequence. The chipping sequence is multilevel because it is not restricted to the alphabet $\{+1, -1\}$ as are PN-coded DS-SS systems. Instead, it is based on the modulated square root Nyquist pulse shapes.

Pursuant to the discussion in Chapter 2, it is clear that optimal performance of the simple matched filter outputs is possible to implement through a perfect rake receiver structure. However, a perfect rake receiver is prohibitively complex to implement, because the exact time delays are unknown and must be estimated with sufficient granularity. Even an approximate rake structure is computationally intensive. It involves several "fingers" scanning for delays where the channel impulse response is significant [1]. Since, however,

the flexible analysis filter bank structure offers the same performance as the rake receiver at only a marginally higher complexity than the rigid matched filter structure—and at a significantly lower complexity than the rake receiver structure—the flexible analysis filter bank plus MRC is preferred. In addition to the decreased computational complexity, it is possible for the system to automatically adapt to channel conditions (through the MRC). This results in significant performance benefits. The system is more robust to timing lock drift. Moreover, the filter bank outputs may be used for sensing the spectrum usage (a key component for effective dynamic spectrum access, see Chapter 4). And, like the flexible synthesis filter bank, the analysis filter bank offers the ability to modify spreading codes on the fly, or even decode orthogonal codes from the same filter bank outputs (e.g., for the downlink of a multiuser system).

In addition to the above advantages, the simple matched filter outputs are readily computed from the flexible filter bank outputs by a simple summation of the latter. In light of this fact and the other advantages of the filter bank structure, this thesis highly recommends that the flexible analysis filter bank approach be adopted for present and future systems. These advantages come at a cost of only a modest increase in complexity. The relative simplicity of the simple matched filter structure seems to be attractive, but it suffers from a disproportionate loss in performance compared to the filter bank plus MRC. On the other hand, the simple matched filter may find advantages in multiple access networks employing FB-MC-SS because the spreading code orthogonality in the downlink would be preserved. This observations was noted for OFDM-based MC-SS systems in [24]. The filter bank structure is still probably preferable for these systems due to its ability to share part of the processing computation of multiple users' codes. That is, the same outputs of an analysis filter bank can be used to decode several orthogonal codes. Such considerations will be examined in future research.

6.3 Timing Recovery and Tracking

Timing recovery at the receiver is an essential part of any communications system. In order for the data to be decoded properly, it must be sampled at the Nyquist rate with an appropriate phase. This unknown parameter must be estimated from the received signal. This is further complicated by the sampling clock offset between the transmitter and receiver. A constant average frequency offset between the clocks will cause a linear drift in the correct timing phase. Besides this linear drift, the sampling clock frequency may also be affected by random clock jitter—a time-variation in the sampling clock frequency.

This means that the drift may oscillate and it further motivates the need for tight tracking algorithms.

Two techniques are proposed in this section for timing recovery. The first technique is based on a periodic scanning of the symbol time. This technique requires that a good reference source is available. For example, a global positioning system (GPS) signal can be used to discipline several clocks wirelessly [93].

6.3.1 Scanning Technique

Timing acquisition with the scanning technique is broken into two parts, a sample slider or a variable delay and the maximization of a utility function. The variable delay is a device that allows one to shift the timing phase at the output of our filter bank (or rigid matched filter) to an arbitrary delay D. Many options are open to a designer for implementation of this variable delay. For a description of one convenient option, see Appendix C.

Mathematically, the sample slider can be represented by a variable delay z^{-D} where D is an integer such that $0 \leq DT_s < T_b$, where T_b is the baud interval and T_s is the sampling interval. L is the total number of subcarriers in the system (active and inactive), and it is the integer value $L = T_b/T_s$. In terms of L, D is restricted to the range $0 \leq D < L$. Delays outside this range wrap back to delays within this range. For advice on dealing with this wrap around problem, refer to Appendix C.

The scanning technique is very simple to understand. Essentially, we compute outputs at all L possible sampling times and average the signal power at these times. If we use the simple matched filter outputs, this results in us observing a sharp peak that we can lock to. For a discussion of the benefits of using the simple matched filter outputs (possibly computed from the filter bank outputs), see Section 6.3.3.

Once locked, tracking the timing phase is possible by continually scanning and updating a running average for each phase offset. This is possible as long as the output of the filter bank is being oversampled. By rotating the coefficients, any phase offset can be calculated by the pipelined filter at any given time. We only require the address of the polyphase components to be read out properly. In one clock cycle, we compute the current output symbol. In the next clock cycle, we compute a sample at an arbitrary delay to measure the power output and update the running average for that output. In this way, we can track the timing phase as long as it varies slowly. Oversampling by a higher factor requires more resources, but allows the scanning to be completed more often, thus offering a more reliable tracking mechanism.

If the scanning technique is used for tracking, it is recommended that one concentrate on timing delays near the currently estimated timing delay. In the case of oscillator drift and jitter, the correct timing phase for the next symbol is more likely to be near the current correct estimate for the present symbol. So, looking at $L-1$ other possible phases is unnecessary and will degrade the performance of the tracking algorithm.

We noted in Section 6.2.2 that the matched filter outputs at the current delay of our system can be calculated by summing the despread subcarrier outputs of the filter bank (see Appendix C for more details). Now, we explain how samples in the vicinity of the current delay may be approximated from the subcarrier outputs. Suppose we desire to compute the simple matched filter output at a small offset, Δ, from the current delay of our system, τ. Recall that the subcarrier outputs are narrow band signals that approximate the frequency response of the received signal. A delay in a narrow band signal is well approximated by a phase shift (for a complex exponential signal, this is not an approximation, but an exact relationship). To estimate the delayed version of the wideband matched filter outputs, we can compute a linear phase shift on the subcarriers prior to the summation. Given the subcarrier outputs $z_k[n] = z_k(nT_b - \tau)$ for a particular baud interval T_b and delay τ, we can compute an estimate of the simple matched filter output at a small additional delay, Δ, as

$$z(nT_b - \tau + \Delta) \approx \sum_{k=0}^{L-1} z_k(nT_b - \tau) e^{\pm 2\pi f_k \Delta}. \tag{6.7}$$

This may be especially useful during tracking to track the outputs near the current estimate of the correct timing phase.

One final observation is in order. It is possible to adjust the delay at the input to the filter bank in addition to the technique described in Appendix C by dropping or inserting a sample at the system input. This possibility seems simple, but it has the disadvantage that a transient occurs in the filter output. As a result, every time the timing phase is adjusted, the disturbed output of the analysis filter bank (because of the incurred transient) may lead to incorrect detection of a number of symbols. This reduces the effectiveness of our scanning technique, because we must wait for the transient to pass prior to beginning our average. This effect is less pronounced if the number of active subcarriers is much smaller than the IFFT size. In that case, however, the computational complexity may be unacceptably high.

6.3.2 Early/Late Gate Technique

The early/late gate technique is a classical technique for timing recovery in single carrier systems [4]. To track the timing phase, we require samples of the matched filter output of

each subcarrier slightly before and slightly after the present time, at times $nT_b - \tau[n] + \Delta$ and $nT_b - \tau[n] - \Delta$, where Δ is some small delay and $\tau[n]$ is the estimate of the correct timing phase at time n. Recall that approximations to these quantities can be calculated following (6.7). Otherwise, these may be calculated by oversampling the subcarrier outputs of the filter bank.

The early/late gate technique consists of computing an estimate for the error in the current timing phase. This can be done by using the simple matched filter output

$$e_0[n] = |z[nT_b - \tau[n] + \Delta]|^2 - |z[nT_b - \tau[n] - \Delta]|^2 \tag{6.8}$$

or else it can be done with the individual subcarrier outputs

$$e_1[n] = |z_k[nT_b - \tau[n] + \Delta]|^2 - |z_k[nT_b - \tau[n] - \Delta]|^2. \tag{6.9}$$

These two different error functions result in optimizing two very different utility functions. The algorithm performance implications of this choice are discussed in Subsection 6.3.3.

Once an estimate of the error is available, we can update our next estimate of the timing phase using a first order loop filter as

$$\tau[n+1] = \tau[n] + \mu e[n], \tag{6.10}$$

where μ is a stepsize parameter chosen to be sufficiently small to guarantee convergence, but sufficiently large to respond quickly to changes in the optimal timing phase.

There is a well-known deficiency in the usage of first order loop filters for PLLs. The estimated phase lags in the presence of a frequency offset. A constant average offset in the oscillator frequency (even a small one) used by the transmitter and receiver for DAC and ADC, respectively, causes a frequency offset. This means that the timing phase will always lag behind the true value unless a second order loop filter is used. This filter should accumulate the error signal. For more information on the effective design of second order PLLs, see [4] and [94].

6.3.3 Discussion: Timing Recovery and Tracking

Successful symbol timing phase recovery at the FB-MC-SS receiver is crucial for successful communication of the FB-MC-SS receiver. The two methods of timing recovery presented in the previous sections are both trying to maximize a utility function. The

maximization of this utility function results in the correct timing phase. Consider the following two utility functions:

$$\Lambda_0(\tau) = \mathbf{E}\left[\left|\sum_{k=0}^{L-1} z'_k(\tau)\right|^2\right], \tag{6.11}$$

and

$$\Lambda_1(\tau) = \sum_{k=0}^{L-1} \mathbf{E}\left[\left|z'_k(\tau)\right|^2\right] \tag{6.12}$$

where $\mathbf{E}[\cdot]$ represents the expectation operator (taken over the ensemble of waveforms), $z'_k(t)$ represents the signal from the kth subcarrier filter at time t after despreading (following the same notation used in Chapter 3), and τ is the delay being considered. Take note that the resulting output of the summation in (6.11) is equivalent to the simple matched filter output at time τ. Either utility function may be used in either of the two timing recovery methods discussed previously (i.e., scanning or early/late gate). In each case, however, there is clearly a pessimal and superior performing utility function. Which function is best-suited to the task of timing recovery is dependent on the technique chosen. Specifically, (6.12) is best used for the early/late gate technique, while (6.11) is preferred for the scanning technique.

To better understand which utility function works best with which technique, three plots of the utility functions are provided for three different processing gains. Refer to Figures 6.5–6.7. The correct timing phase has been set to $\tau = 0$. The solid lines correspond to the utility function calculated from the simple matched filter output, $\Lambda_0(\tau)$. The dashed lines correspond to the utility function calculated from the average of the individual subcarrier outputs, $\Lambda_1(\tau)$.

To simplify our discussion, we define two quantities, B_0 and B_1. We define B_0 to be the length of time in the interval from the first null of $\Lambda_0(\tau)$ at a delay less than zero to the first null of $\Lambda_0(\tau)$ at a delay greater than zero. We define B_1 similarly but use $\Lambda_1(\tau)$ instead of $\Lambda_0(\tau)$. We call B_m the *dilation factor* for the timing recovery utility function $\Lambda_m(\tau)$. This quantity may be expressed mathematically as

$$B_m = \tau_{m,+1} - \tau_{m,-1}, \tag{6.13}$$

where $\tau_{m,+1}$ corresponds to the first time $\Lambda_m(\tau) = 0$ as τ varies from $\tau = 0$ towards positive infinity (by increasing τ) and $\tau_{m,-1}$ corresponds to the first time $\Lambda_m(\tau) = 0$ as τ varies in the opposite direction. Due to the symmetry of the utility functions, $\tau_{m,+1} = -\tau_{m,-1}$. For

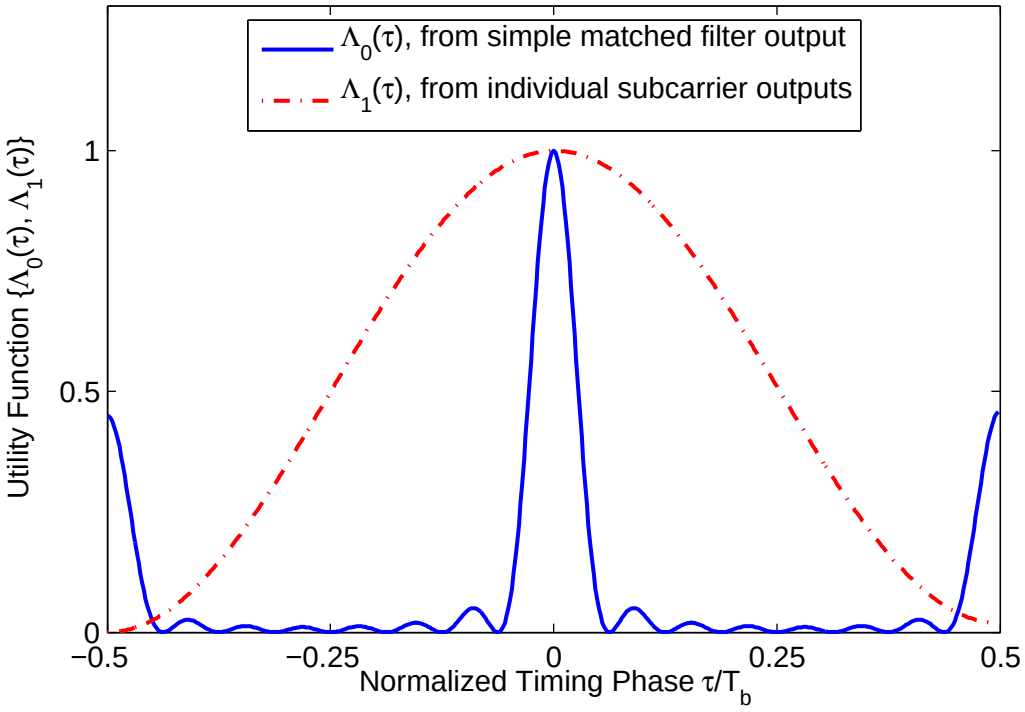

Figure 6.5. This figure presents timing utility functions with processing gain of 16.

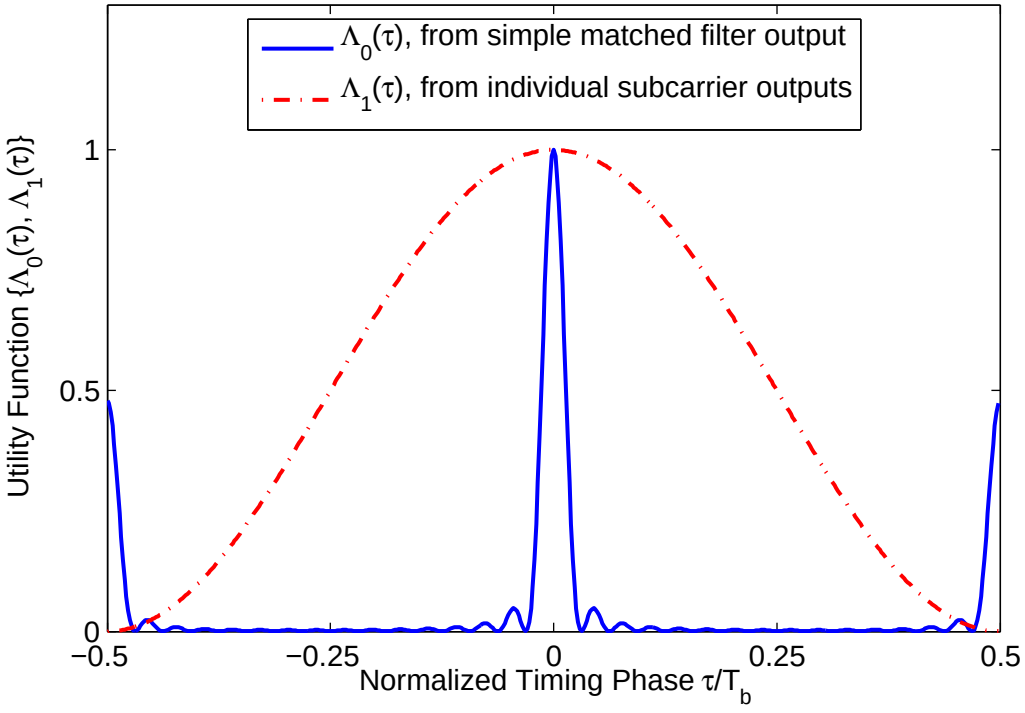

Figure 6.6. This figure presents timing utility functions with processing gain of 32.

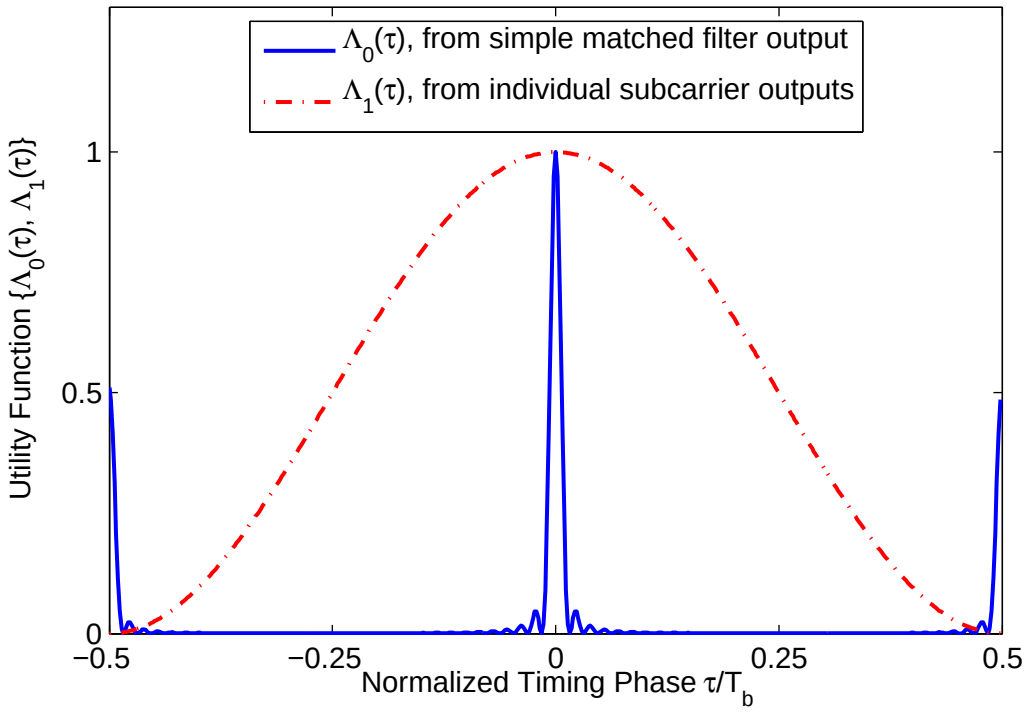

Figure 6.7. This figure presents timing utility functions with processing gain of 64.

the parameters we have used—specifically, the prototype filter roll-off ($\alpha = 1.0$), the baud interval (T_b), and the processing gain ($2L$)—the quantity B_0 has a closed-form solution given by

$$B_0 = \frac{T_b}{L}. \tag{6.14}$$

Clearly, as the processing gain increases for a given baud interval, B_0 decreases. The shape of the utility function, $\Lambda_0(\tau)$, is equivalent to summing L equally spaced sine waves. This summation results in a periodic sinc-like function with period equal to T_b and two local maxima at the timing instants, $\tau = \pm T_b/2$. These are the instants furthest from the correct timing phase.

Now consider the shape of $\Lambda_1(\tau)$. As the processing gain increases, the shape of $\Lambda_1(\tau)$ remains constant. It is simply a raised sinusoidal shape with a maximum at the correct sampling instant and minima at the least correct sampling instants. This is exactly what we expect from the single carrier equivalent timing recovery systems [4]. As a result of this unchanging shape, it is clear that the dilation factor B_1 must also be constant. Thus, we can observe from Figures 6.5–6.7 that the dilation factor for $\Lambda_1(\tau)$ is equal to

$$B_1 = T_b. \tag{6.15}$$

This is the largest dilation factor possible for a given baud interval T_b. This large dilation factor indicates that $\Lambda_1(\tau)$ varies much more slowly from its maximum to lower values as the delay τ is varied. The dilation factor of $\Lambda_0(\tau)$ is an adjustable system parameter. It decreases as the number of active subcarriers, L, increases. As L approaches infinity, the dilation factor, B_0, approaches zero. This extreme case results in a utility function with a perfect impulse at the correct timing.

From this analysis, it is clear that the two utility functions are very different. The function $\Lambda_1(\tau)$ is gradual and its global maximum corresponds to its local maximum. Furthermore, the derivative of this function at any point (except exactly at the minimum) indicates the direction one should move to locate the maximum. This is precisely what is required for the early/late gate timing recovery technique to be effective.

The function $\Lambda_0(\tau)$ has a very sharp peak. Its derivative outside of the main pulse is basically useless in determining the direction to follow. For this reason, it will only be effective with the early/late gate technique in the case that it is initialized correctly. If the lock is ever lost, then the early/late gate technique will be lost and randomly wander around until it stumbles back into the main pulse again. This would result in unnecessary and unacceptable bursts of data being lost.

On the other hand, $\Lambda_0(\tau)$ provides a very clear peak that is easily distinguished in the presence of uncorrelated noise and interference sources. For this reason, it is a perfect fit for the scanning technique. Given a sufficiently large processing gain (by increasing L), it can be used to identify and determine all unique multipath components. In the case of using the simple matched filter for communication, this may be extremely helpful. Applying $\Lambda_1(\tau)$ to the scanning technique is also possible. However, $\Lambda_1(\tau)$ results in a much less precise estimate of the timing phase.

If a suitable reference clock source (e.g., a GPS disciplined clock) is available, then the scanning technique can be used to lock to the correct timing. In this case, the drift should be very slight so that updates to the timing phase during tracking can be handled effectively by monitoring only those outputs near the correct sample timing. These can be estimating using (6.7) or computed explicitly by oversampling the filter bank outputs.

If a suitable reference clock source is unavailable, then the early/late gate technique provides a more stable solution for tracking the timing phase. In this case, the gradual utility function $\Lambda_1(\tau)$ should be used for the reasons discussed previously. If the early/late gate technique is used for tracking, it should be accompanied by a second order loop filter which integrates the error. Without an appropriate second order loop filter, the constant

drift between the transmitter and receiver sampling clocks may cause the algorithm to perform poorly.

In some setups, a hybrid technique is useful. Scanning can be used to initially obtain a close estimate, then early/late gate can be used for tracking. This is the setup that was used for the implementation in [33]. It has a relatively fast convergence, and then tracks the timing update to avoid the problems associated with timing drift.

6.4 Carrier Recovery and Tracking

Successive symbols (or samples) of the received signal contain all of the necessary information for carrier recovery. In the presence of a carrier frequency offset, successive samples are rotated. It is possible to estimate the amount of offset by measuring the amount of rotation. Initial carrier acquisition should be activated after the initial estimate of the correct timing phase (e.g., using one of the algorithms in Section 6.3) has converged. This is important, because the information needed for carrier recovery is contained in the signal when sampled at the appropriate timing.

Once again, we have the option of dealing with subcarriers on an individual basis and averaging the result or dealing with the simple matched filter outputs. Figure 6.8 shows a comparison of the simple matched filter output and the output for single subcarrier with index $k = 1$. Figure 6.9 shows the same comparison in the presence of a carrier frequency offset. The plot includes markers $(*)$ at the correct sampling instants. Notice that in Figure 6.8, these correspond to the transmit symbol stream exactly. This is the case for $z(t)$ and $z_1(t)$, but $z_1(t)$ is at a lower power level since is is only one subcarrier out of 128 total subcarriers. The sequence used for the construction of this output was $\{+1, +1, -1, -1, -1, +1, -1, +1\}]$.

Examining Figure 6.9, it is obvious that something is wrong with the samples at the correct timing instants. They appear to be rotating as a direct result of the carrier frequency offset. Also, the samples at the instants spaced $T_b/2$ away from the correct symbol spacings are strange. Due to aliasing and poor overlapping filters, these components do not have the characteristic of being $-s[n]$ when $s[n] = s[n-1]$ and 0 when $s[n] = -s[n-1]$ as was discussed in Section 6.3.

To better understand, we examine the subcarrier outputs under the flat channel approximation. Using this approximation, the output of the kth subcarrier matched filter may be written

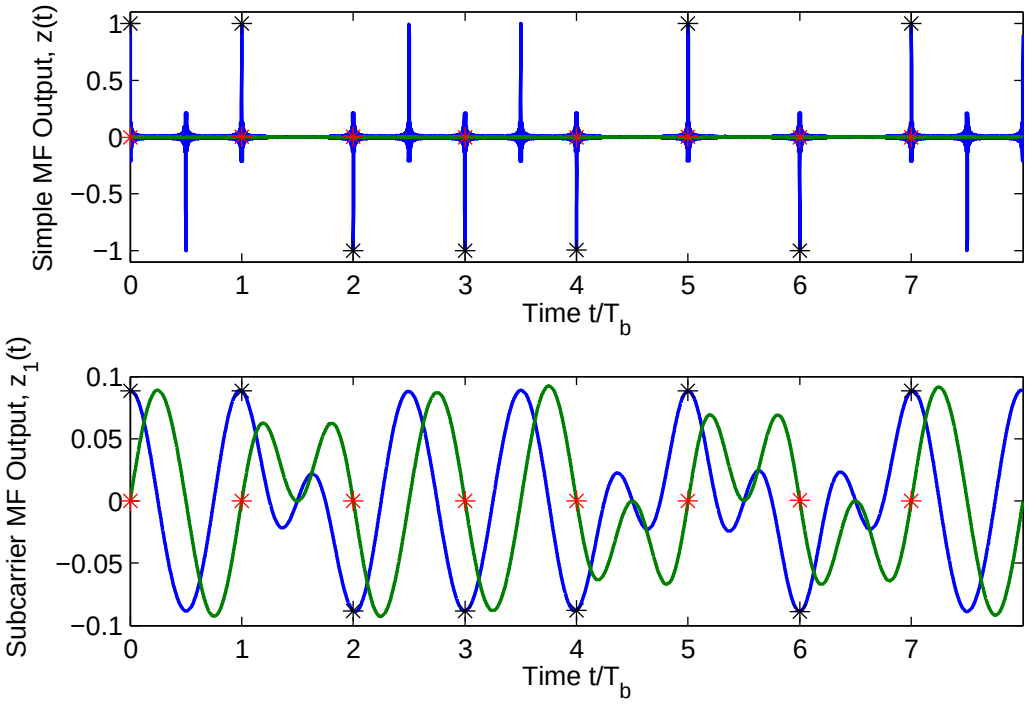

Figure 6.8. Comparison of a single subcarrier output $z_1(t)$, and the simple matched filter output $z(t)$ without carrier offset. The system processing gain is 256.

$$z_k(t) = \left(\sum_{n=-\infty}^{+\infty} s[n]\gamma_k C_{BB}(f_k) p_T(t - nT_b) e^{j2\pi f_k t} \right) \star \left(p_R(t) e^{j2\pi(f_k + \Delta f_c)t} \right). \tag{6.16}$$

Interestingly, when Δf_c is a multiple of the subcarrier spacing, $f_1 = 1/LT_b$, several subcarrier filters will align and yield output signals with the Nyquist property. The spreading code will be off by some integer multiple, but timing recovery will function normally. This is one of the primary reasons that timing recovery should always be done prior to carrier recovery for the proposed FB-MC-SS system.

6.4.1 Coarse Carrier Recovery

Coarse carrier recovery is necessary whenever the RF local oscillator performance is insufficient to guarantee that the receiver subcarrier frequencies are overlapping the correctly transmitted subcarrier frequencies. If the subcarrier bandwidths are chosen sufficiently large, this is not a problem. However, a large bandwidth subcarrier results in a poorer performance (due to ISI caused by a non-flat subcarrier channel distortion as well as a reduction in processing gain). The resulting received signal will be spread differently than expected by the despreader. Specifically, it will be rotated by an integer number of

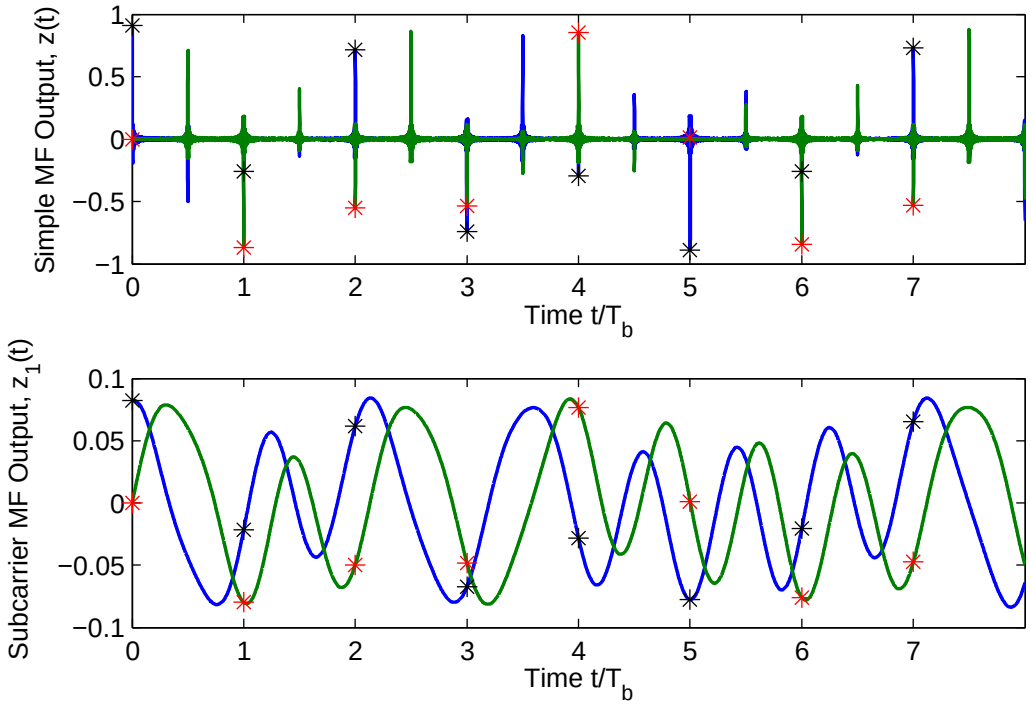

Figure 6.9. Comparison of a single subcarrier output $z_1(t)$, and the simple matched filter output $z(t)$ with carrier offset. The system processing gain is 256.

subcarriers. This is the problem that coarse carrier recovery attempts to correct. It ignores any offset smaller than one subcarrier spacing and leaves such offsets to be dealt with by the fine carrier recovery algorithms.

The idea is very simple and relies on cross-correlating the known spreading sequence with the subcarrier outputs. In other words, we compute the quantity

$$\zeta_c(p) = \left| \sum_{k=0}^{L-1} \gamma^*_{(k-p)} z_k(nT_b) \right|^2 \tag{6.17}$$

for various integer values of p to find the one that maximizes the utility function, $\zeta_c(p)$. Here, we ignore any subcarrier that falls out of our IFFT length. If it is required to ignore too many chips, this reduces the processing gain of the system. However, if the system uses oversampling (e.g., only half of the possible subcarrier bandwidth is used), then the reduction in processing gain is unlikely to occur, because the shift would have to be $L/2T_b$ which presumably would be very large (and therefore unlikely). This is true even for low cost RF oscillators.

We note that in practice, one should only be required to scan through a small number of possible offsets, p. The exact value of p can be determined by carefully examining

the data sheets for the oscillators used at the transmitter and receiver. From there, one may calculate the maximum possible offset. It is then recommended to test all possible offsets (using a technique similar to the scanning approach for timing recovery described in Subsection 6.3.1).

Once the maximum offset has been identified, the frequency of the demodulator at the input to the filter bank is adjusted by pf_1 where f_1 is the subcarrier spacing used in the filter bank. After coarse carrier recovery is complete, there still may be a small residual offset. This is handled by the fine carrier recovery algorithms described in Subsection 6.4.2. Coarse carrier recovery is only required at the beginning of transmission, before fine carrier recovery is begun.

6.4.2 Fine Carrier Recovery

Without loss of generality, we assume that the system is centered such that the optimum timing phase is zero, i.e., $\tau_o = 0$. This allows us to omit it from the indexing operations for brevity and clarity. We perform the following transformation of the symbol stream to extract the carrier offset information,

$$\zeta_f(nT_b) = \text{sign}\left(|z((n-1/2)T_b)| - 1/2\right) z(nT_b)z^*((n-1)T_b) \tag{6.18}$$

where the subscript f is used because this quantity is used as part of the fine carrier recovery algorithms. Note that the first factor, $\text{sign}\left(|z((n-1/2)T_b)| - 1/2\right)$, acts as a kind of equalizer allowing the technique to be independent of the transmitted symbol sequence. As noted previously, the samples $z((n-1/2)T_b)$ are equal to $-s[n] = -s[n-1]$ when the symbols are the same (with a rotation caused by the channel). When the underlying symbols are different and there is no offset, the sample $z((n-1/2)T_b)$ is zero. When there is a frequency offset, it remains small. See Figure 6.9 for visual evidence of this claim.

The fact that we are using the underlying symbols, one might consider this technique to be a decision-directed technique. However, the symbol information is extracted from the signal itself. We do not require a decision of each symbol value to construct (6.18). We extract only the desired information rather than waiting for the output of a symbol detector. This process has two advantages. First, it is faster to compute since we do not need to wait for a decision on the symbol to be made. Second, it prevents decision error propagation from affecting our carrier recovery algorithm. Thus, we may also think of this as a blind technique—a technique that requires no knowledge of the transmit symbol sequence.

From the quantity $\zeta_f(nT_b)$, we can directly obtain an estimate of the residual carrier frequency offset as

$$\Delta\hat{f}_c = \frac{1}{2\pi T_b}\angle\left\{\frac{1}{M}\sum_{n=0}^{M-1}\zeta(nT_b)\right\}. \tag{6.19}$$

A single complex multiplier can compute $\zeta(nT_b)$ as in (6.18) and this may be passed through an efficient moving average filter. This technique can be derived graphically by looking at the examples presented in Figure 6.8 and Figure 6.9. From these, it is clear that the rotation between adjacent symbols results in the BPSK constellation rotating. Multiplying two of these symbols together with one conjugating results in a product with a constant phase offset. The carrier frequency offset may be extracted from this information. We combine our estimates in an average in the same spirit as [11] where it was shown that such a combining leads to an maximum likelihood estimate for other multicarrier systems (i.e., OFDM).

It is clear from this derivation that the frequency offset is resolvable to within $\pm 1/2T_b$. We have already guaranteed that our offset lies in this range using coarse carrier recovery. The only thing left is to track the offset so that any jitter or drift in the oscillators' frequencies does not cause excessive degradation to our system.

6.4.3 Modifications for Tracking

For tracking the carrier offset, the complex number $\zeta(nT_b)$ is calculated as in (6.18). This sequence is passed through an efficient moving average filter. Then the angle and magnitude of the average are calculated using a coordinate rotation digital computer (CORDIC) algorithm [95]. This provides us with an estimate of the carrier frequency offset (6.19). Once we have obtained this offset, it is unlikely to change quickly or abruptly. Thus, the system should avoid changing abruptly. To achieve this, one may use the estimate with a small stepsize parameter. This is expressed in the following discrete time update equation,

$$\Delta\hat{f}_c[n] = \Delta\hat{f}_c[n-1] + \mu\frac{1}{2\pi T_b}\angle\left\{\frac{1}{M}\sum_{n=0}^{M-1}\zeta(nT_b)\right\}. \tag{6.20}$$

A very important change to $\zeta_f(nT_b)$ may be made for the purposes of tracking. We note that the simple matched filter outputs were used to calculate $\zeta_f(nT_b)$. It is equally possible to use the subcarrier outputs themselves. This has the added advantage that we may calculate a weighted average according to the MRC. This offers us an additional robustness in the presence of strong narrow band jamming. This is only possible once estimates of the

MRC weights are available which is why we did not use it earlier. However, for the purposes of a more robust tracking algorithm, we may calculate

$$\zeta'_f(nT_b) = \text{sign}\left(\left|\sum_{k=0}^{L-1} w_k z_k((n-1/2)T_b)\right| - 1/2\right)\sum_{k=0}^{L-1} w_k z_k(nT_b) z_k^*((n-1)T_b) \qquad (6.21)$$

where $\zeta'_f(nT_b)$ is the modified quantity, $z_k(t)$ is the subcarrier output, and w_k is the MRC weight associated with the kth subcarrier output. This change is especially required if strong narrow band jamming is expected to occur over some portion of the transmission band.

6.4.4 Discussion: Carrier Recovery and Tracking

The carrier recovery happens just after timing synchronization as been achieved. First, the coarse carrier recovery is estimated and corrected. Shortly after correcting for the coarse carrier offset, the fine carrier recovery is activated. Once this results in reliable channel estimates and MRC weights, the fine tracking is activated using the MRC to compute the update equation.

The order of operation here is very important and should be enforced by implementing an appropriate state machine (either in software on the host or in the FPGA). An alternative based on differential encoding/decoding is explored in Section 6.7. The advantage of the differential encoding/decoding is that it reduces the effects of carrier offset, sampling clock drift, and greatly simplifies channel estimation (by producing a new "effective" channel).

As noted above, the carrier recovery laid out here depends on the output of the filter bank being oversampled by at least 2. Without this oversampling, the blind carrier recover can be replaced by a decision-directed method, but those methods rely on accurate symbols before convergence can be guaranteed. This is not realistic, so the proposed technique is the blind technique described above.

6.5 Channel Estimation

After carrier recovery, the filter bank outputs pass through a despreader block and are sent via a first-in first-out (FIFO) buffer to the host controller. The general purpose processor (GPP) performs a least squares estimate of the channel coefficients. If desired, channel updates can occur with each new symbol. It is, however, more practical to update the channel only occasionally to reduce the communication overhead required between the host and the FPGA. The channel coefficients are fed back from the controller to the FPGA and are used to equalize (align the amplitude and phase) of the filter bank outputs.

If each subcarrier filter is sufficiently narrow band, the channel gain for each subcarrier is well-approximated by a constant. This is the flat channel approximation. The constant should be equal to the complex baseband frequency response evaluated at the subcarrier center frequency. Thus, the received symbol on subcarrier k yields

$$z_k(nLT_b) = s[n]\gamma_k C_{BB}(f_k) + \theta_k(nLT_b). \tag{6.22}$$

Here, $s[n]$ is the transmit symbol, γ_k is the spreading gain, $C_{BB}(f_k)$ is the baseband equivalent channel gain evaluated at the subcarrier frequency f_k, and $\theta_k(nLT_b)$ is an additive interference-plus-noise term. We assume the channel impulse response is K samples long and define the following vectors and matrices.

$$\mathbf{A} = \begin{bmatrix} 1 & 1 & \cdots & 1 \\ e^{j2\pi f_0 T_b} & e^{j2\pi f_1 T_b} & \cdots & e^{j2\pi f_{N-1} T_b} \\ \vdots & \vdots & \ddots & \vdots \\ e^{j2\pi f_0 K T_b} & e^{j2\pi f_1 K T_b} & \cdots & e^{j2\pi f_{N-1} K T_b} \end{bmatrix}^H \tag{6.23}$$

$$\mathbf{\Gamma} = \text{diag}\{\gamma_0, \gamma_1, ..., \gamma_{N-1}\} \tag{6.24}$$

$$\mathbf{z}(nT_b) = \left[z_0^*(nT_b), z_1^*(nT_b), ..., z_{N-1}^*(nT_b)\right]^H \tag{6.25}$$

$$\boldsymbol{\theta}(nT_b) = \left[\theta_0^*(nT_b), \theta_1^*(nT_b), ..., \theta_{N-1}^*(nT_b)\right]^H \tag{6.26}$$

Let the vector $\mathbf{c}$ represent the (time-domain) channel impulse response. Now, (6.22) can be rewritten into a matrix equation involving the channel impulse response as follows.

$$\mathbf{z}(nT_b) = s[n]\mathbf{\Gamma A c} + \theta(nT_b) \tag{6.27}$$

This can be used at each time instant to obtain a least squares estimate for the channel impulse response, $\mathbf{c}$. However, when the channel is known to be a slow fading channel, the updates can occur much less frequently. Since BPSK is used, the least-squares solution can estimate the channel within a phase offset of π without knowledge of $s[n]$.

Based on these equations, a least squares estimate of the channel is possible based on the reception of a single symbol as

$$\hat{\mathbf{c}}[n] = \hat{s}[n]\left(\mathbf{A}^H\mathbf{A} + \rho\mathbf{I}\right)^{-1}\mathbf{A}^H\mathbf{\Gamma}^H\mathbf{z}(nT_b), \tag{6.28}$$

where we have included $\rho\mathbf{I}$ as a regularization parameter to counter balance the presence of noise in the subcarriers. It is also possible to identify extremely noisy subcarriers and remove those rows from the least squares estimation. Note that multiplying by $\hat{s}[n]$ is

optional if there is another mechanism for distinguishing between the π phase ambiguity of the result. It has been found experimentally that averaging (6.27) over multiple time instants prior to calculating the least squares estimate is beneficial in practice. To perform this average, one must take care not to cancel out the useful information. For example, if $s[n]$ and $s[n-1]$ are opposite in sign, then adding them will result in the useful parts cancelling out. A practical means of accomplishing this using the preliminary estimate from (6.28) is given by first defining the following quantity,

$$\mathbf{d}[n] = \mathbf{A}^H \mathbf{\Gamma}^H \mathbf{z}(nT_b), \tag{6.29}$$

and using it to obtain the estimate,

$$\hat{\mathbf{c}}[n] = (1-\beta)\hat{\mathbf{c}}[n-1] + \beta \text{sign}\left(\text{Re}\left\{\hat{\mathbf{c}}^H[n-1]\mathbf{A}^H\mathbf{d}[n]\right\}\right)\left(\mathbf{A}^H\mathbf{A}\right)^{-1}\mathbf{d}[n], \tag{6.30}$$

where β is a parameter chosen to control the system responsiveness to changes in the channel variation. Valid choices for β are $0 < \beta < 1$.

Finally, we note that it is often more convenient to maintain a vector of the frequency response instead of the channel impulse response. This vector is easily obtained from the channel impulse response as $\hat{\mathbf{C}}_{BB} = \mathbf{A}\hat{\mathbf{c}}$.

6.6 MRC Weight Estimation

The MRC is a critical component for the robust system operation. If the MRC weights are estimated correctly, the system will have optimal performance. If the weights are not updated correctly or quickly enough, the system performance will be degraded. We examine first a decision-directed method for estimating the interference-plus-noise variance.

It is preferable to estimate MRC weights after equalizing the data streams, because then they become much less dependant on amplitude. This leads us to the first technique, decision-directed MRC weight updates.

6.6.1 Decision-Directed Method

The simplest scheme for estimating the variance of the interference-plus-noise term on each subcarrier is based on subtracting an estimate of the current symbol as

$$\hat{\sigma}_k^2[n] = \frac{1}{M}\sum_{m=0}^{M-1} |z_k'((n-m)T_b) - C_{BB}(e^{j2\pi f_k})\hat{s}[n-m]|^2. \tag{6.31}$$

This is a simple estimator, but it requires knowledge of the symbols. Trying to use the MRC to calculate the symbols and then using the symbols to calculate the MRC seems

suspicious. Although it can be done, if there are errors in one side, it will have a significant impact on the other due to this reliance.

6.6.2 Semiblind Method

Signals at various outputs of the analysis filter bank are phase aligned. These phase-aligned signals are called $z'_k(nT_b)$ and are computed as

$$z'_k(nT_b) = \frac{\gamma_k^* z_k(nT_b)}{C(f_k)}. \tag{6.32}$$

At this point, an estimate of the noise and interference variance $\sigma_k'^2$ for each subcarrier is required and must be tracked so that the system is able to adapt to interference dynamically. Using BPSK modulation, this can be accomplished with the following estimator.

$$\hat{\sigma}_k'^2 = \frac{1}{M} \sum_{n=0}^{M-1} |z'_k(nLT_s)|^2 - 1 \tag{6.33}$$

where M controls how quickly the system responds to changes. The averaging is computed efficiently with one block RAM, one adder, one subtractor, and an arithmetic shift. Once the noise variances are known, they must be inverted and stored in a block RAM for usage as part of the MRC block.

The decision statistic from the maximal ratio combiner is computed as

$$\hat{s}[n] = \sum_{k=0}^{N-1} \frac{\frac{1}{\hat{\sigma}_k'^2} z'_k(nLT_s)}{\sum_{m=0}^{N-1} \frac{1}{\hat{\sigma}_m'^2}}. \tag{6.34}$$

The MRC block cycles through the phase-aligned filter bank outputs and multiplies each by its associated MRC weight, accumulating the products. The accumulated total is used to make a decision regarding the symbol. The symbols are converted to bits and sent through a DMA FIFO to the host controller. The host controller sends the data over ethernet to the host PC for analysis.

6.6.3 Discussion: MRC Weight Estimation

The decision-directed technique of (6.31) is useful in situations where the symbols can be estimated reliably. This is especially true when FB-MC-SS operates in a band without much interference. In this case, the subcarrier SNRs remain the same.

One problem that has been encountered experimentally from implementing (6.33) is that it has a hard time detecting when a signal is not present. That is, if the noise level is the only signal on a particular subcarrier (due to spectral sculpting of the signal around

primary users for instance), it continues to suppose that the symbol exists. This could be fixed with a statistical hypothesis test periodically run on each different subcarrier. If the hypothesis that the signal is not present is greater than some threshold, that subcarrier should be ignored. This was not a problem with (6.31).

6.7 Differential Encoding

To alleviate the problems of timing offset and carrier offset, a differential encoding at the transmitter may be used. This encoding will be called $s'[n]$ and it is given as

$$s'[n] = s'[n-1]s[n] \tag{6.35}$$

which leads to a required decoding stage at the receiver to obtain the information sequence,

$$s[n] = s'[n](s'[n-1])^*. \tag{6.36}$$

If this differential encoding is applied at the transmitter, the received sequence on the kth subcarrier, $z_k[n] = z_k(nT_b)$, becomes

$$z_k[n] = s'[n]c_k e^{j\frac{2\pi\Delta_T k}{L}nT_b} e^{j2\pi\Delta_F nT_b} + \nu_k[n]. \tag{6.37}$$

where $\Delta_T k$ is the frequency offset induced by the sampling clock oscillator mismatch at the kth subcarrier and Δ_F is the frequency offset induced by the carrier oscillator mismatch (constant for all subcarriers). Now, the original symbol sequence can be recovered through some clever manipulations of this sequence without channel estimation, carrier recovery, or sampling frequency offset correction. It should be noted that the correct timing phase is still required on each subcarrier signal. This can be accomplished in the same manner as the case without differential encoding (e.g., through scanning or early/late gate). The outputs of the differential detector are computed as follows

$$z_k[n](z_k[n-1])^* = \left(s'[n]c_k e^{j\left(\frac{2\pi\Delta_T k}{L}+2\pi\Delta_F\right)nT_b}\right)\left(s'[n-1]c_k e^{j\left(\frac{2\pi\Delta_T k}{L}+2\pi\Delta_F\right)(n-1)T_b}\right)^* + \xi_k[n] \tag{6.38}$$

where $\xi_k[n]$ represents the altered noise and unwanted cross-terms. This can be manipulated through basic algebra to yield

$$z_k[n](z_k[n-1])^* = s'[n](s'[n-1])^*|c_k|^2 e^{j\frac{2\pi\Delta_T k}{L}T_s} e^{j2\pi\Delta_F T_s} + \xi_k[n]. \tag{6.39}$$

Now, we can replace the first two factors on the right-hand side, $s'[n](s'[n-1])^*$, with $s[n]$ from (6.36) to obtain

$$z_k[n](z_k[n-1])^* = s[n]|c_k|^2 e^{j\frac{2\pi\Delta_T k}{L}T_s} e^{j2\pi\Delta_F T_s} + \xi_k[n]. \tag{6.40}$$

This has resulted in a new (pseudo) channel c'_k given by the following

$$c'_k = |c_k|^2 e^{j\frac{2\pi\Delta_T k}{L}T_s} e^{j2\pi\Delta_F T_s} \tag{6.41}$$

which we can estimate using any technique we wish. We note that for a small enough Δ_T and a small enough Δ_F, this is approximately equal to $|c_k|^2$ which is purely real. Following this assumption, the differentially decoded outputs are in fact (slightly) rotated and scaled versions of the information sequence. This can be seen from

$$z_k[n](z_k[n-1])^* = s[n]c'_k + \xi_k[n]. \tag{6.42}$$

To perform maximum ratio combining at the receiver, one simply needs to estimate the new signal-to-noise ratio for each subcarrier k,

$$\mathtt{SNR}_k = \frac{|c'_k|^2}{\sigma^2_{\xi_k}}, \tag{6.43}$$

and use these to form the new maximum ratio combining weights.

Differential encoding/decoding has given us insights into how we might be able to estimate Δ_T and Δ_F in our system. In addition, it greatly simplifies the receiver removing the need for many of the synchronization blocks required in the nondifferentially encoded case. However, it should be noted that this comes at a price. That price is a loss in performance. This results because our matched filters are slightly off, and we are multiplying two noisy symbols to obtain a (slightly) noisier symbol.

6.8 Summary and System Design Advice

A snapshot of the spectrum measured over-the-air with an FB-MC-SS system in operation is presented in Figure 6.10. Note the strong null associated with the multipath channel. The MRC automatically adapts the FB-MC-SS signal to obtain optimal performance in the presence of such problems. Also, it is important to notice that the signal has a sharp roll-off from its passband to its stopband. The roll-off of FB-MC systems in general is much sharper than other multicarrier systems.

For the proper operation of an FB-MC-SS communications system, all of the subsystems presented in this chapter must be implemented correctly. Primarily, this consists of sampling the baseband signal, locating and locking to the correct timing phase, correcting the carrier frequency offset, estimating the channel coefficients, estimating the maximum ratio combining weights, and ultimately detecting which symbol was transmitted.

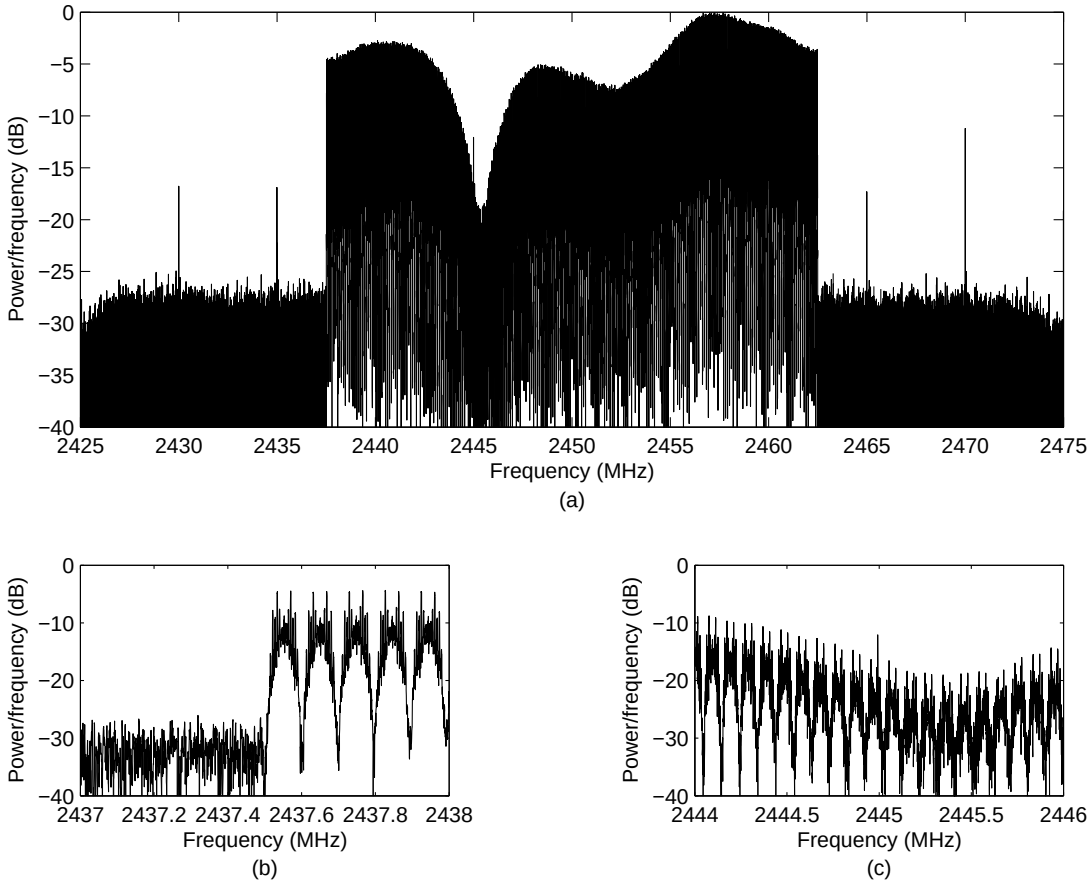

Figure 6.10. This figure shows the measurement of the spectrum of an FB-MC-SS system operating over-the-air in a laboratory environment. Part (a) is a zoomed out version of the spectrum. Part (b) is zoomed in on the edge of the FB-MC-SS band. Part (c) is zoomed in on the null area.

A simpler option is to use differential encoding. This technique only requires the received signal to be locked to the correct timing, and the effective channel is in a very simple form. These advantages are not free. The differential encoding is known to cause some degradation in system performance [1]. Following the timing lock and channel estimation, an MRC detector may be used to estimate the symbols. Small carrier frequency offsets will not degrade the system performance much, but larger offsets would still need to be corrected. Correcting smaller offsets will result in better system performance.

Due to the performance losses associated with differential encoding, we focus on the former (coherent) receiver. To implement this system, the subsystems in that have been discussed must be turned on and off in a specific order. This can be accomplished via a

state machine (either on the FPGA or on the host). The order that these steps must be executed is given now.

1. Timing recovery on
2. Wait for a lock
3. Coarse carrier recovery on
4. Wait for a lock
5. Coarse carrier recovery off
6. Fine carrier recovery/tracking on
7. Wait for a lock
8. Channel estimation on
9. MRC weight estimation on
10. Detector on

This results in a system that will activate and, if the expected FB-MC-SS signal is present, will properly decode the transmitted symbol stream.

The appendices have hints on dealing with some of the finer details of system implementation. For example, a description of calculating arbitrary outputs in a single symbol period from a polyphase filter bank is given in Appendix C. Finally, Appendix D provides a brief introduction to the effects of fixed point numbers. It includes an overview of how these effects influence the implementation of the FB-MC-SS system and makes a few suggestions that, if followed, can greatly improve performance of the system.

CHAPTER 7

CONCLUSION AND FUTURE WORK

7.1 Conclusion

This thesis studied the class of multicarrier spread spectrum systems that are built based on filter banks, focusing on spreading in the frequency domain. We refer to this class as FB-MC-SS systems. The idea of constructing communication systems based on FB-MC-SS has been in the literature for the past two decades. However, all published works have been limited to basic theoretical studies of the idea. This thesis, for the first time, reports a practical implementation of an FB-MC-SS system. The proposed and developed design is based on the filtered multitone (FMT) modulation [96]. In FMT, the subcarrier bands do not overlap. This yields an isolated signal for each subcarrier (chip) of the system.

In terms of theory, we gave a detailed analysis to show that the proposed FMT-based FB-MC-SS system provides the maximum possible processing gain compared with other multicarrier spread spectrum systems. This was shown in Appendix A. We also compared the performance of our design with that of a direct-sequence spread spectrum (DS-SS) system with an optimal rake receiver. This study showed that when the processing gain of both systems is large and the channel is subject to an additive white noise, both systems (FB-MC-SS and DS-SS) result in equivalent performance. This observation is important because while the FB-MC-SS design that is presented in this thesis is very practical and can be easily implemented, the optimum rake receiver for DS-SS is very difficult (if not impossible) to implement.

On the practical side, the propsed FMT-based FB-MC-SS system was implemented on a software-defined radio (SDR) platform. Its functionality was tested in a harsh radio environment. Algorithms for symbol timing acquisition and carrier recovery as well as their tracking were developed. Their satisfactory functionality was tested on the SDR platform through physical experimentation. We also compared the results of the FB-MC-SS transceiver to a DS-SS transceiver to show its robust performance when the received signal

is subject to strong parial band interference.

The thesis also discussed two applications of the proposed FB-MC-SS system. FB-MC-SS was identified as an ideal candidate for a control channel in cognitive radio systems. It allows transmission at a level comparable or below that of other users' noise levels. This allows the system to remain almost invisible to the primary users of the spectrum. It can also easily be adapted to avoid transmission over portions of the spectrum that are in use by the primary users after these portions have been identified. In addition, the receiver filter bank provides a high quality spectrum sensing mechanism that allows occupied portions of the spectrum to be identified efficiently and correctly.

The second application of FB-MC-SS is as a spread spectrum system in general. These systems have found usage in applications ranging from defense to personal communications. Judging by the equivalent performance of FB-MC-SS and DS-SS in the same bandwidth, it is possible to see that applications where DS-SS has been found useful are the same applications where FB-MC-SS will also be useful. Of course, the added advantages of FB-MC-SS are brought to the table.

7.2 Future Work

This section discusses the future work. Some of this work is already being looked at. The other parts are in the pipeline to be examined at a later time.

7.2.1 Cognitive Radio Networks

One of the most attractive applications of FB-MC-SS is the promise it holds to operate as a control channel for cognitive radio networks. At present, several experiments with the system operating over-the-air show the promise of using it as a control channel. However, it has not been fully deployed in a real operating environment. Attempts to apply FB-MC-SS in cognitive radio networks are ongoing.

In addition to obtaining information about the physical layer, higher layers need to be looked at. Of particular interest to cognitive radios is an interaction between the physical layer and the medium access control (or link) layer. The effectiveness of this interaction either enhances or reduces the ability of a cognitive radio to meet the requirement of operating without impact to the primary users. Cross layer optimizations are extremely important to avoid interfering with primary users and still maintain a high quality of service for secondary users. More research needs to be done in this important area.

7.2.2 Multiuser Scenario

A very important application of spread spectrum systems is related to multiuser scenarios. Multiuser spread spectrum systems rely on orthogonal (or pseudo-orthogonal) codes to separate the various users. In the single user scenario, the MRC detector results in an optimal performance. In the presence of multiple users, this detector must be modified to one that maintains the orthogonality of the various users' codes. Further research in this area needs to be done to identify the best a detection algorithm that performs optimally.

Additionally, the synchronization algorithms have been designed with a single user in mind. Most of these still apply in the presence of multiple users for the downlink. However, the uplink should be considered. For example, each user will have a different multipath channel impulse response. In this scenario, what is the best timing phase for multiuser detection? Additional information may be available in the presence of multiple user signals to provide answers. This question and ones like it are extremely important for multiuser systems.

7.2.3 Algorithms

The algorithms presented in Chapter 6 were focused on having a simple implementation with a reasonable performance. However, with the notable exception of the channel estimation, no derivation of the optimality of the algorithms is given. It would be an interesting problem to consider the optimal joint estimator for carrier offset, sampling clock offset, timing phase, channel estimation, and interference-plus-noise variance. This problem involves a highly correlated multidimensional probability density function, and it will most likely require extensive simulation and analysis to understand it fully. Such information would be useful to determine and compare the performance of practical algorithms to the performance of theoretically optimal (even if impractical) algorithms.

APPENDIX A

DERIVATION OF PROCESSING GAINS

This appendix derives the processing gain for an FMT-based spread spectrum system. It is shown that the processing gain is the same for FMT modulation versus other multicarrier modulation formats. FMT leads to a simple implementation and better narrow band interference suppression. For these reasons, it is chosen as the modulation of choice for the FB-MC-SS system considered in this thesis.

Consider an FMT-based spread spectrum transceiver system that consists of the L-fold expander, the transmit filter $g[n]$, an additive white Gaussian noise (AWGN) channel, and an FMT-based spread spectrum receiver consisting of the matched filter $g^*[-n]$, an L-fold decimator, and a gain of $1/N$, as in Figure A.1. As noted earlier in this chapter, when the channel is AWGN, the receiver in Figure A.1 delivers the same output as the MRC. Hence, the output $\hat{s}[n]$ is that of an optimum detector. We also recall the definition for the processing gain

$$\mathcal{G} = \frac{\rho_{\text{out}}}{\rho_{\text{in}}} \tag{A.1}$$

where ρ_{in} and ρ_{out} denote SNR at the receiver input and output, respectively.

It also follows from Figure A.1 that

$$\rho_{\text{in}} = \frac{\sigma_x^2}{\sigma_\nu^2} \tag{A.2}$$

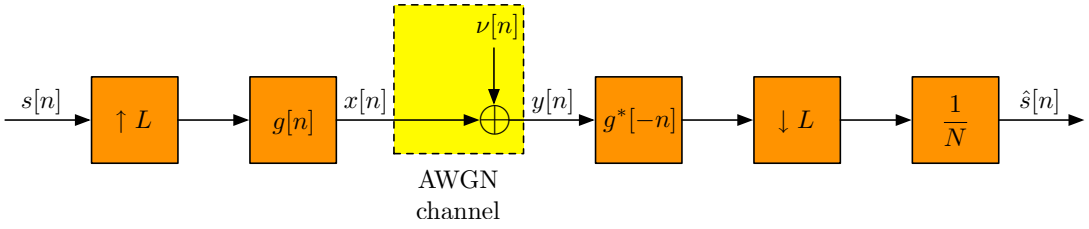

Figure A.1. An FMT-based spread spectrum transceiver model with an AWGN channel.

and thus,

$$\rho_{\text{in}} = \frac{N\sigma_s^2}{L\sigma_\nu^2} \tag{A.3}$$

where σ_x^2 and σ_ν^2 are the variances of $x[n]$ and $\nu[n]$, respectively, and the second line follows since

$$\sigma_x^2 = \sigma_s^2 \times \frac{1}{L} \times \frac{1}{2\pi}\int_0^{2\pi} |G(e^{j\omega})|^2 d\omega,$$

and it follows from (3.4) that

$$\frac{1}{2\pi}\int_0^{2\pi} |G(e^{j\omega})|^2 d\omega = \frac{N}{2\pi}\int_0^{2\pi} |H(e^{j\omega})|^2 d\omega = N.$$

On the other hand, the detector output $\hat{s}[n]$ may be written as

$$\hat{s}[n] = s[n] + \nu_{\text{out}}[n] \tag{A.4}$$

where $\nu_{\text{out}}[n]$ is the noise at the detector output. Moreover, it follows from Figure A.1 that

$$\sigma_{\nu_{\text{out}}}^2 = \sigma_\nu^2 \times \frac{1}{2\pi}\int_0^{2\pi} |G^*(e^{j\omega})|^2 d\omega \times \frac{1}{N^2} = \frac{\sigma_\nu^2}{N}. \tag{A.5}$$

Hence

$$\rho_{\text{out}} = \frac{\sigma_s^2}{\sigma_{\nu_{\text{out}}}^2} = \frac{N\sigma_s^2}{\sigma_\nu^2} \tag{A.6}$$

Substituting (A.3) and (A.6) into (A.1), we obtain $\mathcal{G} = L$.

The interesting result here is that the processing gain depends on the total bandwidth used (L times the width of the prototype filter). It does not depend on having a uniform power distribution in the band, and it does not depend maximizing the number of subcarriers, N, used in the band. This observation may be counter intuitive. Following the results from DS-SS, one's intuition may suggest that the processing gain should be equal to the number of spreading gains of the system. In FMT-based spread spectrum, this is equal to the number of subcarriers, N. This peculiar result is related to the magnitude response of the pulse-shaping filter $g[n]$. Recall from Figure 3.3(a) that $g[n]$ is a multiband filter with N subcarrier bands. The receiver matched filter $g^*[-n]$ also has the same magnitude response. When the channel noise passes through this matched filter, its spectrum is shaped and, accordingly, part of its power is removed. The signal part of the received signal, $x[n]$, on the other hand, has a multiband spectrum that matches the receiver matched filter and thus passes through it without any spectral removal.

Therefore, one finds that FB-MC-SS using FMT obtains the same processing gain as more complicated schemes that use overlapping subcarriers. Consequently, it sees a similar

performance, but it greatly simplifies the implementation as discussed elsewhere in this thesis. In addition, the subcarrier signals achieve better spectral isolation which leads to a better narrow band interference suppression effect. For these reasons, FMT is the multicarrier modulation of choice for the FB-MC-SS modulation scheme developed in this thesis.

APPENDIX B

DERIVATION OF MRC WEIGHTS

This appendix derives the MRC estimator given by (3.28). Substituting the channel gain estimates, $\hat{C}_{BB}(e^{j2\pi f_k})$, for the actual channel gains, $C_{BB}(e^{j2\pi f_k})$, in (3.25), after a simple rearrangement, we obtain

$$s'_k[n] = \frac{\gamma_k^*}{\hat{C}_{\mathrm{BB}}(e^{j2\pi f_k})} z_k(nT), \tag{B.1}$$

where

$$s'_k[n] = s[n] + \frac{\gamma_k^*}{\hat{C}_{\mathrm{BB}}(e^{j2\pi f_k})} \vartheta_k(nT), \quad \text{for } k = 0, 1, \cdots, N-1, \tag{B.2}$$

are a set of noisy estimates of $s[n]$. The goal is to combine these noisy estimates to construct an unbiased estimate of $s[n] = \mathbf{w}_o^H \mathbf{s}'[n]$ with a minimum variance. Here, $\mathbf{s}'[n]$ has the corresponding entries $s'_k[n]$ for its kth element. This construction can be made as

$$\hat{s}[n] = \mathbf{w}_o^{\mathrm{H}} \mathbf{s}'[n] \tag{B.3}$$

where

$$\mathbf{w}_o = \arg\min_{\mathbf{w}} E[|\mathbf{w}^{\mathrm{H}} \boldsymbol{\vartheta}'[n]|^2] \qquad \text{subject to the constraint } \mathbf{w}^{\mathrm{H}}\mathbf{u} = 1, \tag{B.4}$$

$\boldsymbol{\vartheta}'[n]$ has the elements $\frac{\gamma_k^*}{\hat{C}_{\mathrm{BB}}(e^{j2\pi f_k})} \vartheta_k(nT)$, and $\mathbf{u}$ is a vector of length N with elements of 1. This problem can be solved using the method of Lagrange multipliers, [42]. The result is

$$\mathbf{w}_o = \frac{1}{\mathbf{u}^T \mathbf{R}^{-1}_{\vartheta'\vartheta'} \mathbf{u}} \mathbf{R}^{-1}_{\vartheta'\vartheta'} \mathbf{u} \tag{B.5}$$

where $\mathbf{R}_{\vartheta'\vartheta'} = E[\boldsymbol{\vartheta}'[n] \boldsymbol{\vartheta}'^{\mathrm{H}}[n]]$. Moreover, the variance of the estimation error is obtained as $E[|\mathbf{w}_o^{\mathrm{H}} \boldsymbol{\vartheta}'[n]|^2] = 1/(\mathbf{u}^T \mathbf{R}^{-1}_{\vartheta'\vartheta'} \mathbf{u})$. Hence, assuming that $E[|s[n]|^2] = 1$, the signal to interference plus noise ratio (SINR) at the decision device input is obtained as

$$\frac{E[|s[n]|^2]}{E[|\mathbf{w}_o^H \boldsymbol{\vartheta}'[n]|^2]} = \mathbf{u}^T \mathbf{R}^{-1}_{\vartheta'\vartheta'} \mathbf{u}. \tag{B.6}$$

Since in our design the subcarrier bands are nonoverlapping, $\mathbf{R}_{\vartheta'\vartheta'}$ is a diagonal matrix. Then, using σ_k^2 to denote the variance of $\vartheta_k(nT)$, we obtain

$$\mathbf{R}_{\vartheta'\vartheta'} = \begin{bmatrix} \frac{\sigma_0^2}{|\hat{C}_{\mathrm{BB}}(e^{j2\pi f_0})|^2} & 0 & \cdots & 0 \\ 0 & \frac{\sigma_1^2}{|\hat{C}_{\mathrm{BB}}(e^{j2\pi f_1})|^2} & \cdots & 0 \\ \vdots & \vdots & \ddots & \vdots \\ 0 & 0 & \cdots & \frac{\sigma_{N-1}^2}{|\hat{C}_{\mathrm{BB}}(e^{j2\pi f_{N-1}})|^2} \end{bmatrix}. \tag{B.7}$$

Using (B.7) in (B.5). Following the principal of maximum ratio combining, we obtain the minimum variance estimate with the weight vector

$$\mathbf{w}_o = \frac{1}{\sum_{k=0}^{N-1} \frac{|\hat{C}_{\mathrm{BB}}(e^{j2\pi f_k})|^2}{\sigma_k^2}} \begin{bmatrix} \frac{|\hat{C}_{\mathrm{BB}}(e^{j2\pi f_0})|^2}{\sigma_0^2} \\ \frac{|\hat{C}_{\mathrm{BB}}(e^{j2\pi f_1})|^2}{\sigma_1^2} \\ \vdots \\ \frac{|\hat{C}_{\mathrm{BB}}(e^{j2\pi f_{N-1}})|^2}{\sigma_{N-1}^2} \end{bmatrix}. \tag{B.8}$$

Here, σ_k^2 is the variance of $\vartheta_k(nT)$ which was obtained by averaging the magnitude squared output of (3.26).

APPENDIX C

IMPACTS OF SAMPLING CLOCK DRIFT

Due to offsets and jitter between the sampling clocks used at the transmitter and receiver, the optimal timing phase is randomly time-varying. The sampling clock offset results in an optimal phase that, on average, varies linearly with time. The sampling clock jitter results in random fluctuations in the optimal timing phase. If the correct offset is not tracked continuously, this results in a pair of related, but distinct, problems.

The first problem results from incorrectly sampling the matched filter output. Recall that the matched filter output is a Nyquist pulse (due to the square root Nyquist pulse used at the transmitter and receiver). Thus, the output must be sampled at the correct timing phase to avoid ISI. This is true for single carrier and multicarrier systems. Indeed, it is true for all digital communications systems.

The second problem is more subtle. It involves the rotation of the phase of subcarrier outputs due to the clock mismatch that accumulates over time. This occurs even when the interval is shorter than the sampling quantization level (continuous-time) where we call it a subsampling timing offset. This problem is discussed in more details in Section C.1.

As the mismatch accumulates, eventually a new sampling time at the output results in lower ISI than the current time. This is tracked through the timing recovery algorithms presented earlier in this chapter. This problem is a result of incorrect timing at the same quantization level as the receiver sampling clock. Additionally, the phase rotation is still an issue. A structure for adjusting the output of the polyphase filter bank without a transient is given in Section C.2.

A third problem, called the wrap around problem, is associated with a mismatch at the symbol quantization level. This is an extension of the method used to compute an output at a variable offset.

C.1 Phase Rotation Problem

The phase rotation on each subcarrier output results from the receiver polyphase filter structure. The polyphase filter structure uses aliasing to downconvert the sampled signal

$$z_k[n] = p[n]e^{j2\pi f_k n T_s} \tag{C.1}$$

to baseband. Here, $p[n]$ is a Nyquist-L filter, $f_k T_s$ is the normalized subcarrier frequency at the input rate of the filter bank. If $f_k T_s = k/L$ as it was designed at the transmitter, then decimating the signal at the appropriate timing phase results in

$$z_k[nL] = p[nL] \tag{C.2}$$

as expected. Now, consider what happens when $f_k T_s = (k + \epsilon)/L$. Decimating at the correct sampling phase results in

$$z_k[nL] = p[nL]e^{j2\pi\epsilon n/L}. \tag{C.3}$$

Thus, the symbols rotate over time, resulting in some symbols being added out of phase if not compensated. This reduces the system processing gain. The rotation is related to the optimal sampling time moving on a small enough scale that it cannot be tracked (unless a much finer quantization of time is used). For example, the optimal timing phase may lie halfway between sample $z_k[nL]$ and $z_k[nL + 1]$ at sample $z_k[nL + 1/2]$. This value is not possible to compute from the output of the polyphase filter bank without unacceptable increases in the algorithm complexity.

To correct this problem, phase compensators should be used on the subcarrier outputs to compensate for the rotation during equalization. This requires the phase offsets to be tracked. We note that the rotation is a linear function of the subcarrier frequencies. Therefore, it is possible to estimate it well using a least-squares technique since there are N active subcarrier signals, and only 1 unknown parameter (the linearly varying rate of rotation). If no phase compensator is used, then the system will suffer a loss in processing gain. The reduction can be reduced by increasing the IFFT size of the analysis filter bank, but this requires more resources and may be prohibitive for some designs.

C.2 Variable Delay

Whenever the delay accumulates to one complete sampling period, the filter bank output should be computed at a new delay and the phase equalizers should be adjusted. The variable delay block used to compute an output at an arbitrary input sampling phase allows

the system to stay on track in this case. This section now explains the signal processing details for computing an output at a specified delay using a modification to the classical analysis polyphase filter bank structure. A similar approach could be used for designs that employ the rigid matched filter when implemented using a polyphase structure. The details of that approach are essentially the same as described here, but the polyphase filter outputs are summed instead of passing them to the IFFT for further processing.

To implement the analysis polyphase filter bank, the prototype filter $h[n]$ is divided into its L polyphase components, $E_0(z)$ through $E_{L-1}(z)$. We assume that $h[n]$ has been time-limited to a duration of K baud intervals where K is a small positive integer (typically 4 or 5). If this is not the case (i.e., the filter is time-limited to a fractional number of baud intervals), one may of course zero-pad $h[n]$. With this assumption, the Z-Transform of $h[n]$ is

$$H(z) = \sum_{n=0}^{KL-1} h[n]z^{-n}. \tag{C.4}$$

The kth polyphase component of $H(z)$ is thus given by

$$E_k(z) = \sum_{l=0}^{K-1} h[k + lL]z^{-l}. \tag{C.5}$$

Note that the prior assumption implies that $h[n]$ has KL coefficients. Hence, each polyphase component has K coefficients.

If we wish to include a variable delay D at a granularity of one sample (i.e., the shift must be an integer number of input sampling periods) in our filter implementation, then we can achieve this by constructing a new prototype filter with delayed coefficents. This can be made more clear by recalling that the system output of the filter $h[n]$ to an input signal with Z-Transform $X(z)$ is

$$Y_1(z) = X(z)H(z) \tag{C.6}$$

and the output with respect to a delayed version is

$$Y_2(z) = z^{-D}X(z)H(z). \tag{C.7}$$

Due to the associative property of multiplication, we can group the variable delay either with the input signal to obtain

$$Y_2(z) = X_D(z)H(z) \tag{C.8}$$

where $X_D(z) = z^{-D}X(z)$ or we can group the delay with the filter to obtain

$$Y_2(z) = X(z)F(z) \tag{C.9}$$

where $F(z)$ is a based on a new filter, $f[n]$, which is identical to $h[n]$ delayed by D samples. Recall that $F(z)$ is time-limited, whereas $X(z)$ in general is not. Thus, shifting $H(z)$ is easier and may be done without a transient in the output provided that the tap delay line for $f[n]$ is the same tap delay line used for $h[n]$ prior to the shift.

As noted above, the new prototype filter, $f[n]$, is equal to a shifted version of the old prototype filter, i.e., $f[n] = h[n - D]$. This follows from the grouping choice made in (C.9). Explicitly, we have $F(z) = z^{-D}H(z)$. We decompose this filter into its polyphase components. The kth polyphase component is obtained as

$$E'_k(z) = \sum_l h[k + lL - D]z^{-l} \tag{C.10}$$

where it is understood that $h[n]$ is zero outside of the range $0 \leq n < KL$. Careful examination of (C.10) and its comparison with (C.5) reveals that

$$E'_k(z) = \begin{cases} z^{-1}E_{L+k-D}(z) & k < D \\ E_{k-D}(z) & k \geq D. \end{cases} \tag{C.11}$$

Therefore, we recognize that we can compute the output of the analysis filter bank at any delay D that we choose. We may do so in real-time without any transients by circularly shifting the polyphase component filters and adding a unit delay whenever $k < D$.

In our design, $h[n]$ is a square root Nyquist filter. For simplicity, we ignore multipath effects, the spreading code, and noise/interference to improve presentation clarity. Examine the impulse response of the kth subcarrier filter, $H_k(z)$, which may be expressed as

$$H_k(z) = H(ze^{-j\frac{2\pi kn}{L}}). \tag{C.12}$$

One important observation is that the filters are not centered at baseband (with the possible exception of the zeroth subcarrier). The output of the filter bank for the kth subcarrier is then a modulated version of a Nyquist filter, $p[n] = h[n] \star h[n]$. The output of the kth filter to an impulse may be expressed as

$$z_k[n] = p[n]e^{j\frac{2\pi kn}{L}}. \tag{C.13}$$

We have used $z_k[n]$ to represent the filter bank outputs to remain consistent with the usage elsewhere in this thesis. This should not be confused with z from the Z-Transform. The distinction should be clear from context, because the time domain signal, $z_k[n]$, will always be accompanied by a time index. When decimated at the correct timing phase, the impulse response is simply the Kronecker delta function (i.e., $p[nL] = \delta[n]$) as expected. However,

if we are off of the true timing phase by $m \neq 0$ samples, this results in the complex impulse response $p[nL+m]$ being rotated by $2\pi km/L$ radians.

This observation has important ramifications for computing the simple matched filter outputs from the filter bank outputs. Therefore, it is important to consider this effect when the scanning technique associated with the utility function $\Lambda_0(\tau)$ in this chapter is chosen for timing phase acquisition. This technique relies on computing the simple matched filter outputs. To avoid an additional filter, it is best to obtain the simple matched filter outputs from the outputs of the filter bank. Without compensation, each subcarrier output is rotated by a linear phase offset. Summing these outputs to compute the matched filter output will fail, because the outputs will cancel each other (due to their phase misalignment).

To better understand the problem, consider the Z-Transform of the modulated filter for the kth subcarrier, denoted $H_k(z)$. This may be expressed as

$$H_k(z) = \sum_{n=0}^{KL-1} h[n] e^{j\frac{2\pi kn}{L}} z^{-n}. \tag{C.14}$$

Now, consider the delayed version of this filter, $z^{-D}H_k(z)$. This may be expressed as

$$z^{-D}H_k(z) = \sum_{n=D}^{KL-1+D} h[n-D] e^{j\frac{2\pi k(n-D)}{L}} z^{-n}. \tag{C.15}$$

Now, we may replace the index n by another index $n' = n - D$ to obtain

$$z^{-D}H_k(z) = z^{-D} \sum_{n'=0}^{KL-1} h[n'] e^{j\frac{2\pi kn'}{L}} z^{-n'}. \tag{C.16}$$

This is the correct output that we desire. Take particular note of the complex exponential modulating this filter. Note that it begins at a sample that is delayed D times, but its initial phase at the starting instant is 0 radians. In deriving the variable delay previously, we did not consider the initial phase of the complex exponential modulating our filters. In fact, we have it set up so that the phase of the complex exponential is 0 radians at $n = 0$ instead of 0 radians at $n = D$. If no compensation is performed, we will have actually implemented

$$e^{j\frac{2\pi kD}{L}} z^{-D}H_k(z) = z^{-D} \sum_{n'=0}^{KL-1} h[n'] e^{j\frac{2\pi k(n'+D)}{L}} z^{-n'}. \tag{C.17}$$

Note the additional phase rotation factor out front. This is the linear phase offset that we referred to previously.

From the discussion above, it should be clear that one may compensate for this effect by multiplying the filter bank outputs, $z_k[n]$, with the appropriate phase compensation.

This ensures that the complex exponential has zero phase at the desired delay D. A block diagram of this system is presented in Figure C.1. The phase is determined both by the desired delay D and by the subcarrier index k, thus we obtain a new output

$$\dot{z}_k[n] = z_k[n]e^{-j\frac{2\pi kD}{L}}. \tag{C.18}$$

The output $\dot{z}_k[n]$ should be used in place of $z_k[n]$ when computing the simple matched filter outputs and associated quantities such as the utility function $\Lambda_0(\tau)$. If additional latency is acceptable, there is an efficient option for computing $\dot{z}_k[n]$. One may circularly shift the output signals from the polyphase filters before inputting them to the IFFT. It is a well-known property of the IDFT that circularly shifting the input results in a linear phase offset at the output [4]. Exploiting this well-known property of the IDFT does not require storage for the complex exponential values nor does it require an additional multiplier. It does, however, require an additional buffer to circularly shift the signals, and it increases the latency of computation by approximately L clock cycles. A block diagram of this structure is presented in Figure C.2.

Another important observation is that the modulated Nyquist pulse does not affect the envelope of the output impulse response. This, in turn, implies that it does not affect the utility function $\Lambda_1(\tau)$ described in this appendix. In the case that timing

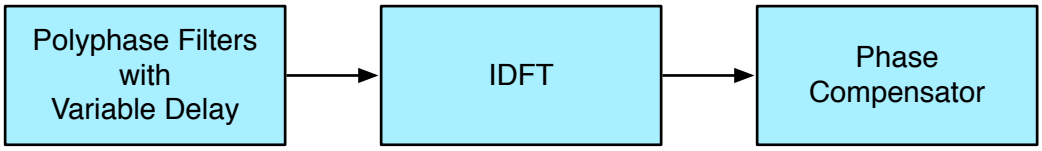

Figure C.1. Proposed architecture for adding a variable delay to the analysis filter bank. The phase compensator multiplies each subcarrier output by the appropriate amount.

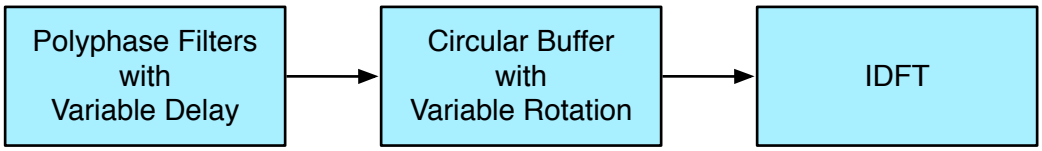

Figure C.2. Proposed architecture for adding a variable delay to the analysis filter bank. The circular buffer is used to compensate for the phase rotation.

recovery is accomplished using the early/late gate technique, the outputs do not need to be compensated before being used to compute the error signal.

For practical implementations, the input is fed serially from the analog-to-digital converter to the processing blocks. A down counter keeps track of which polyphase component is to be computed. Then, the correct coefficients are loaded from a set of block RAMs initialized with the coefficients, $h[n]$. Following this, a column of multiplexers is used to zero pad the first coefficient or the last. Finally, these outputs go to the chain of multiply-accumulators to compute the next filter output. This is just one example implementation that uses the technique described in this appendix. Other implementations derived from the technique described in this appendix are also possible.

In the case of sampling clock offsets, the timing phase will drift. This requires that delays greater-than $L-1$ or less-than 0 are eventually required. This requires additional processing to handle cases when the a delay is required that wraps from $NL+L-1$ to $(N+1)L$. This implementation detail is extremely important for practical systems.

APPENDIX D

FINITE WORD LENGTH

At the time of this writing, FPGAs are not equipped to deal with floating point numbers efficiently. The reason for this is that floating point arithmetic requires far more resources than integer arithmetic. For this reason, most DSP designs in FPGAs are required to use integer (or equivalently fixed point) arithmetic if the real-time performance, parallelism, and low latency of FPGAs are desired for a particular application.

We assume that fixed point numbers are required. We briefly review the structure of these numbers. We assume the two's complement representation is used. The leftmost bit in the representation is the most significant bit (MSB)—the bit with the highest weight. The rightmost bit is the least significant bit (LSB)—the bit with the lowest weight. There is a binary point. The weight of the bit to the left of the binary point is one. The weights increase and decrease as powers of 2.

Consider a number $(b_3\, b_2\, b_1\, b_0\, .\, b_{-1}\, b_{-2}\, b_{-3}\, b_{-4})_2$ as a collection of bits. The subscript 2 indicates that this is a binary representation. The value of this number may be expressed in terms of its bits as

$$(b_3\, b_2\, b_1\, b_0\, .\, b_{-1}\, b_{-2}\, b_{-3}\, b_{-4})_2 = -b_3 \times 2^3 + \sum_{n=-4}^{2} b_n \times 2^n. \tag{D.1}$$

From this equation, it should be clear that $(1000.0000)_2$ is the most negative number allowed by the representation with a value of -8. The most positive number allowed is $(0111.1111)_2$ with a value $4 + 2 + 1 + 1/2 + 1/4 + 1/8 + 1/16 = 127/16$. Notice that if this were an 8-bit integer, it would be equal to 127. The denominator exists only because we chose to interpret the number this way. Fixed point and integer arithmetic have a one-to-one correspondence.

It is important for the DSP designer to be familiar with the effects of finite word length. In this appendix, we include only details relevant for the system under consideration. Other components may be affected by finite word length effects. Notably, we avoid discussing the

effect on digital oscillators since the other effects are more important for the FB-MC-SS design.

D.1 Finite Word Length Effects

A lot of rounding options are available for calculations in a digital signal processing system. Sometimes, the choice has very little effect on the output signal. Other times, it has a very significant effect. Consider the following cosine signal,

$$x[n] = -\cos(2\pi n/16), \tag{D.2}$$

operating at a normalized frequency of 0.25. This signal is not realizable in a fixed point system, because it requires infinite precision numbers. Floating point numbers do a good job of approximating infinite precision numbers, especially for the range of numbers required by this signal.

To see the effects of rounding visually, we can perform a simple test. The first rounding algorithm that we will explore is the *truncation* algorithm. This algorithm truncates the high order bits of the infinite precision number to fit it into a smaller number. We arbitrarily choose to round our words to 8 bit numbers with 6 fractional bits. We have plotted the DFT for this signal before and after truncation in Figure D.1. From the figure, it is obvious that the effect of rounding has been to inject a (relatively small) DC offset in our signal. This is probably not an issue at this point. It is roughly 36 dB lower than the tones from our cosine. However, if we had chosen a smaller word length, the strength of the tone at DC would increase. If we were to pass this tone to a PLL expecting a pure (filtered) tone, issues may arise. That is one example that shows why it is important to understand the effects of finite word lengths on practical signal processing.

To understand why the truncation algorithm causes this distortion is quite simple. Consider the number $(00.1010)_2 = 5/8$. Let us assume that the output is desired to be a 4-bit number with only two fractional bits. After truncation, the number would be $(00.10)_2 = 1/2$. Now, consider a negative number $(11.0110)_2 = -5/8$. After truncating, we obtain $(11.01)_2 = -3/4$. In the positive case, the number was rounded down since $1/2 < 5/8$, and in the negative case, the number was rounded down since $-3/4 < -5/8$. Thus, we can expect that to happen when rounding any nonzero number. Furthermore, this results in a bias that is roughly half of the LSB of the resulting word length. This bias shows up on the plot. In our example, we expect this to contribute a total amount of $2^{-6} = -36$ dB which it does.

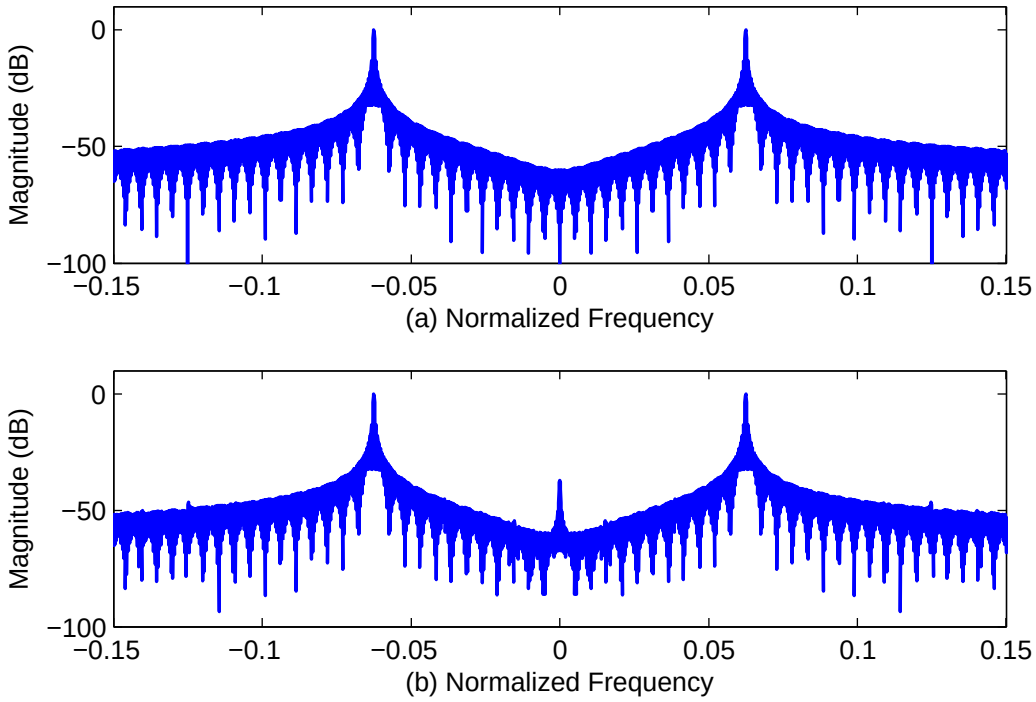

Figure D.1. A comparison of the spectrum of a cosine before and after truncating from real numbers to 8 bit fixed point numbers with 6 fractional bits. Above (a) shows the signal before rounding. Below (b) shows the signal after rounding.

In hardware, one can use more complicated rounding schemes (with an associated cost in terms of area). There are a lot of different rounding schemes available, but a simple one would be to always round toward zero. We have plotted the results for this scheme in Figure D.2. The unwanted spike at DC has disappeared. There are still artifacts throughout the signal that could be corrected by a more complicated rounding scheme.

D.2 Considerations for DSA Applications

Besides the effects of rounding, our finite word lengths are only able to represent signals in certain ranges of power levels. This is very important as far as cognitive radios are concerned. The primary users occupying the spectrum may be transmitting nearby with high power levels. If one cannot represent a low power signal in addition to the high power signal, there is little hope that the desired low power signal can be recovered through filtering. To illustrate this, we will design a multiband FIR filter and perform quantization of its coefficients to our desired word length. This will allow us to see what happens to low power signal signals.

Figure D.3 demonstrates what can happen. Prior to rounding, there are three distinct

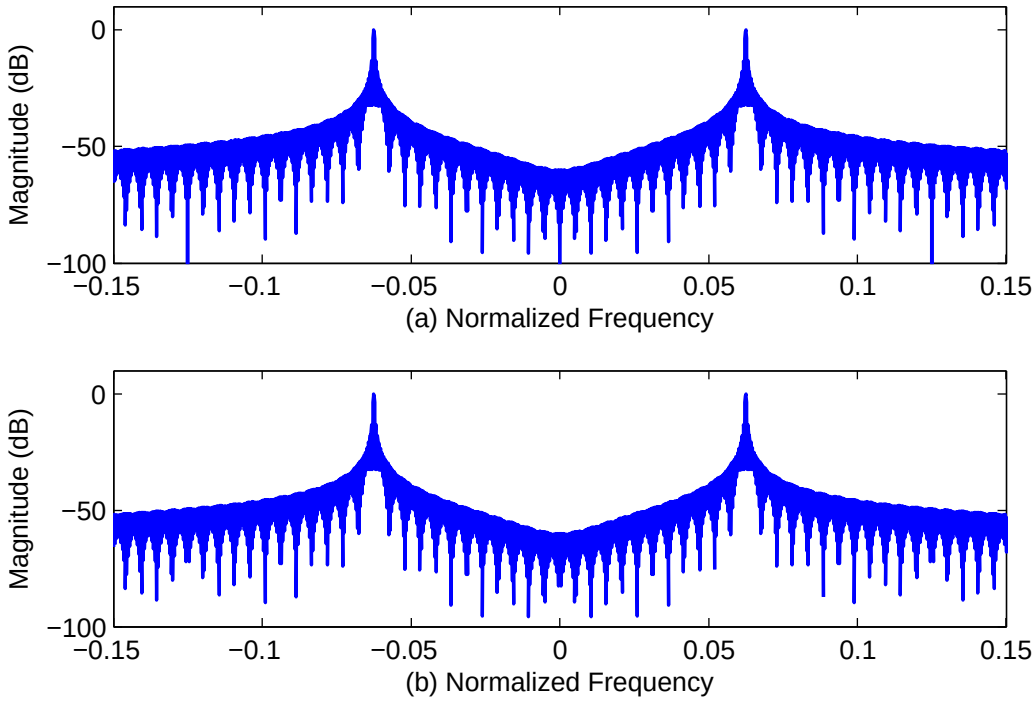

Figure D.2. A comparison of the spectrum of a cosine before and after rounding toward zero to 8 bit fixed point numbers with 6 fractional bits. Above (a) shows the signal before rounding. Below (b) shows the signal after rounding.

signals. After rounding, the signal on the right-hand side is lost in the noise. This means that the bits where this signal was located have been truncated during the rounding process. Thus, it is unlikely that any useful data will be recovered.

This has very real impacts on dynamic spectrum access systems where low power secondary users are expected to coexist with primary users. The next subsection describes how these considerations play a role in designing the filter bank system.

D.3 Considerations for FB-MC-SS

The transmitter implementation is very simple, but it is important to note that the precision of the IFFT input controls the precision of the spreading sequence that may be used. In addition, the transmitter should be tuned to make full use of the dynamic range of its DAC. Otherwise, one may see artifacts and distortion in the signal that complicate the receiver (or just cause errors).

The receiver implementation has a considerable number of places where word length is important. First, an automatic gain controller of some sort should be used at the input to the filter bank. This should be tuned to be sensitive to generic signals in the area,

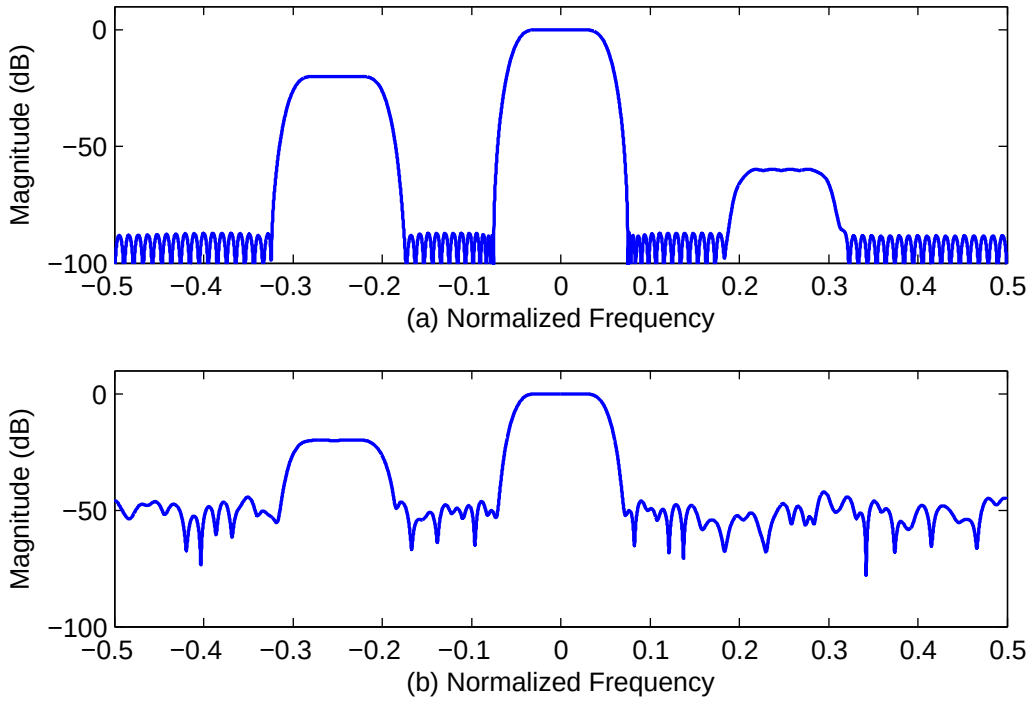

Figure D.3. A comparison of the spectrum of a multiband filter before and after rounding toward zero. Above (a) shows the signal before rounding. Below (b) shows the signal after rounding to 12 bits with 10 fractional bits.

especially for dynamic spectrum access scenarios. Clipping any signal causes harmonics to appear across the entire sampling bandwidth. This will decrease system performance significantly, because it violates the concept of spectrum isolation on which FB-MC-SS is predicated.

The challenge with making oneself sensitive to other systems in the environment is that one may not know exactly what range of amplitudes are likely at the filter bank outputs. It is crucial that the proper word lengths are chose at the filter bank outputs. A good choice when using a Virtex-5 FPGA is to use the DSP48 slices on the FPGA for the polyphase analysis filter bank, then convert the filter bank outputs to 24-bit words and pass them to a 24-bit IFFT operation. This allows a large dynamic range even in the presence of signals that are much stronger than the FB-MC-SS system. Here, we reduce our system word length down to 16-bit words to avoid wasting resources.

Choosing the correct 16 bits is crucial for robust system performance. If the bits used are too high, then the FB-MC-SS signal will be lost in the noise and suffer a performance loss from unnecessary noise. If the bits used are too low, then the FB-MC-SS signal will saturate

or wrap around. Either case yields a significant problem in terms of performance. In the case of saturation, the MRC weight for this subcarrier will be ∞ (due to the variance being 0). It will also cause problems for channel estimation. Note that saturating or wrapping the value of a high power interference is okay as long as we detect the overflow and avoid using this subcarrier in the system further. In the case that the FB-MC-SS signal wrap around, the symbols will be wrapped to an incorrect state prior to channel estimation and symbol detection. Obviously, saturation and wrap around of the FB-MC-SS signal will cause the system to underperform and eventually fail.

For this reason, it is extremely important that the designer be aware of the effects associated with finite word lengths. The designer should experiment in fixed point simulations with large interferences present. If the system is to be used near and around other systems, then the choice of word lengths will have a large impact on overall system performance.

REFERENCES

[1] J. G. Proakis and M. Salehi, *Digital Communications*, 5th ed. McGraw-Hill Science/Engineering/Math, 2007.

[2] D. Tse, *Fundamentals of Wireless Communication.* Cambridge University Press, 2005.

[3] A. Goldsmith, *Wireless Communications.* Cambridge University Press, 2005.

[4] B. Farhang-Boroujeny, *Signal Processing Techniques for Software Radios.* Lulu, 2nd edition, 2010.

[5] G. Falciasecca and B. Valotti, "Guglielmo marconi: The pioneer of wireless communications," in *Microwave Conference, 2009. EuMC 2009. European*, Sept 2009, pp. 544–546.

[6] J. A. C. Bingham, "Multicarrier modulation for data transmission: an idea whose time has come," *Communications Magazine, IEEE*, vol. 28, no. 5, pp. 5–14, May 1990.

[7] B. Saltzberg, "Performance of an efficient parallel data transmission system," *IEEE Trans. on Comm. Tech.*, vol. 15, no. 6, pp. 805–811, December 1967.

[8] R. Chang, "High-speed multichannel data transmission with bandlimited orthogonal signals," *Bell Sys. Tech. J.*, vol. 45, pp. 1775–1796, December 1966.

[9] L. Cimini, "Analysis and simulation of a digital mobile channel using orthogonal frequency division multiplexing," *Communications, IEEE Transactions on*, vol. 33, no. 7, pp. 665–675, Jul 1985.

[10] B. Hirosaki, "An orthogonally multiplexed qam system using the discrete fourier transform," *Communications, IEEE Transactions on*, vol. 29, no. 7, pp. 982–989, Jul 1981.

[11] P. H. Moose, "A technique for orthogonal frequency division multiplexing frequency offset correction," *Communications, IEEE Transactions on*, vol. 42, no. 10, pp. 2908–2914, Oct 1994.

[12] T. Schmidl and D. Cox, "Robust frequency and timing synchronization for ofdm," *Communications, IEEE Transactions on*, vol. 45, no. 12, pp. 1613–1621, Dec 1997.

[13] D. Landstrom, J. Arenas, J.-J. van de Beek, P. Borjesson, M.-L. Boucheret, and P. Odling, "Time and frequency offset estimation in ofdm systems employing pulse shaping," in *Universal Personal Communications Record, 1997. Conference Record., 1997 IEEE 6th International Conference on*, Oct 1997, pp. 279–283 vol.1.

[14] J.-J. van de Beek, M. Sandell, and P. Borjesson, "Ml estimation of time and frequency offset in ofdm systems," *Signal Processing, IEEE Transactions on*, vol. 45, no. 7, pp. 1800–1805, Jul 1997.

[15] B. Farhang-Boroujeny, "OFDM versus filter bank multicarrier," *IEEE Signal Processing Magazine*, vol. 28, no. 3, pp. 92–112, May 2011.

[16] W. Rhee, J. Chuang, and L. Cimini, "Performance comparison of ofdm and multitone with polyphase filter bank for wireless communications," in *Vehicular Technology Conference, 1998. VTC 98. 48th IEEE*, vol. 2, May 1998, pp. 768–772 vol.2.

[17] M. Bellanger, "Physical layer for future broadband radio systems," in *Radio and Wireless Symposium (RWS), 2010 IEEE*, Jan 2010, pp. 436–439.

[18] ——, "Efficiency of filter bank multicarrier techniques in burst radio transmission," in *Global Telecommunications Conference (GLOBECOM 2010), 2010 IEEE*, Dec 2010, pp. 1–4.

[19] B. Farhang-Boroujeny and R. Kempter, "Multicarrier communication techniques for spectrum sensing and communication in cognitive radios," *IEEE Communications Magazine*, vol. 46, no. 4, pp. 80–85, April 2008.

[20] R. Pickholtz, "Theory of spread-spectrum communications– a tutorial," *Communications, IEEE Transactions on*, vol. 30, no. 5, pp. 855–884, May 1982.

[21] S. S. Rappaport and D. M. Grieco, "Spread-spectrum signal acquisition: Methods and technology," *IEEE Commun. Mag.*, vol. 22, no. 6, pp. 6–21, June 1984.

[22] A. J. Viterbi, "Spread spectrum communications: Myths and realities," *Communications Magazine, IEEE*, vol. 40, no. 5, pp. 34–31, May 2002.

[23] L. B. Milstein, "Interference rejection techniques in spread spectrum communications," *Proceedings of the IEEE*, vol. 76, pp. 657–671, 1988.

[24] S. Hara and R. Prasad, "Overview of multicarrier CDMA," *IEEE Communications Magazine*, vol. 35, no. 2, pp. 126–133, Feb. 1997.

[25] L.-L. Yang and L. Hanzo, "Multicarrier DS-CDMA: A multiple access scheme for ubiquitous broadband wireless communications," *Communications Magazine, IEEE*, vol. 41, no. 10, pp. 116–124, October 2003.

[26] S. Kondo and L. B. Milstein, "Performance of multicarrier DS CDMA systems," *IEEE Trans. Communications*, vol. 44, no. 2, pp. 238–246, Feb. 1996.

[27] G. K. Kaleh, "Overview of multicarrier CDMA," *IEEE Trans. Communications*, vol. 44, no. 7, pp. 886–893, July 1996.

[28] K. Cheun, K. Choi, H. Lim, and K. Lee, "Anti jamming performance of a multicarrier direct-sequence spread-spectrum system," *IEEE Trans. Communications*, vol. 47, no. 12, pp. 1781–1784, Dec. 1999.

[29] D. L. Wasden, J. Loera, H. Moradi, and B. Farhang-Boroujeny, "Design and implementation of a multicarrier spread spectrum communication system," *Military Communications Conference, 2012 - MILCOM 2012*, pp. 1–7, Oct-Nov 2012.

[30] S. Haykin, "Cognitive radio: Brain-empowered wireless communications," *IEEE Journal on Selected Area in Communications*, vol. 23, no. 2, pp. 201–220, Feb. 2005.

[31] T. Weiss and F. J. et al., "Spectrum pooling: An innovative strategy for the enhancement of spectrum efficiency," *IEEE Communications Magazine*, vol. 42, no. 3, pp. 8–14, 2004.

[32] J. Zhao, H. Zheng, and G.-H. Yang, "Distributed coordination in dynamic spectrum allocation networks," *Proc. IEEE DySPAN*, pp. 259–268, Nov. 2005.

[33] D. L. Wasden, H. Moradi, and B. Farhang-Boroujeny, "Design and implementation of an underlay control channel for cognitive radios," *Selected Areas in Communications, IEEE Journal on*, vol. 30, no. 10, pp. 1875–1889, November 2012.

[34] D. Wasden, J. Loera, A. Majid, H. Moradi, and B. Farhang-Boroujeny, "Design and implementation of an underlay control channel for cognitive radios," in *Dynamic Spectrum Access Networks (DYSPAN), 2012 IEEE International Symposium on*, Oct 2012, pp. 280–281.

[35] W. Rhee, J. Chuang, and L. Cimini, "Performance comparison of ofdm and multitone with polyphase filter bank for wireless communications," in *Vehicular Technology Conference, 1998. VTC 98. 48th IEEE*, vol. 2, May 1998, pp. 768–772 vol.2.

[36] L. Rugini and P. Banelli, "Ber of ofdm systems impaired by carrier frequency offset in multipath fading channels," *Wireless Communications, IEEE Transactions on*, vol. 4, no. 5, pp. 2279–2288, Sept 2005.

[37] T. Pollet, M. Van Bladel, and M. Moeneclaey, "Ber sensitivity of ofdm systems to carrier frequency offset and wiener phase noise," *Communications, IEEE Transactions on*, vol. 43, no. 234, pp. 191–193, Feb 1995.

[38] P. P. Vaidyanathan, *Multirate Systems and Filter Banks*. Englewood Cliffs, NJ: Prentice-Hall, 1993.

[39] B. Farhang-Boroujeny and C. G. Yuen, "Cosine modulated and offset QAM filter bank multicarrier techniques: a continuous- time prospect," *EURASIP Journal on Applied Signal Processing, 2010, special issue on Filter Banks for Next Generation Multicarrier Wire- less Communications*, p. 16 pages, doi:10.1155/2010/165654 2010.

[40] D. Chu, "Polyphase codes with good periodic correlation properties," *IEEE Trans. Info. Theory*, vol. 18, no. 4, pp. 531–532, Jul. 1972.

[41] R. E. Best, *Phase Locked Loops*. McGraw-Hill, 1998.

[42] B. Farhang-Boroujeny, *Adaptive Filters: Theory and Applications*. John Wiley and Sons, 1998.

[43] F. C. Commission. (2002, Nov) Report on the spectrum efficiency working group. [Online]. Available: http://www.fcc.gov/spf/reports.html

[44] R. Etkin, A. Parekh, and D. Tse, "Spectrum sharing for unlicensed bands," *Selected Areas in Communications, IEEE Journal on*, vol. 25, no. 3, pp. 517–528, April 2007.

[45] Q. Zhao and A. Swami, "A survey of dynamic spectrum access: Signal processing and networking perspectives," in *Acoustics, Speech and Signal Processing, 2007. ICASSP 2007. IEEE International Conference on*, vol. 4, April 2007, pp. IV–1349–IV–1352.

[46] W. Hu, D. Willkomm, M. Abusubaih, J. Gross, G. Vlantis, M. Gerla, and A. Wolisz, "Cognitive radios for dynamic spectrum access - dynamic frequency hopping communities for efficient ieee 802.22 operation," *Communications Magazine, IEEE*, vol. 45, no. 5, pp. 80–87, May 2007.

[47] C. Cordeiro, K. Challapali, D. Birru, and N. Sai Shankar, "Ieee 802.22: the first worldwide wireless standard based on cognitive radios," in *New Frontiers in Dynamic Spectrum Access Networks, 2005. DySPAN 2005. 2005 First IEEE International Symposium on*, Nov 2005, pp. 328–337.

[48] C. Stevenson, G. Chouinard, Z. Lei, W. Hu, S. Shellhammer, and W. Caldwell, "Ieee 802.22: The first cognitive radio wireless regional area network standard," *Communications Magazine, IEEE*, vol. 47, no. 1, pp. 130–138, January 2009.

[49] Z. Quan, S. Xui, A. Sayed, and H. Poor, "Optimal multiband joint detection for spectrum sensing in cognitive radio networks," *IEEE Trans. Signal Proc.*, vol. 57, no. 3, pp. 1128–1140, March 2009.

[50] B. Farhang-Boroujeny, "Filter bank spectrum sensing for cognitive radios," *IEEE Trans. Signal Proc.*, vol. 56, no. 5, pp. 1801–1811, May 2008.

[51] P. D. Sutton, K. E. Nolan, and L. E. Doyle, "Cyclostationary signatures in practical cognitive radio applications," *IEEE Journal on Selected Area in Commun.*, vol. 26, no. 1, pp. 13–24, Jan. 2008.

[52] B. Farhang-Boroujeny and C. Furse, "A robust detector for multicarrier spread spectrum transmission over partially jammed channels," *IEEE Trans. Signal Proc.*, vol. 53, no. 3, pp. 1038–1044, March 2005.

[53] B. F. Lo, I. F. Akyildiz, and A. M. Al-Dhelaan, "Efficient recovery control channel design in cognitive radio ad hoc networks," *IEEE Trans. Vehicular Tech.*, vol. 59, no. 9, pp. 4513–4526, Nov. 2010.

[54] I. F. Akyildiz, W.-Y. Lee, M. C. Vuran, and S. Mohanty, "Next generation/dynamic spectrum access/cognitive radio wireless networks: A survey," *Computer Networks*, vol. 50, no. 13, pp. 2127–2159, Sept. 2006.

[55] I. F. Akyildiz, W.-Y. Lee, and K. R. Chowdhury, "CRAHNs: Cognitive radio ad hoc networks," *Ad Hoc Networks*, vol. 7, no. 5, pp. 810–836, July 2009.

[56] S. M. Mishra, A. Sahai, and R. W. Brodersen, "Cooperative sensing among cognitive radios," *IEEE International Conference on Communications, ICC '06*, vol. 4, pp. 1658–1663, June 2006.

[57] D. Cabric and R. Brodersen, "Physical layer design issues unique to cognitive radio systems," *Personal, Indoor and Mobile Radio Communications*, vol. 2, pp. 759–763, Sept. 2005.

[58] L. Cao and H. Zheng, "Distributed spectrum allocation via local bargaining," *in proceedings of Second Annual IEEE Comm. Society Conference on Sensor and Ad Hoc Communications and Networks*, pp. 475–486, Sept. 2005.

[59] K. R. Chowdhury and I. F. Akyildiz, "OFDM-based common control channel design for cognitive radio ad hoc networks," *IEEE Trans. on Mobile Computing*, vol. 10, pp. 228–238, 2011.

[60] B. Hamdaoui and K. G. Shin, "OS-MAC: An efficient MAC protocol for spectrum-agile wireless networks," *IEEE Transactions on Mobile Computing*, vol. 7, no. 8, pp. 915–930, Aug. 2008.

[61] D. Cabric, S. Mishra, D. Willkomm, R. Brodersen, and A. Wolisz, "A cognitive radio approach for usage of virtual unlicensed spectrum," *in proceedings: 14th IST Mobile and Wireless Communications Summit, Dresden, Germany*, June 2005.

[62] C. Cordeiro and K. Challapali, "C-MAC: A cognitive MAC protocol for multi-channel wireless networks," *in Proc. IEEE Int. Symp. on Dynamic Spectrum Access (DySPAN)*, pp. 147–157, Apr. 2007.

[63] J. Jia, Q. Zhang, and X. Shen, "HC-MAC: a hardware constrained cognitive MAC for efficient spectrum management," *IEEE Journal on Selected Area in Commun.*, vol. 26, no. 1, pp. 106–117, 2008.

[64] C. Cormio and K. R. Chowdhury, "A survey on MAC protocols in cognitive radio wireless networks," *Ad Hoc Networks*, vol. 7, no. 7, pp. 1315–1329, Sept. 2009.

[65] B. F. Lo, "A survey of common control channel design in cognitive radio networks," *Physical Communication*, vol. 4, pp. 26–39, 2011.

[66] D. Cabric, S. Mishra, and R. Brodersen, "Implementation issues in spectrum sensing for cognitive radios," *IEEE Journal on Selected Area in Commun.*, vol. 1, no. 11, pp. 772–776, Nov. 2004.

[67] R.-R. Chen, K.-H. Teo, and B. Farhang-Boroujeny, "Random access protocols for collaborative spectrum sensing in multi-band cognitive radio networks," *IEEE Journal of Selected Topics in Signal Processing*, vol. 5, no. 2, pp. 124–136, Feb. 2011.

[68] T. Chen, H. Zhang, G. M. Maggio, and I. Chlamtac, "Cogmesh: A cluster-based cognitive radio network," *Proc. IEEE DySPAN*, p. 168178, Apr. 2007.

[69] L. A. DaSilva and I. Guerriero, "Sequence-based rendezvous for dynamic spectrum access," *in Proc. IEEE Int. Symp. on Dynamic Spectrum Access (DySPAN)*, pp. 1–7, October 2008.

[70] C. Cormio and K. R. Chowdhury, "Common control channel design for cognitive radio wireless ad hoc networks using adaptive frequency hopping," *Ad Hoc Networks*, vol. 8, pp. 430–438, 2010.

[71] M. E. Sahin and H. Arslan, "System design for cognitive radio communications," *Proc. IEEE CrownCom*, pp. 1–5, June 2006.

[72] M. Petracca, R. Pomposini, F. Mazzenga, R. Giuliano, and M. Vari, "An always available control channel for cooperative sensing in cognitive radio networks," in *Wireless Days (WD), 2010 IFIP*, Oct 2010, pp. 1–5.

[73] K. Bian, J.-M. Park, and R. Chen, "A quorum-based framework for establishing control channels in dynamic spectrum access networks," *in Proc. of MobiCom*, pp. 25–36, 2009.

[74] N. C. Theis, R. W. Thomas, and L. A. DaSilva, "Rendezvous for cognitive radios," *IEEE Trans. on Mobile Computing*, vol. 10, pp. 216–227, 2011.

[75] A. Masri, C.-F. Chiasserini, C. Casetti, and A. Perotti, "Common control channel allocation in cognitive radio networks through UWB multihop communications," *in: The First Nordic Workshop on Cross Layer Optimization in Wireless Networks at Levi, Finland*, 2010.

[76] S. Srinivasa and S. Jafar, "Cognitive radios for dynamic spectrum access - the throughput potential of cognitive radio: A theoretical perspective," *Communications Magazine, IEEE*, vol. 45, no. 5, pp. 73–79, May 2007.

[77] P. D. Welch, "The use of fast fourier transform for the estimation of power spectra: A method based on time averaging over short, modified periodograms," *Audio and Electroacoustics, IEEE Transactions on*, vol. 15, no. 2, pp. 70–73, Jun 1967.

[78] D. Thomson, "Spectrum estimation and harmonic analysis," *Proceedings of the IEEE*, vol. 70, no. 9, pp. 1055–1096, Sept 1982.

[79] B. Farhang-Boroujeny, "Filter bank spectrum sensing for cognitive radios," *Signal Processing, IEEE Transactions on*, vol. 56, no. 5, pp. 1801–1811, May 2008.

[80] T. Eng and L. B. Milstein, "Coherent DS-CDMA performance in Nakagami multipath fading," *Communications, IEEE Transactions on*, vol. 43, no. 234, pp. 1134–1143, 1995.

[81] J. Min and H. Samueli, "Synchronization techniques for a frequency-hopped wireless transceiver," *Vehicular Technology Conference, 1996. Mobile Technology for the Human Race, IEEE 46th*, vol. 1, pp. 184–187, 1996.

[82] L.-L. Yang and L. Hanzo, "Performance of generalized multicarrier DS-CDMA over Nakagami-m fading channels," *Communications, IEEE Transactions on*, vol. 50, no. 6, pp. 956–966, June 2002.

[83] V. M. DaSilva and E. S. Sousa, "Performance of orthogonal CDMA codes for quasi-synchronous communication systems," *Proceedings of IEEE*, vol. ICUPC '93, pp. 995–999, October 1993.

[84] D. N. Rowitch and L. B. Milstein, "Convolutionally coded multicarrier DS-CDMA systems in a multipath fading channel– part i: Performance analysis," *IEEE Trans. Commun.*, vol. 47, pp. 1570–1582, 1999.

[85] ——, "Convolutionally coded multicarrier DS-CDMA systems in a multipath fading channel– part ii: Narrow-band interference suppression," *IEEE Trans. Commun.*, vol. 47, pp. 1729–1736, 1999.

[86] H. Wei, L.-L. Yang, and L. Hanzo, "Time- and frequency-domain spreading assisted MC DS-CDMA using interference rejection spreading codes for quasi-synchronous communications," *Vehicular Technology Conference*, vol. VTC2004-Fall, pp. 390–393, 2004.

[87] L. Vandendorpe, "Multitone spread spectrum multiple access communications system in a multipath rician fading channel," *IEEE International Conference on Communications, ICC '94*, pp. 1638–1642, 1994.

[88] W. Xu and L. B. Milstein, "On the performance of multicarrier rake systems," *IEEE Transactions on Communications*, vol. 49, no. 10, pp. 1812–1823, October 2001.

[89] S. A. Abbas, "Ber performance of the rake receiver in a realistic mobile radio channel," *Vehicular Technology Conference, 1998. VTC '98. 48th IEEE*, vol. 3, pp. 2037–2041, 1998.

[90] K. J. Kim, S. Y. Kwon, E. K. Hong, and K. C. Whang, "Effect of tap spacing on the performance of direct-sequence spread-spectrum rake receiver," *Communications, IEEE Transactions on*, vol. 48, no. 6, pp. 1029–1036, June 2000.

[91] P. Boyer, "Performance based on selective multipath reception," *Communications, IEEE Transactions on*, vol. 52, no. 2, pp. 280–288, February 2004.

[92] M. Patzold, *Mobile Radio Channels*, 2nd ed. Wiley, 2012.

[93] E. D. Kaplan and C. J. Hegarty, *Understanding GPS: Principles and Applications*, 2nd ed. Artech House, 2006.

[94] F. M. Gardner, *Phaselock Techniques*, 3rd ed. John Wiley and Sons, Inc., 2005.

[95] J. E. Volder, "The CORDIC trigonometric computing technique," *IRE Transactions on Electronic Computers*, vol. EC-8, no. 3, pp. 330–334, 1959.

[96] G. Cherubini, E. Eleftheriou, and S. Olcer, "Filtered multitone modulation for very high-speed digital subscriber lines," *Selected Areas in Communications, IEEE Journal on*, vol. 20, no. 5, pp. 1016–1028, Jun 2002.